Uncertainties in the Realisation of the SPRT Subranges of the ITS-90

CCT-WG3 on Uncertainties in Contact Thermometry
D.R. White (MSL), M. Ballico (NMIA), V. Chimenti (CEM),
S. Duris (SMU), E. Filipe (IPQ), A. Ivanova (VNIIM), A. Kartal Dogan (UME),
E. Mendez-Lango (CENAM), C. Meyer (NIST), F. Pavese (IMGC), A. Peruzzi (NMi-VSL),
E. Renaot (LNE-INM), S. Rudtsch (PTB), K. Yamazawa (NMIJ, AIST).

ABSTRACT

This document summarises the uncertainties in the realisation of the standard platinum resistance thermometer (SPRT) subranges of ITS-90 between the triple point of neon (24.5561 K) and the freezing point of silver (961.78 ºC). The document provides users of ITS-90 with guidance for assessing the uncertainty in their SPRT calibrations and temperature measurements. A secondary purpose is to promote harmonisation of the assessment of calibration and measurement capabilities as defined under the CIPM's arrangement for the mutual recognition of national measurement institutes (CIPM 1999). The document describes all known sources of uncertainty and influence variables, identifies key references in the literature that discuss, model or evaluate each effect, gives an indication of the typical magnitudes of the uncertainties, and gives propagation laws so that total uncertainty may be determined.

Contents

1. Introduction and scope 4
2. Effects common to all fixed points 5
    2.1. Residual gas pressure 5
    2.2. Hydrostatic pressure 6
    2.3. Impurity effects 7
    2.4. Isotope effects 13
3. Water Triple point 15
    3.1. Residual gas pressure 15
    3.2. Impurities 15
    3.3. Isotopic composition 16
    3.4. Strain, crystal defects, and crystal size 18
    3.5. Buoyancy effect 18
    3.6. Thermal effects 18
4. Cryogenic Fixed points (e-H_2, Ne, O_2, Ar) 19
    4.1. Impurities 19
    4.2. Isotopic composition 19
    4.3. Isomer equilibration (e-H_2) 21
    4.4. Strain and crystal defects 22
    4.5. Static thermal effects 22
    4.6. Dynamic thermal effects 23
    4.7. Determination of the liquidus point 23
5. Metal fixed points (Hg, Ga, In, Sn, Zn, Al, Ag) 24
    5.1. Immersion and thermal effects 24
    5.2. Isotope effects 25
    5.3. Determination of the liquidus point 26
6. The SPRT 27
    6.1. Oxidation 27
    6.2. Impurities 29
    6.3. Vacancies and crystal defects 30
    6.4. Strain and hysteresis 30
    6.5. Long term drift and uncertainty 31
    6.6. Insulation and leakage effects 31
7. Interpolation error and non-uniqueness 34
    7.1. Type 1 non-uniqueness (subrange inconsistency) 34

7.2. Type 3 non-uniqueness 36

8. Resistance measurement 39

8.1. Reference resistor 39

8.2. Connecting cables and lead resistances 40

8.3. The resistance bridge 41

8.4. Self heating 43

9. Total uncertainty in SPRT measurements 46

9.1. The fixed-point sensitivity coefficients 46

9.2. Methods for calculating total uncertainty 47

9.3. Uncertainty in SPRT resistance at the triple point of water (reported value) 47

9.4. Uncertainty in SPRT resistance ratio at the fixed points 48

9.5. An approximate expression for total uncertainty in the interpolated resistance ratio, W_r 49

9.6. Total uncertainty in temperature 51

9.7. Total uncertainty for capsule SPRTs used 'in-house' 51

9.8. Total uncertainty for capsule SPRTs used outside the calibration laboratory 52

9.9. Total uncertainty for long-stem SPRTs used 'in-house' 53

9.10. Total uncertainty for long stem SPRTs used in a calibration bath 54

9.11. Total uncertainty in fixed point comparisons 56

Glossary 58

Appendix A: Summary of typical ranges of fixed-point uncertainties 60

Appendix B: Table of sensitivity coefficients and useful constants for the fixed points 61

Appendix C: The ITS-90 interpolations and the propagation of uncertainty 62

C.1. The mathematical structure of ITS-90 62

C.2. Propagation of uncertainty 64

C.3. Simplifying and reducing uncertainty 66

Appendix D: The ITS-90 SPRT interpolating functions 70

D.1. Two methods for calculating the sensitivity coefficients 70

D.2. The interpolating functions for each subrange 71

References 81

1. Introduction and Scope

The primary purpose of this document is to provide users of the International Temperature Scale of 1990 (ITS-90) with guidance for assessing the uncertainty in calibrations and temperature measurements employing standard platinum resistance thermometers (SPRTs). A secondary purpose is to promote harmonisation of the assessment of calibration and measurement capabilities as defined under the CIPM's arrangement for the mutual recognition of national measurement institutes (CIPM 1999). Accordingly, the document provides a brief description of all known sources of uncertainty and influence variables, identifies key references in the literature that discuss, model or evaluate each effect, gives an indication of the magnitudes of the uncertainties, and gives propagation laws so that total uncertainty may be determined.

The guide covers all of the known influence effects in the most commonly used SPRT subranges between the triple point of neon (24.5561 K) and the freezing point of silver (961.78 ºC). Since the hydrogen point is required for the calibration of SPRTs for the neon–water subrange, effects associated with the realisation of the triple point of equilibrium hydrogen (13.8033 K) are included. For the hydrogen–water subrange, which extends below 24.5561 K, the SPRT must also be calibrated at two additional points near 17.0 K and 20.3 K with the actual temperatures determined by either ITS-90 gas thermometer or ITS-90 vapour-pressure thermometer. Discussion of these two additional points is beyond the scope of this guide. For further information refer to ITS-90 (Preston-Thomas 1990), the *Supplementary Information for the ITS-90* (BIPM 1990), and to the published literature describing ITS-90 realisations over this sub-range.

Because most of the effects discussed here are the subject of ongoing research, the methods and models described for assessing uncertainty are suggested and not prescribed, and the user of the document is free to adopt any approach consistent with current physical knowledge and uncertainty practice. In particular, more information will be found in more recent research literature.

Although the guide occasionally notes the impact of different measurement techniques on uncertainty, it is not a guide on technique or on the realisation of the scale and should be read in conjunction with the *Supplementary Information for the ITS-90* and the *Mise en Pratique for the Realisation of the Kelvin* (BIPM 2006). Indeed, familiarity with the *Supplementary Information*, the *Mise*, and the principles of the ITS-90 is assumed.

Numerical values for uncertainties given here are for indicative purposes only. Users of the guide are expected to determine values appropriate to their equipment and procedures. Additionally, it is not essential that distinct values are determined for each source of uncertainty; usually it is sufficient that all terms have been identified and assessed.

In the interests of promoting harmonisation and ensuring consistency with the ISO *Guide to the Expression of Uncertainty in Measurement* (ISO 1995), we have endeavoured to adhere to the following principles:

- Unless otherwise stated all uncertainties are expressed as standard uncertainties.
- Where uncertainties are estimated with low confidence, the reporting of effective degrees of freedom (ISO 1995, Section G4) is encouraged so users of the uncertainty are able, if required, to calculate realistic values for confidence intervals.
- All uncertainty terms are associated with a physical cause. This ensures that each source of uncertainty has a mathematical model allowing estimation and propagation of uncertainty.
- Corrections are applied where bias (systematic error) is known, including in most cases where the correction is less than the uncertainty. This is done to maximise the information retained in reported measurement results and to prevent the accumulation of significant bias. We follow the sign convention that corrections are always added to the measurement.
- Where Type A assessments are employed, all of the sources of the uncertainty should be identified and the measurements should draw samples from the whole of the distribution associated with each source. This practice prevents both 'double counting' and underestimates of uncertainty. This requirement may preclude the use of non-specific uncertainty terms such as repeatability or reproducibility (ISO 1993).

Appendix A provides a complete tabular summary of the typical range of uncertainties at each of the fixed points. The figures in Section 9 provide graphical examples of the total propagated uncertainties.

Acknowledgement
CCT Working Group 3 gratefully acknowledges the contributions of previous members of the working group (Bonnier *et al*. 2005), other members of the CCT, colleagues in the various NMIs, and equipment suppliers for helpful discussions and responses to requests for information or research. We also acknowledge the members of CCT Working Group 1 for their contributions to definitions and, particularly, for the work on impurities in fixed points and isotopic effects in the equilibrium-hydrogen and neon points.

2. Effects common to all fixed points

This section discusses four effects common to all of the fixed points, namely residual gas pressure, hydrostatic pressure, impurity effects and isotopic effects. Additional effects or additional details relating to specific fixed points may be found in Sections 3, 4, and 5.

2.1 *Residual gas pressure*

Fixed-point cells are generally classified as sealed or 'open'. Sealed cells are sealed at the time of manufacture so that the internal pressure cannot be measured or controlled during use. Open cells may be open to the atmosphere or subject to control of the gas pressure and composition. In triple-point cells, the pressure of the gas above the surface of the liquid in the cell is ideally due to the vapour pressure of the fixed-point substance only. In melting and freezing points, the pressure above the surface of the liquid should be the standard atmosphere, 101 325 Pa. Note that residual gasses in the cryogenic fixed points are usually treated as impurities, so an additional uncertainty term due to residual gas pressure is unnecessary.

Measurements made in cells at a different internal pressure, p_{meas}, should be corrected for the pressure difference:

$$\Delta T_p = -\frac{dT}{dp}\left(p_{\text{meas}} - p_0\right) , \tag{2.1}$$

where p_0 is the ideal/nominal pressure and dT/dp is the pressure coefficient defined by ITS-90 (values are given in Appendix B). For melting and freezing points in open cells without any pressure control or measurement, the pressure is determined by the weather and altitude at the location of the measurement. This leads to pressure variations (standard uncertainty) with weather, over periods of days, of about 2 kPa (2% atm.), and pressure differences with altitude of 20 kPa or more, leading to corrections of 1.5 mK or more.

The uncertainty in the pressure correction is given by

$$u^2\left(\Delta T_p\right) = \left(\frac{dT}{dp}\right)^2 u^2\left(p_{\text{meas}}\right) + u^2\left(\frac{dT}{dp}\right)\left(p_{\text{meas}} - p_0\right)^2 , \tag{2.2}$$

where $u(p_{\text{meas}})$ is the uncertainty in the pressure inside the cell and $u(dT/dp)$ is the uncertainty in the pressure coefficient. If the cell is subject to pressure control or measurement, the uncertainty in the pressure may be 10 Pa, or lower.

The uncertainty in the pressure coefficient is practically negligible, and ranges from about 0.2% for the triple point of water to a few percent for the other fixed points (McAllan 1982). In open cells, the pressure coefficient is easily confirmed by changing the gas pressure. The current values used for the fixed points are also consistent with values calculated from the Clausius-Clapeyron equation:

$$\frac{dT}{dp} = \frac{T_{\text{fp}}\Delta V}{\Delta H_{\text{f}}} , \tag{2.3}$$

where ΔH_{f} is the molar heat of fusion, T_{fp} is the fixed-point temperature, and ΔV is the molar volume change.

With sealed metal fixed-point cells, the internal cell pressure is not measurable, and the operator must rely on the manufacturer of the cell having sealed the cell at the correct pressure. With the usual procedures, and in the absence of leaks, the pressure in the cell when at the fixed-point temperature is approximately[1]

[1] During the manufacture of sealed cells, the filled crucible is placed in a glass or fused silica container with a long capillary, which is also attached to the gas filling system. The capillary is first sealed at the gas supply end when the cell is at the fixed-point temperature. Later when the cell is cold, the capillary is removed by resealing the cell close to the crucible. At the time the cell is filled with gas at the fixed-point temperature, the gas in that part of the container around the fixed point is described by $pV_{\text{fp}} = n_{\text{fp}}RT_{\text{fp}}$, where n_{fp} is the number of moles of gas in the space in the fixed-point cell, of volume V_{fp}. The gas in the capillary obeys a similar relationship $pV_{\text{c}} = n_{\text{c}}RT_{\text{c}}$, where the subscript, c, refers to the capillary. When the capillary is later removed, the large fraction, $V_{\text{fp}}/(V_{\text{c}}+V_{\text{fp}})$, of the total quantity of the gas is retained in the cell, and this leads to a the result given. According to the result, the smaller the capillary volume and the closer the capillary temperature to the fixed-point temperature when first sealed, the smaller the error in the cell pressure. The capillary temperature is, unfortunately, not single valued but may range between room temperature, 300 K, and 1900 K (the melting point of silica), depending on the details of the manufacturing process. The average, T_{c}, will be somewhere in between. The capillary volume is normally as small as practical, perhaps less than 2% of the total.

$$p = p_0\left(1+\left(\frac{V_c}{V_c+V_{fp}}\right)\left(\frac{T_{fp}-T_c}{T_c}\right)\right), \tag{2.4}$$

where V_{fp} is the volume of gas in the cell, V_c is the volume of gas in the capillary used to fill the cell with gas during the manufacture of the cell, and T_c is the average temperature of the gas in the capillary when it is sealed. A capillary volume of 1% of V_{fp}, and an average temperature, T_c, range in of 300 K to perhaps near the fixed-point temperature, suggests uncertainties in pressure in the range from 1% to 5% (1 kPa to 5 kPa).

2.2 *Hydrostatic pressure*

The practical realisation of the fixed points, with a thermometer well surrounded by at least one solid-liquid interface, results in a vertical pressure gradient along the length of the thermometer well with the pressure determined by the depth of liquid above the sensing element of the thermometer. The measured temperature must be corrected for the hydrostatic pressure difference between the surface of the liquid, where the fixed-point temperature is defined, and the thermal centre of the sensing element of the SPRT. The correction is

$$\Delta T_{hyd} = -\frac{dT}{dh}\left(h_{liq}-h_{SPRT}\right), \tag{2.5}$$

where h_{liq} is the vertical elevation of the surface of the molten material in the cell when the measurement is taken, h_{SPRT} is the vertical elevation of the thermal centre of the sensing element, and dT/dh is the hydrostatic-pressure coefficient defined by ITS-90 (values are given in Appendix B). Note that the hydrostatic and pressure coefficients are related by

$$\frac{dT}{dh} = \rho g \frac{dT}{dp}, \tag{2.6}$$

where ρ is the density of the liquid and g is the acceleration due to gravity. The range of values for hydrostatic corrections varies considerably between fixed points, with corrections for mercury cells often more than 1 mK.

The uncertainty in the hydrostatic correction is given by

$$u^2\left(\Delta T_{hyd}\right) = \left(\frac{dT}{dh}\right)^2\left[u^2\left(h_{liq}\right)+u^2\left(h_{SPRT}\right)\right]+u^2\left(\frac{dT}{dh}\right)\left(h_{liq}-h_{SPRT}\right)^2, \tag{2.7}$$

where $u(h_{liq})$ and $u(h_{SPRT})$ are the uncertainties in the elevations, and $u(dT/dh)$ is the uncertainty in the hydrostatic pressure coefficient.

The uncertainties in the hydrostatic correction coefficients are assumed to be low, as for the pressure coefficients (Section 2.1), since the two are so closely related. However, there is an additional contribution of a few tenths of a percent due to variations in the local value of the gravitational acceleration, g. For most fixed points, the uncertainty in the coefficient values determined from immersion characteristics is much higher than the values inferred from the dT/dp values. However, there are suggestions of a discrepancy between measured and calculated values of the hydrostatic-pressure coefficient for the water triple point (see, for example, McAllan 1982, Sakurai 2002, Nakanishi and Sakurai 2005) where the magnitude of the measured coefficient is usually a few percent higher than the value inferred from (2.6). Given the relatively large measurement uncertainties and a weak correlation of the effect with thermometer-well diameter (e.g., see the data from Stock and Solve 2006), some unresolved physical effect is a more likely explanation. For most applications, the contribution of the uncertainty in the hydrostatic-pressure coefficient is small (see also (9.27)).

For long-stem SPRTs, the uncertainty in the location of the thermal centre of sensing element is compounded by the differential thermal expansion of SPRT lead wires and the SPRT sheath. For example, the differential expansion in a 600 mm long SPRT with platinum leads and fused-silica sheath is about 6 mm at the silver point. The uncertainty in the liquid level in the cell is also compounded by the expansion of the fixed-point cell and its contents, and the change in volume of the fixed-point substance on melting. For example, the depth of material in aluminium-point cells increases several millimetres when heated to the freezing point, then exhibits a further 7.2% volume increase on melting. Some of the material constants required for such calculations are presented in Appendix B.

The corrections for hydrostatic-pressure effects in the cryogenic points are much smaller than for the high-temperature fixed points, because of the size and construction the cells. However, the uncertainties have a similar magnitude to those for the high-temperature fixed points. The uncertainty still depends on the uncertainty

in the location of the thermal centre of the SPRT, and on the depth of the liquid surrounding the SPRT. Usually the liquid does not always cover the SPRT and the depth increases as the liquid fraction increases.

2.3 *Impurity effects*

Impurity effects are usually the most significant source of uncertainty in fixed-point realisations. Recent improvements in the accuracy and limits of detection in the chemical analysis of impurities in fixed-point substances have made it feasible to model and correct for some impurities. This has had a considerable impact on both the realization technique (Mangum *et al*. 1999a, 2000a) and uncertainty analysis (Fellmuth *et al*. 2005c). Throughout this section, we refer only to impurity effects. However, the same observations and models apply to dilute isotopic effects (Section 2.4).

Before discussing the assessment of uncertainties due to impurities, we provide background discussion on the melting phenomenon, the effect of impurities, and a short derivation of Van't Hoff's relation. Prince (1966) provides a tutorial description of all aspects of the problem and the interpretation of phase diagrams, Lambert (2002a, 2002b) provides good background reading on the understanding of the thermodynamic potential and entropy, and the derivation of Van't Hoff's relation comes from Ubbelohde (1965).

Melting and freezing

All chemical reactions and phase transitions involve a balance between the tendency for systems to occupy the lowest energy state, and for the thermal energy in the system to be dispersed as far as possible. The dispersal of thermal energy (i.e., atomic and molecular kinetic energy) is maximised when the system has access to as many microscopic (quantum-mechanical) states as possible. The number of microscopic states is measured by the entropy. The balance between the two tendencies is described in terms of the thermodynamic potential of the system (in this case, the Gibbs' free energy)

$$G = H - TS\,, \tag{2.8}$$

where H is the enthalpy, T is thermodynamic temperature, and S is the entropy. The enthalpy is the total energy of the system, $H = E + PV$, comprising the internal energy plus the potential energy due to volume and pressure. Systems tend to reorganise themselves spontaneously to minimise the thermodynamic potential.

In the solid phase, atoms are constrained to move in potential wells (a small volume centred on positions in the crystal lattice) with relatively few microscopic states available. In the liquid phase, atoms are able to move within a large volume with access to a large number and high density of microscopic states. Liquids therefore have higher entropy than solids. For atoms to move from the solid phase to the liquid phase they require energy to lift themselves out of the potential wells, and this change in potential is the origin of the enthalpy of fusion. The liquid phase therefore has both higher entropy and higher enthalpy than the solid phase. Figure 2.1 plots the typical thermodynamic potentials for solid and liquid phases. Note that the two curves cross so that the minimum thermodynamic potential is achieved with the system in different phases depending on the temperature.

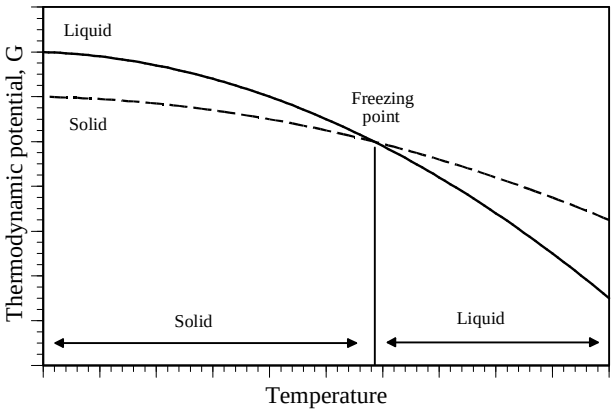

Figure 2.1: The variation of thermodynamic potential with temperature for the solid and liquid phases.

At the freezing point, T_f, the thermodynamic potentials of the solid and liquid phases are equal, that is

$$H_S - T_f S_S = H_L - T_f S_L\,, \tag{2.9}$$

so that the increase in enthalpy due to the enthalpy of fusion $\Delta H_{\mathrm{f}} = H_{\mathrm{L}} - H_{\mathrm{S}}$ in the liquid is exactly offset by an increase in the entropy $\Delta S_{\mathrm{f}} = S_{\mathrm{L}} - S_{\mathrm{S}}$:

$$\Delta S_{\mathrm{f}} = \frac{\Delta H_{\mathrm{f}}}{T_{\mathrm{f}}}. \tag{2.10}$$

Impurity effects

When two substances are mixed together, the total volume available to atoms or molecules of both substances is increased, which increases the number of available microscopic states (i.e., the entropy). The presence of impurities in a fixed-point substance therefore alters the entropy of the two phases and the temperature at which the thermodynamic potentials of the solid and liquid phases are the same.

The increase in the entropy due to dilution by an impurity, in either phase, is

$$\Delta S = -R\left(X \ln X + X_{\mathrm{imp}} \ln X_{\mathrm{imp}}\right), \tag{2.11}$$

where X is the mole fraction of the fixed-point substance, X_{imp} is the mole fraction of the impurity, and R is the gas constant. The first term is the increase in entropy due to the dilution of the fixed-point substance (note $X < 1$, so the entropy is increased), and the second term is due to the dilution of the impurity. In a typical fixed point, the concentration of the impurity is very low and the second term of (2.11) can be neglected. This means that the increase in the entropy depends only on the mole fraction of the fixed-point substance. That is, the chemical properties of the impurities have no direct impact on the fixed-point temperature: all that matters is the degree of dilution they cause in the fixed-point substance[2]. Additionally, because X is very close to 1, the expression for the entropy increase (2.11) can be simplified further, i.e., $RX \ln X \approx R\ln(1 - X_{\mathrm{imp}}) \approx -RX_{\mathrm{imp}}$.

The freezing temperature with the impurity, $T_{\mathrm{f,imp}}$, can now be determined by equating the thermodynamic potentials with the increased entropy included for both the solid and liquid phases:

$$H_{\mathrm{S}} - T_{\mathrm{f,imp}}\left(S_{\mathrm{S}} + RX_{\mathrm{imp,S}}\right) = H_{\mathrm{L}} - T_{\mathrm{f,imp}}\left(S_{\mathrm{L}} + RX_{\mathrm{imp,L}}\right), \tag{2.12}$$

and hence, so long as the temperature change is small and the enthalpy of fusion (2.10) is the same in the presence of impurities (which is true for sufficiently low impurity concentrations and negligible temperature change), then

$$T_{\mathrm{f,imp}} = T_{\mathrm{f}} + K_{\mathrm{f}}\left(X_{\mathrm{imp,S}} - X_{\mathrm{imp,L}}\right), \tag{2.13}$$

where $K_{\mathrm{f}} = RT_{\mathrm{f}}^2 / \Delta H_{\mathrm{f}}$ is called the cryoscopic constant (Note: the constant $A = 1/K_{\mathrm{f}}$ is occasionally used and also called the cryoscopic constant). Equation (2.13) is one of many variations of Van't Hoff's relation. The values of K_{f} for all of the ITS-90 fixed points are given in Appendix B.

One important consequence of (2.13) is that impurities can both raise and lower freezing points. This can also be seen in Figure 2.1, where increased entropy for either of the two phases will lower the respective curves. Thus, dilution of the liquid phase causes the freezing point to be depressed, and dilution of the solid phase causes the freezing point to be elevated.

Equation (2.13) can be expressed in terms of the mole fraction of the impurity in the liquid phase:

$$T_{\mathrm{f,i}} = T_{\mathrm{f}} + K_{\mathrm{f}}(k_0 - 1)X_{\mathrm{imp,L}} = T_{\mathrm{f}} + m_{\mathrm{L}} X_{\mathrm{imp,L}}, \tag{2.14}$$

or in terms of the mole fraction of the impurity in the solid phase

$$T_{\mathrm{f,i}} = T_{\mathrm{f}} + K_{\mathrm{f}} \frac{(k_0 - 1)}{k_0} X_{\mathrm{imp,S}} = T_{\mathrm{f}} + m_{\mathrm{S}} X_{\mathrm{imp,S}}, \tag{2.15}$$

where $k_0 = X_{\mathrm{imp,S}} / X_{\mathrm{imp,L}}$ is called the equilibrium distribution coefficient for the impurity (also called the segregation coefficient or partition coefficient, and fractionation coefficient when applied to isotopic impurities).

[2] Freezing-point depression, boiling-point elevation, and osmosis are phenomena that depend only on the numbers of atoms or molecules, and are described as colligative properties. Van't Hoff received the first Nobel Prize awarded for Chemistry in 1901 for the explanation of the effects.

The parameters m_S and m_L, the slopes of the two lines, are the sensitivity coefficients giving the change in the freezing temperature with impurity concentration.

In fixed points, the observed behaviour with a single impurity in low concentrations is described by one of the two simple binary phase diagrams shown in Figure 2.2 (Prince 1966, Sloan and McGhie 1988). The figures plot the liquidus temperature (onset of freezing with cooling) and solidus temperature (onset of melting with heating) versus impurity concentration. At sufficiently low concentrations, the liquidus and the solidus are linear and described by the expressions (2.14) and (2.15) respectively. Since the two expressions are different parameterisations of the same relation, they can be equated, and hence, the ratio of the slopes is also given by the distribution coefficient, $k_0 = m_L/m_S = X_{imp,S}/X_{imp,L}$. Note too that the slopes are constrained by the relation $1/m_S - 1/m_L = 1/K_f$, independent of the solubility of the impurity in either phase. (These results are true only at sufficiently low concentrations where the solidus and liquidus are straight lines, it not true generally.)

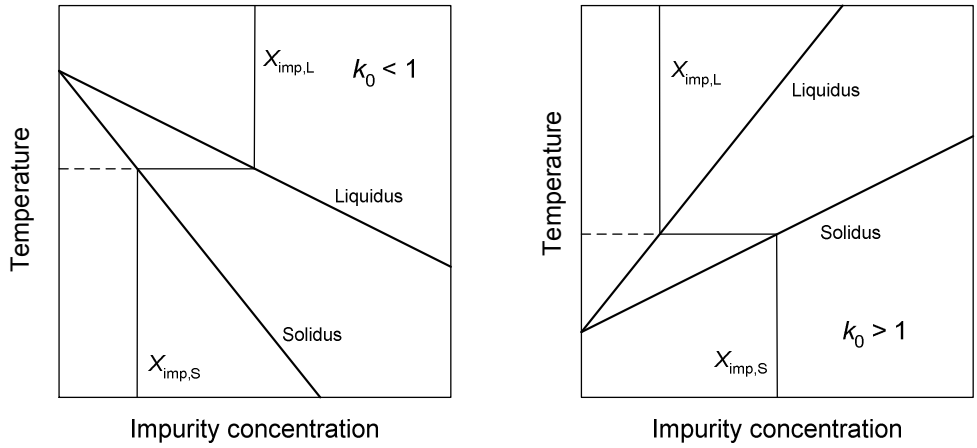

Figure 2.2: Simplified schematic representation of the binary phase diagrams for impurities at low concentrations. At temperatures above the liquidus, all of the material is liquid, below the solidus, all of the material is solid, and between the solidus and liquidus, solid and liquid coexist at equilibrium.

Segregation during freezing

Consider a fixed point, in a molten state with an impurity of concentration $X_{imp.L}$, and subject to slow cooling. As it cools, the temperature eventually falls to the liquidus temperature and a small amount of solid forms. Under equilibrium conditions (chemical and thermal), the liquidus and solidus temperatures (as indicated by the horizontal lines in Figure 2.2) must be the same. This can be true only if the ratio of the impurity concentrations in the solid and liquid is equal to the distribution coefficient. Consequently, as a freeze progresses, solid will form with a different impurity concentration to that in the liquid. This segregation of impurities between the solid and liquid phases causes the concentration of the impurities in the remnant liquid to increase ($k_0 < 1$) or decrease ($k_0 > 1$), which in turn causes the liquidus temperature for the remnant liquid to change. If the impurities are distributed uniformly in the remnant liquid, and there is no diffusion within the solid, then the liquidus temperature of the remnant liquid changes with the liquid fraction of the substance, F, ($0 < F < 1.0$):

$$T_{f,imp}(F) \approx T_f + K_f X_{imp,L}(k_0 - 1)F^{k_0 - 1}, \tag{2.16}$$

where $X_{imp,L}$ is the initial concentration of the impurity (when it is uniformly distributed through the molten fixed-point substance). The factor $(k_0 - 1)F^{k_0 - 1}$ is plotted in Figure 2.3 for several values of k_0 to show the effects of impurities with different k_0 values on the shape of the freezing curve.

While there is a continuous range of possible k_0 values from 0 to very large values, there are two distinct families of freezing-point behaviour. The most common case is for impurities with $k_0 < 1$ (i.e., the impurity is less soluble in the solid), so the impurities cause a freezing-point depression. A special case is $k_0 = 0$, where the impurity is completely insoluble in the solid. Equation (2.16) then simplifies to Raoult's law for freezing-point depression and the observed fixed-point temperature changes with liquid fraction according to

$$T_{f,imp}(F) = T_f - K_f X_{imp,L}\frac{1}{F}. \tag{2.17}$$

For systems with impurities with $k_0 = 0$, plots of temperature versus $1/F$ provide a direct measure of the impurity concentration (see Figure 2.3(b)), and extrapolations to $1/F = 0$ can be used to determine T_f. In practice, few impurities have $k_0 = 0$ exactly, and it is extremely unlikely that a fixed point will have only impurities with $k_0 = 0$, so (2.17) is at best approximate for most fixed points and quite misleading for others. If (2.17) is fitted to the observed freezing curve for a fixed-point with many different impurities with different k_0 values, the fit tends to confuse temperature elevation and depression because impurities with distribution coefficients of k_0 and $1/k_0$ yield freezing curves with similar slopes (compare the curves in Figure 2.3 for $k_0 = 0.5$ and $k_0 = 2$). The fits also underestimate the temperature depression in samples with significant concentrations of impurities with k_0 values in the range 0.1 to 1 (Fellmuth *et al*. 2003a, Fellmuth and Hill 2006).

The second regime of Figure 2.3 is for impurities with $k_0 > 1$, in which case the observed temperature is always elevated. Note the asymmetry in the curves of Figure 2.3(a); impurities with low values of k_0 have the greatest effect at the end of the freezing curves, while impurities with large k_0 values have the greatest effect at the beginning of the freezing curve.

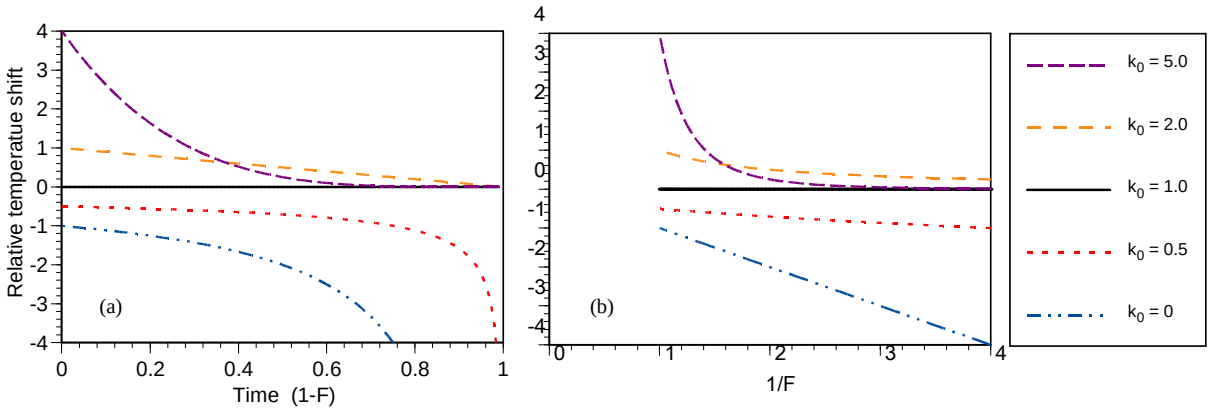

Figure 2.3: Idealised freezing curves for fixed points with impurities with different distribution coefficients according to the factor $(k_0 - 1)F^{k_0 - 1}$ of Equation (2.16): (a) plotted against the frozen fraction $1 - F$ (approximately proportional to elapsed time), (b) plotted against $1/F$ (linear in the case for $k_0 = 0$).

Non-equilibrium effects

The discussion of segregation effects described above assumes that impurities are uniformly distributed throughout the liquid as it freezes. In practice, several non-equilibrium effects affect the distribution of impurities. These include diffusion effects, convection, the non-uniform advancement of the interface due to the formation of particular crystalline structures (Sloan and McGhie 1988), and the fact that freezing points are often realised with two solid-liquid interfaces. Diffusion effects are particularly significant. As freezing progresses the impurities rejected from the solid ($k_0 < 1$) build up in front of the solid-liquid interface, and only slowly diffuse throughout the remaining liquid. For $k_0 > 1$, the analogous effect occurs with a depleted region in front of the interface. In either case, when the freeze happens very quickly relative to diffusion rates, no segregation is observed, and the entire sample freezes at one temperature. Thus, the effect of rapid freezing is to prevent segregation. For a planar solid-liquid interface in an infinite liquid, the effective distribution coefficient is (Burton *et al*. 1953)

$$k_{\text{eff}} = \frac{k_0}{k_0 + (1 - k_0)\exp\left(-V\delta/D\right)}, \tag{2.18}$$

where V is the interface velocity, δ is the $1/e$ thickness of the liquid layer in front of the interface where the impurity has become enriched or depleted, and D is the diffusion coefficient for the impurity. Note that k_{eff} approaches 1.0 as the interface velocity increases. If freezing rates approach or exceed the diffusion rates, freezing curves become flatter according to the value of k_{eff} (suggesting high purity), while the temperature is still elevated or depressed according to the value of k_0.

This effect places limitations on fixed-point realisation techniques. For example, limitations in the thermal conductivity of materials make it practically impossible to freeze fixed points sufficiently quickly to prevent segregation (Jimeno-Largo *et al*. 2005). On the other hand, the time taken for some impurities to fully diffuse and equilibrate over distances of many millimetres in the liquid phase may be many tens of hours. Consequently, the shape and temperature range of freezing curve can depart significantly from the equilibrium curves shown in Figure 2.3.

Complications with diffusion effects, multiple impurities of different k_0 values acting together, and thermal effects arising from non-uniformity of the furnace or cryostat temperature, make it practically impossible to relate the observed broadening of the freezing range to impurity concentrations or to infer good quantitative estimates of the temperature depression or elevation. Consequently, the only point on a freezing curve amenable to modelling (from which the fixed-point temperature is determined) is the liquidus point: the point at which freezing first commences.

Melting points

The discussions above apply directly if the fixed point is a freezing point. In practice, the gallium point and the cryogenic points are realised as melting points. Ideally, the melting curve reflects (almost literally) the freeze that precedes the melt. Suppose, for example, a substance containing impurities with $k_0 < 1$ is initially frozen slowly to produce a freezing curve similar to the lower curves of Figure 2.3 (a). When the same fixed-point cell is heated, the first volumes of the fixed-point substance to melt are those with the highest impurity concentration (lowest solidus temperature), and the temperature rises gradually as the purer volumes of the substance melt. If the temperature across the fixed-point cell is uniform for both the freezing and melting processes, and the melt and freeze heating rates are constant (not necessarily the same) and both rates are slow enough to allow complete diffusion of the impurities in the liquid phase, then the observed melting curve will be a time-reversed version of the freezing curve. Seldom are all of these conditions met.

If the melt follows a fast freeze where very little segregation occurs, then the resulting melting curve will also be flat, although there will be differences between melt and freeze due to non-equilibrium effects. In practice, the finite impurity-diffusion rates mean that non-equilibrium effects are nearly always apparent in the differences between the melting and freezing curves. Note that the liquidus point for a fixed point realised as a melting point is where the melt is complete.

Validity of the model

Van't Hoff's relation is a very good approximation for all systems in equilibrium at given sufficiently low concentrations of impurities. However, the range of validity of the relation is difficult to predict. At the low concentrations typical of fixed-point substances, and in the absence of nearby phase transitions (e.g., due to the formation of other compounds at very low concentration), the equation is expected to be valid.

The effect of nearby phase transitions can be to introduce strong curvature into the solidus and liquidus in the binary phase diagram. In these cases, the linear equations for the solidus and liquidus (2.14) and (2.15) may be accurate only at impracticably low impurity levels. Systems with phase transformations at impurity concentrations below 1% are quite common and are called "zero-percent" systems because they occur very close to the 0% axis on 0%-100% phase diagrams. It is not known how many such systems have phase transformations at concentration below, say, 0.001%. Connolly and McAllan (1980) report an example of iron as an impurity in tin, which forms a Sn-$SnFe_2$ eutectic at an iron concentration of 0.0011% (atomic). Although the eutectic temperature is 8.1 mK below the freezing point of pure tin, for iron concentrations of less than 0.0011% the freezing range never exceeds 1 mK. In the extreme case, a sample of impure tin with the eutectic composition will give rise to a perfectly flat freezing curve 8.1 mK below the true freezing point. That is, phase transitions at very low concentrations can result in large changes in the liquidus temperature that are not betrayed by large slopes in the freezing or melting curves. This means a flat freezing or melting curve is a necessary but not sufficient indicator of purity Connolly and McAllan (1980) identified over 70 zero-percent systems amongst metals used as fixed points.

Impurities giving rise to phase transformations at low concentrations are difficult for several reasons. Firstly, as illustrated by the iron-tin example, they can give rise to relatively flat freezing curves (suggesting high purity) while causing large changes in the fixed-point temperature. Secondly, the relevant (low-concentration) liquidus slopes are very different from those at the higher concentrations usually reported in phase diagrams. Thirdly, the solidus and liquidus slopes may be linear only for a very narrow range of measurable impurity concentrations, making the slopes difficult to measure. Finally, if the impurity concentration is outside the linear region, then it is difficult to apply corrections.

Corrections and uncertainties for liquidus temperatures: the SIE Method

Because the effects of the impurities depend only on the total numbers of impurity atoms in the solid and liquid phases, Van't Hoff's relation (2.13) can be rewritten,

$$T_{\mathrm{f,imp}} - T_{\mathrm{f}} = K_{\mathrm{f}} \sum_i \left(X_{i,\mathrm{S}} - X_{i,\mathrm{L}} \right) \tag{2.19}$$

where the index *i* ranges over all of the different impurities in the substance. This can be rewritten as

$$\Delta T_{\text{imp}} = T_{\text{f}} - T_{\text{f,imp}} = -K_{\text{f}} \sum_i (k_{0,i} - 1) X_{i,\text{L}} = -\sum_i m_{i,\text{L}} X_{i,\text{L}} \,, \tag{2.20}$$

where $m_{i,\text{L}}$ is the liquidus slope for each impurity (see (2.14)). That is, an overall correction for impurities can be made by *summing the individual estimates* (SIE) of the corrections for each impurity. The uncertainty in the impurity correction, due to propagated uncertainties in the various parameters, is:

$$u^2\left(\Delta T_{\text{imp}}\right) = \sum_i \left[u^2(X_{i,\text{L}}) m_{i,\text{L}}^2 + u^2(m_{i,\text{L}}) X_{i,\text{L}}^2 \right]. \tag{2.21}$$

While the SIE method can be applied to the cryogenic fixed points (see Section 4), it is not yet fully realisable for any of the metal fixed points. The method requires knowledge of all of the liquidus slopes for the various impurities and complete data is not yet available for any of the metal fixed points.

Many of the liquidus slopes can be derived from published binary phase diagrams, e.g., Massalski *et al*. (1990), Baker *et al*. (1992), Villars *et al*. (1995), but usually the diagrams do not have sufficient resolution to calculate the liquidus slopes for zero-percent systems. Computer programs for thermodynamic calculations are also capable of computing phase diagrams using databases of the thermodynamic properties of the materials (Eriksson and Hack 1990, Jansson *et al*. 1993). The cryogenic fixed points have relatively few impurities that affect the liquidus point and most of the liquidus slopes are well known (see Section 4.1). At present the most complete table for the metal fixed points is for tin (Fellmuth and Hill 2006). Research continues to complete the tables of the liquidus slopes for the other combinations of fixed-point substances and impurities. Ripple *et al* (2008) list the impurities commonly found in the metal fixed points.

The chemical analyses are also a limitation for the SIE method. Some combinations of elements and impurities remain difficult to analyse, so the uncertainties in the concentrations can be unacceptably large. In addition, the uncertainty estimates for chemical analyses may not be expressed in a manner consistent with the ISO uncertainty guide. Until recently, the common practice in chemical testing was to use the repeatability or reproducibility of measurements, commonly expressed as the limits of detection, as the basis for the uncertainty assessment. This may still be the practice in many laboratories. Such assessments often omit other significant sources of uncertainty including sampling effects, segregation effects within a sample, contamination of the analysis equipment, and calibration effects. Thus, uncertainties in chemical analyses may be larger than reported, and the magnitude of $u(X_{i,\text{L}})$ may be comparable to $X_{i,\text{L}}$ itself. Where the uncertainty of the impurity concentrations is large compared to other uncertainties, it is important to compute the degrees of freedom associated with the standard uncertainty (2.21) to ensure that the expanded uncertainty can be properly computed.

Pavese (2009) reviews the available information for making SIE assessments for the cryogenic fixed points (see Section 4.1). Fellmuth and Hill (2006) present the example of an SIE analysis applied to tin. They also discuss and demonstrate the limitations of thermal analysis in the assessment of impurity effects, and compare the SIE method to other methods. See Widiatmo *et al*. (2006), and Renaot *et al* (2008b) for similar studies on aluminium, Yamazawa *et al* (2007b) on tin, and Widiatmo (2008) on silver.

Corrections and uncertainties for liquidus temperatures: the OME Method

In the absence of detailed information on the liquidus slopes and concentrations of individual impurities, estimates of corrections and uncertainty can be based on an *overall maximum estimate* (OME) of impurity concentration.

The manufacture of high-purity metals by zone refining relies on the segregation of impurities that occurs on freezing. Thus, impurities with extreme values of distribution coefficient are preferentially removed. Given this observation, we assume that the liquidus temperature change for most remnant impurities lies in the range

$$\left| T_{\text{liq}} - T_{\text{pure}} \right| < \Delta T_{\text{OME, max}} = K_{\text{f}} X_{\text{tot,L}} \,. \tag{2.22}$$

where $X_{\text{tot,L}} = \sum_i X_{i,\text{L}}$ is the sum of all of the impurity mole-fractions. See Appendix B for the values of K_{f} for all fixed-point substances.

Empirically it is observed that most impurities have $k_0 < 1$, and cause the freezing point to be depressed. However, most fixed-point substances have some impurities with $k_0 > 1$ (exceptions are hydrogen and neon), and these impurities tend to have a much greater effect at the liquidus temperature (see Figure 2.3). Therefore, in the absence of additional information it is assumed that the correction is zero. If it is assumed that any liquidus temperature in the range (2.22) is equally likely, then the uncertainty in the liquidus temperature is given by

$$u\left(\Delta T_{\mathrm{OME}}\right) = \frac{\Delta T_{\mathrm{OME,\,max}}}{\sqrt{3}} = \frac{K_{\mathrm{f}} X_{\mathrm{tot,L}}}{\sqrt{3}} \,. \tag{2.23}$$

Where supplier assays are incomplete, i.e., lacking uncertainties or detection limits, or the list of detected elements is incomplete, often no further claim can be made beyond the nominal purity (e.g., 99.9999% by weight, metallic elements only). Note that purities derived via the expression 1 – Σ(detected impurities) are unsupportable because manufacturer assays may indicate little more than "no impurities detected".

The SIE method generally yields smaller uncertainties than the OME method. Note again, that zero bias is assumed and no correction is applied for the OME method.

Corrections and uncertainties for liquidus temperatures: The Hybrid SIE-OME Method

Although the tables for the liquidus slopes for the metal fixed points are incomplete, there is useful data for many of the fixed points. It is therefore possible to combine the SIE method for the impurities with known liquidus slopes and the OME method for the remaining impurities.

Validation

Whatever method is chosen for assessing the uncertainty due to impurities, corroborating experimental evidence for the uncertainty assessment should be sought. This is particularly so if the chemical analyses are for samples taken prior to assembly of the cell; the cell material and assembly process are significant sources of impurities, especially for the high-temperature fixed points (Widiatmo *et al*. 2005, 2006).

Corroborating evidence in support of an impurity assessment can be found from the analysis and comparison of melting and freezing curves. In most cases, the flatter the curve, the more pure the fixed-point substance, and the closer the measured fixed point is to the correct temperature. Note that a flat freezing or melting curve does not prove the substance is pure; phase transitions at low concentrations can also give rise to flattened curves. The observed curve shapes should at least be consistent with the known impurity concentration. Extrapolation of the freeze plateaus to the liquidus point using a function of F or $1/F$ (Strouse 2003b), and plots of liquidus point versus freezing rate (Widiatmo *et al*. 2005, 2006, 2008, Yamazawa *et al*. 2007b) all provide a qualitative indication of impurity levels. It should be kept in mind that the impurities are not normally uniformly distributed in metal fixed points unless the cell is held in the molten state for several tens of hours. Additionally, a melt following a very fast (quench) freeze generally leads to a more homogeneous sample with a narrow melt range, whereas a melt following a slow freeze, which allows significant impurity segregation, will have a larger melt range (Strouse 2005, Fellmuth and Hill 2006). Non-equilibrium diffusion effects, effects due to non-uniformities in the furnace or cryostat temperature, or the formation of breaches in solid-liquid interfaces, all complicate the interpretation of freezing and melting curves.

Ultimately, comparison amongst different cells provides the strongest supporting evidence for the purity of a fixed point. When using comparisons of different cells (Mangum *et al.* 1999b, Strouse 2003b), the cells should be manufactured from different sources of fixed-point substances, and preferably made using different procedures (Widiatmo *et al*. 2005). Comparisons performed in the same laboratory using the same equipment are more sensitive to temperature differences because other influence effects will be similar and highly correlated. Further information on the identification of the liquidus point can be found in Section 4 (cryogenic fixed points) and Section 5 (metal fixed points).

2.4 *Isotopic effects*

For an isotopic effect to be manifest in a fixed point, the fixed-point substance must exist as two or more stable isotopes (or isototopologues in the case of molecules such as water). Variations in the isotopic composition, either due to variation in the natural abundances or due to fractionation during purification, lead to small variations in the fixed-point temperatures.

Isotopic effects arise because heavier isotopes have lower vibrational frequencies associated with bonding in the solid and therefore lower-energy states in the solid. This means the lowest energy state for a partially molten system at equilibrium has a slight excess of the heavier isotope in the solid. The solid-liquid fractionation of dilute isotopes leads to a temperature dependence on the isotopic composition of the same form as dilute impurity effects as described by Van't Hoff's relation (2.13).

The concentrations of stable isotopes are normally expressed in terms of 'delta values' and measured with respect to the composition of a standard reference material:

$$\delta_{\mathrm{sample}} = \frac{R_{\mathrm{sample}}}{R_{\mathrm{ref}}} - 1 \,, \tag{2.24}$$

where R is an isotope ratio (e.g., $[^{18}O]/[^{16}O]$ or $[^{2}H]/[^{1}H]$). The delta values are normally expressed in permil (parts per thousand) which has the symbol ‰. Care should be taken to distinguish isotope ratio R and mole fraction X. For example, $R_D = [^{2}H]/[^{1}H]$ while $X_D = [^{2}H]/([^{2}H]+[^{1}H])$. This distinction is especially important where a substance has two or more stable isotopes with a significant abundance (e.g., neon).

The fractionation factor is the ratio of the concentrations of a specific isotope in two different phases. The solid-liquid fractionation factor

$$\alpha_{s\text{-}l} = \frac{R_{solid}}{R_{liquid}} = \frac{1+\delta_{solid}}{1+\delta_{liquid}}, \tag{2.25}$$

is equivalent to the distribution factor k_0 for impurities, as described in Section 2.3. With the exception of deuterium in the equilibrium-hydrogen point, fractionation factors for the fixed points are always close to 1.0. For example, the solid-liquid fractionation factors for water are $\alpha_{s\text{-}l}(^{18}O) \approx 1.003$ and $\alpha_{s\text{-}l}(^{2}H) \approx 1.02$ (Nicholas *et al* 1997). Because of the large relative differences in the atomic masses of ^{1}H and ^{2}H, the fractionation factor for ^{2}H at the hydrogen point is about 4 (Fellmuth *et al* 2005b).

The effect of different isotopic compositions on fixed-point temperatures has been determined empirically only for the hydrogen, neon, and water triple points (see Sections 3.3 and 4.2). A minor problem with these points is that the isotopic composition of the substances used in the measurements that formed the basis of ITS-90 is not known. Hence, comparisons of modern and historical measurements are subject to uncertainty due to the unknown differences in isotopic composition.

Of the remaining ITS-90 fixed points, only aluminium does not have an isotopic effect because it exists as a single stable isotope. However, effects attributable to isotopic composition in the other fixed points have not been detected. In almost all cases, the magnitudes of the effects are thought to be much smaller than impurity effects, and probably difficult to distinguish from impurity effects.

For substances with dilute fractions of isotopes, Van't Hoff's relation, (2.13), with the fractionation factor $\alpha_{s\text{-}l}$ replacing k_0, and the range of isotope mole fractions replacing $X_{imp,L}$, will give the magnitude of expected temperature variations. While some information is available for the variations in isotopic abundances for many of the fixed-point substances, the fractionation factors are not known. An important theoretical contribution to the fractionation factor for a pair of isotopes is the factor $(M_1 - M_2)/M_1M_2$, where M_1 and M_2 are the atomic masses of two different isotopes (Tew 2008). The effects should therefore fall very quickly with increasing atomic mass (and therefore, very approximately, with increasing fixed-point temperature). The second major contribution to the fractionation factor is a term in T^{-2}, which would suggest that the effects fall very quickly with temperature. However, this temperature dependence is exactly compensated by the T^2 dependence in (2.13).

3. Water Triple Point

The triple point of water is the thermodynamic state in which the solid, liquid and vapour phases of water coexist in thermal equilibrium. The SI definition of the kelvin (BIPM 2005) further requires the water to have the isotopic composition:

0.000 155 76 mol ^{2}H per mol ^{1}H,
0.000 379 9 mol ^{17}O per mol ^{16}O, and
0.002 005 2 mol ^{18}O per mol ^{16}O.

This is the isotopic composition of Vienna-Standard Mean Ocean Water (V-SMOW), a standard reference material distributed by International Atomic Energy Agency. Guidelines on the realisation of the water triple point can be found in BIPM (1990), Mangum *et al*. (2000a), and ASTM (2002).

The major effects giving rise to uncertainty in the water triple point are hydrostatic pressure (Section 2.2), impurities (Section 2.3), isotopic composition (Section 2.4), and strain and crystal size effects. Most of the effects depress the temperature and, therefore, amongst a comparison of many cells, the cell realising the highest temperature will usually be closest to the definition.

3.1 *Residual gas pressure*

Further to Section 2.1, the pressure above the surface of the water in the cell is ideally due to the vapour pressure of the water only. In practice, there is usually some residual gas pressure arising from incomplete degassing of the water during manufacture of the cell. The pressure correction can be estimated using the bubble-compression test (White 2004):

$$\Delta T_p = \left(\frac{dT}{dh}\right) h \left(\frac{V_\mathrm{f}}{V_\mathrm{i} - V_\mathrm{f}}\right), \tag{3.1}$$

where V_i is the initial volume of a bubble, trapped in the seal-off tube or McLeod-gage extension on the cell, and V_f is the final volume of the same bubble compressed under a known head of water, h, within the cell. For most cells in good condition, the correction is below 1 μK and therefore negligible. In poor cells, the effect may be several tens of microkelvin. Ideally, poor cells should be avoided for high-accuracy work so that the correction and uncertainty are always negligible. If the application of a correction is unavoidable, the relative uncertainty in the correction can be calculated as

$$\frac{u^2\left(\Delta T_p\right)}{\Delta T_p^2} \approx \frac{u^2(h)}{h^2} + \frac{V_\mathrm{i}^2}{\left(V_\mathrm{i} - V_\mathrm{f}\right)^2}\left(\frac{u^2(V_\mathrm{i})}{V_\mathrm{i}^2} + \frac{u^2(V_\mathrm{f})}{V_\mathrm{f}^2}\right). \tag{3.2}$$

The uncertainty is dominated by uncertainties in the volumes, which are affected by ambient temperature, the internal dimensions of the seal-off tube or McLeod gage, and the effects of surface tension on the bubble. The contribution of the uncertainty in the hydrostatic coefficient is negligible and omitted from (3.2).

3.2 *Impurities*

Impurities in the water of triple-point cells give rise to the most significant source of uncertainty and the most difficult effect to assess. Many of the impurities likely to affect the triple-point have a distribution coefficient $k_0 = 0$ and, therefore, depress the temperature by approximately 1.86 K.mol^{-1}.kg^{-1} or, equivalently, 103 μK for each part per million (mole fraction) of impurity (see Section 2.3). Recent water-triple-point comparisons, (e.g., Renaot *et al*. 2005, Stock and Solve 2006) exhibit results dispersed over ranges exceeding 200 μK, much of which is due to impurities. There are four main sources of impurity.

Chemicals used in the preparation of the water or the glass cells may be a source of contamination during the manufacture of the cell. These may include HF, HCl, and NH_4F, which are soluble in ice; i.e., $k_0 \neq 0$ (see Section 2.3). Most of these materials have a high dissociation constant, so are detectable from measurements of electrical conductivity (see Ballico (1999) for the method). With appropriate care in the manufacture (Zief and Speights 1972), the contribution of impurities in the source water can be kept very low.

Borosilicate glass, from which most cells and their manufacturing plant are made, is weakly soluble in water resulting in a temperature depression at the time of manufacture and additional drift with time. With high quality cells, actual depressions at the time of manufacture can be as low as a few microkelvin (Strouse and Zhao 2007, Tavener and Davies 2007), but depressions of up to −100 μK can be also be inferred from comparisons of some new cells where isotope corrections have been made. The drift rates range up to −20 μK/yr with a mean

rate of −4 μK/yr, although the variation between cells is very large (Hill 2001). With borosilicate cells, the drift rate is likely to increase with time and is very dependent on the treatment of the glass prior to the manufacture of the cells (White *et al*. 2005b). Storage of the cells near 0 ºC and manufacture of the cells from fused silica both reduce the drift rate (Zief and Speights 1972, Strouse and Zhao 2007). The use of fused silica cells may, depending on manufacturing process, result in a higher level of particulate impurities and a higher initial impurity level due to the higher temperature required to melt pure silica and seal the cell.

The other main source of impurity is low-volatility compounds in the source water. For example, light hydrocarbons have a similar boiling point to water so distillation may not remove them. The typical magnitude of this impurity effect is unknown, but anecdotal evidence suggests that cells subjected to a prolonged degassing during manufacture (approx. 2 days) can be 20 μK higher than other cells, after isotope corrections have been applied.

Some impurity is due to the solubility of the residual gas in the cell. However, since one quarter of the difference between the temperature of the ice point and the triple point of water is due to dissolved gasses (Ancsin 1982), it can be inferred that any impurity effect due to dissolved gasses is smaller than the residual-gas-pressure effect, which is usually negligible.

Because the most likely impurities are insoluble in ice and are rejected during the formation of the ice mantle, Raoult's law is applicable. This means that (2.17), giving the expected temperature depression versus melted fraction, allows the determination of the impurity level and temperature depression from measurements of temperature versus frozen fraction (Mendez-Lango 2002). The measurements take ~1 month and achieve uncertainties of the order of 30 μK.

When the first ice-water interface is formed around the thermometer well, the water so formed is purer than the main body of water. Measuring the temperature realised by the cell in this state and again after the cell has been (gently) inverted several times to mix the inner melt with the main body of water, may give an indication of the impurity level (ASTM 2002). This test must be carried out with the first formation of the ice-water interface and measurements must be corrected for self-heating. A similar effect occurs with extended use of a cell over a week or longer. The waters around the well and the main body appear to mix slowly causing a gradual depression of the observed temperature with time (see Stock and Solve (2006) for examples).

The main impurities in cells are usually the salts of the compounds used in the glass, some of which dissolve and ionise in water. The concentration of ionic impurities, such as sodium hydroxide, can be estimated from the measurement of the conductivity of the water, inferred from measurements of cell capacitance versus frequency (Ballico 1999). However, some significant impurities, such as silicic acid, have a low ionisation constant and are not readily detectable by this method. If it is assumed that the impurities are due to the uniform dissolution of borosilicate glass, corrections can be applied (White *et al*. 2005b). However, because leaching contributes to the dissolution, the dissolution of the glass is generally not uniform. The uncertainty in the corrections is therefore large, perhaps 50% of the correction. The method is of little use for correcting the long-term accumulation of impurities in either borosilicate or fused-silica cells.

Triple-point cells can be made with a flask attached so that the mantle is formed from water distilled from the flask (Stimson 1945, see also Tavener 2002). This ensures that non-volatile impurities do not affect the temperature. The effects of volatile impurities remain and care is required to avoid isotopic fractionation effects of up to 50 μK that may occur due during the distillation (Nicholas *et al*. 1997).

The best uncertainty due to impurities is achieved in recently manufactured high-quality cells and is probably below 10 μK (Nguyen and Ballico 2008, Strouse and Zhao 2007, Tavener and Davies 2007). The dispersion of results in recent international comparisons (Stock and Solve 2006, Renaot *et al* 2005) suggests that a depression and uncertainty due to impurities of about 50 μK is more typical for older cells.

3.3 *Isotopic composition*

Natural fractionation effects ensure that most of the continental surface (fresh) water, from which cells are made, is depleted in the heavy isotope ^{2}H and to a lesser extent ^{18}O and ^{17}O, with a strong dependence on the latitude, altitude, and season at the location of the precipitation (Bowen and Revenaugh 2003). The water may be further depleted or enriched during the distillation and degassing processes in the manufacture of the cells, (Nicholas *et al*. 1997). The combination of effects leads to cells that realise temperatures typically ranging between 10 μK above to 110 μK below the ocean-water definition. If the manufacturing process is not well controlled, or involves multiple distillations, cells can be well outside this range. Because of the dependence on source water and processing, the isotopic depression in cells is highly dependent on the cell manufacturer. Recently, some manufacturers have adapted their manufacturing processes to obtain cells with water close the V-SMOW definition. The best of these cells may have an isotopic composition within ±10 μK of the ideal (Strouse and Zhao 2007, Tavener and Davies 2007).

Ideally, the isotopic composition of the cell water should be measured by taking a sample after the cell has been sealed (Nicholas *et al*. 1997, Strouse and Zhao 2007), and a correction applied (Ripple *et al*. 2005, BIPM 2006):

$$\Delta T_{\text{iso}} = -A_{\text{D}}\delta\text{D} - A_{18\text{O}}\delta^{18}\text{O} - A_{17\text{O}}\delta^{17}\text{O}\,, \tag{3.3}$$

where the A_{D}, $A_{18\text{O}}$, and $A_{17\text{O}}$ are the isotopic-depression constants, and the δD, δ^{18}O, and δ^{17}O are differences in isotopic composition from V-SMOW, according to

$$\delta^{18}\text{O} = \left[\frac{\left({}^{18}\text{O}/{}^{16}\text{O}\right)_{\text{sample}} - \left({}^{18}\text{O}/{}^{16}\text{O}\right)_{\text{V-SMOW}}}{\left({}^{18}\text{O}/{}^{16}\text{O}\right)_{\text{V-SMOW}}}\right], \tag{3.4}$$

and similarly for δD and δ^{17}O. The delta values are usually expressed in permil (‰, per thousand) and are usually negative for most cells. The values of δD and δ^{18}O can be determined with standard uncertainties of about 0.5‰ and 0.05‰ respectively; δ^{17}O is difficult to measure but can be estimated from (Meijer 1998):

$$1 + \delta^{17}\text{O} = \left(1 + \delta^{18}\text{O}\right)^{0.528}, \tag{3.5}$$

which applies to all waters. The uncertainties due to the ^{17}O are usually insignificant in any case.

For meteoric waters (precipitation), where only δD has been determined, values for δ^{18}O can be estimated using

$$\delta\text{D} = 8 \times \delta^{18}\text{O} + 0.01\,, \tag{3.6}$$

which is known as the global meteoric water line (Craig 1961). Strictly, this relation applies only to precipitation and not to sea water or water after it has been processed. However, it works sufficiently well to be useful where the ^{18}O concentration is not measured directly (Peruzzi *et al*. 2007).

The most precise set of values for the isotopic depression constants (3.3) are from Kiyosawa (Kiyosawa 1991, White *et al*. 2003a), who measured the melting-point elevation of samples of water enriched with D and ^{18}O. These values, currently recommended for use with the ITS-90, are A_{D} = 628 μK and $A_{18\text{O}}$ = 641 μK. The value of $A_{17\text{O}}$ is inferred as 57 μK. Kiyosawa relied on the manufacturer's assay of the water, possibly neglecting contamination with the other isotopologues (Tew and White 2005), and did not provide any uncertainty analysis. Therefore, the uncertainties in these values are not well known. The degree of consistency with the measurements of White *et al*. (2003a), and the much earlier measurements of LaMer and Baker (1934), suggest standard uncertainties in A_{D}, $A_{18\text{O}}$, and $A_{17\text{O}}$ of the order of 20 μK, 50 μK, and 5 μK, respectively.

The total uncertainty in the isotope correction is given by

$$\begin{aligned} u^2\left(\Delta T_{\text{iso}}\right) = {} & u^2\left(A_{\text{D}}\right)\left(\delta\text{D}\right)^2 + u^2\left(A_{18\text{O}}\right)\left(\delta^{18}\text{O}\right)^2 + u^2\left(A_{17\text{O}}\right)\left(\delta^{17}\text{O}\right)^2 \\ & + u^2\left(\delta_{\text{D}}\right)A_{\text{D}}^2 + u^2\left(\delta_{18\text{O}}\right)A_{18\text{O}}^2 + u^2\left(\delta_{17\text{O}}\right)A_{17\text{O}}^2. \end{aligned} \tag{3.7}$$

The uncertainty is usually dominated by the uncertainties in δD and A_{D}. For cells no more than 100 μK from V-SMOW, the uncertainties in the corrections are less than 4 μK, so are generally negligible.

Most triple-point cells made from continental fresh water can be expected to be within +10 μK and −110 μK of V-SMOW, so a correction of +50 μK and a standard uncertainty of 35 μK will account for typical variations in isotopic composition where no isotopic information is available. Information on the composition may be available from the manufacturer. Some manufacturers provide isotopic assays of the water, and may provide cells with the assay ampoule still attached.

A further, smaller, isotopic effect occurs with isotopic fractionation between water and ice when the cell is in use (Nicholas *et al*. 1997). In theory (Section 2.3), the effect causes the temperature to be dependent on the frozen faction and ranges from no effect for zero frozen fraction, to about −15 μK for a cell nearly fully frozen. In practice, the freezing rates for cells are sufficiently fast and the isotopic equilibration process is so slow that significant fractionation does not occur during the initial freezing of the mantle ((2.18) and Ferrick *et al*. 2002). Measurements of the composition of the water and ice from partly frozen cells support the theory: cells frozen normally over a period of a few hours exhibit isotopic fractionation of no more than 2 μK (Nicholas *et al*. 1997, Renaot *et al* 2008a). One cell frozen slowly over a few days exhibited fractionation of 7 μK (Tavener 2006). However, additional fractionation occurs with freezing at the ice-water interface around the thermometer well. Detailed understanding of the effect of repeated freezing and melting is not known, but it could be responsible for a depression of a several microkelvin and some of the observed non-repeatability of cells.

3.4 *Strain, crystal defects, and crystal size*

The temperature realised in freshly prepared triple-point cells is low, typically by 0.2 mK in cells where the mantle is frozen slowly and as much as 1 mK for quickly frozen cells (Berry 1959, Furukawa and Bigge 1982, Furukawa *et al*. 1997). The effect is reduced to below 100 μK over 2-3 days as the ice anneals, and after a week, the effects are below 30 μK. To achieve temperature stability and reproducibility at the level of 10 μK or so, it is necessary to allow the mantle to anneal for at least 10 days. While the annealing of strain and crystal defects is probably a factor in this effect, Berry's experiments (1959) (see also McAllan 1982) suggest the major cause is due to the relatively high surface energy of small ice crystals. The combination of interfacial tension and curvature of the surface of the ice produces a pressure-related temperature depression described by the Gibbs-Thomson relation

$$\Delta T = \frac{TM}{\rho L}\gamma_{SL}\left(\frac{1}{r_1}+\frac{1}{r_2}\right), \tag{3.8}$$

where ΔT is the temperature depression, L is the molar latent heat, M is the molar mass, ρ is the density, γ_{SL} is the interfacial tension between water and ice (~ 30 mJ/m^2), and r_1 and r_2 are the two orthogonal radii of curvature of the ice crystal. If the two radii are assumed the same, then the temperature depression is about 0.05 μK.m, so that crystals with a 1 mm radius of curvature would cause the temperature to be depressed by about 50 μK. The gradual annealing and re-growth of crystals from ~ 0.2 mm to ~10 mm that takes place over the first few days therefore explains the ~200 μK rise in temperature.

Because of the range of crystal sizes surrounding the thermometer well, each with different radii of curvature (including one negative radius over most of the surface), the actual temperature of the ice-water interface is variable at the level of a few microkelvin. The effect is probably the cause of repeatable features observed in the immersion profile of a cell.

3.5 *Buoyancy effect*

Because the density of ice is less than that of water, the ice mantle floats and pushes against the end of the thermometer well. The pressure on the ice-water interface at this point causes a reduction in the local temperature. The magnitude of the overall effect depends on the volume of ice frozen, the fraction of ice above the water, the shape of the end of the thermometer well, and the thermal resistance between the thermometer and the thermometer well. The resulting cooling of the thermometer can be as large as 20 μK with long-stem SPRTs and 40 μK with capsule SPRTs (White and Dransfield 2005a, Sakurai 2002). The effect is practically eliminated by placing a small (~10 mm) thermally insulating sponge at the bottom of the well. The effect can be further reduced by using, above the foam, an aluminium or galvanised-brass bushing as a thermal shunt (Furukawa and Bigge 1982, Bojkowski and Batagelj 2007). Care must be taken when using a metal shunt that there is no chemical reaction with the water (or ethanol, if used) in the thermometer well, as this will alter the temperature near the shunt.

3.6 *Thermal effects*

To obtain measurements with a repeatability of 10 μK, the mantle must be free of holes or areas where it adheres to the thermometer well. The propagation of infrared radiation along the thermometer well and stem (originating from incandescent lamps) can also be prevented by using a dark cloth or foil. The absence of stray thermal influences is confirmed by carrying out an immersion profile measurement, which demonstrates that the temperature follows the hydrostatic correction, (2.5) (see also Section 5.1). Self-heating corrections must be made.

4. Cryogenic Fixed Points (e-H_2, Ne, O_2, Ar)

The cryogenic fixed points of ITS-90 are the triple points of equilibrium hydrogen, neon, oxygen and argon, each of naturally occurring isotopic composition. Recently, the definition for *e*-H_2 has been modified to specify more accurately the isotopic composition (Steur *et al*. 2005). A similar clarification is expected for neon. The fixed points can be realized in practice with either open (refillable) or permanently sealed cells.

The cryogenic fixed points differ significantly from the high-temperature fixed points in their very low heat of fusion and the low thermal conductance. For this reason, the cryogenic fixed points are usually realized in adiabatic conditions using the so-called calorimetric method. The triple-point cell is slowly frozen, then thermally isolated and time is allowed for the release of strain and equilibration of temperature within the solid. The solid is then slowly melted by intermittent heating, using a series of heat pulses of known energy, alternating with stabilization periods in which the equilibrium temperature is measured as a function of the fraction, *F*, of the sample melted. The triple-point temperature is then determined by fitting a function of the melted fraction *F* to a selected range of measured equilibrium temperatures. For full details, refer to the *Supplementary Information*. Further information on the realization of the points and material properties of the fixed-point substances can be found in Pavese and Molinar (1992), Fellmuth *et al*. (1999, 2003b), and Wolber and Fellmuth (2008). Further information on the realization of the hydrogen point can be found in Fellmuth *et al*. (2005b).

The argon point may also be used for long-stem SPRTs as well as capsule SPRTs. In this case, it is usually treated in a similar manner to the metal fixed points. However, the poor thermal conductance of the argon leads to a small bias in the measurements due to the background heat flux (see Section 4.7 below) and a corresponding increase in the total uncertainty. For technical details on the apparatus, technique, and typical uncertainties for long-stem SPRTs, see Bloembergen *et al*. (1990), Hermier and Bonnier (1990), Ahmed *et al*. (2003), and Pond (2003).

The major sources of uncertainty in the cryogenic points are impurities, isotopic effects, thermal effects and, potentially, effects related to the resistance measurement (Section 8), typically totalling several tenths of a millikelvin. Note, residual gases in the cryogenic fixed-point cells are treated as impurities; an additional uncertainty term due to residual gas pressure is unnecessary.

4.1 *Impurities*

The impurities in the cryogenic points may arise from several sources, including contamination during the filling procedure, degassing of inner surface of the cell, dissolution of bulk materials of the cell, and the development of leaks in the cell seal with aging. The relative contribution of some of these effects depends on whether the cell is sealed or open. Because of the low temperature of the cryogenic fixed points, all but gaseous impurities are easily removed, and only a small number of impurities need to be considered. The distribution coefficient and the liquidus slopes for most of these impurities are given in Table 4.1 (from Pavese 2009). Because chemical assays are readily available and the liquidus and solidus slopes are known, the SIE method should always be applied.

Note that the OME method could be applied, but the narrow range and mostly negative values of distribution coefficients means that the OME method over estimates the uncertainty, and neglects readily made corrections. Note too that the application of Raoult's law for the assessment of impurities in the cryogenic fixed points is not appropriate. Firstly, as noted in Section 2.3, all of the expected impurities have a distribution coefficient, $k_0 > 0$, and some with $k_0 > 1$. Secondly, the plateau shape is affected by the thermal conductance of the frozen material and background thermal flux, and by isotope fractionation effects, and extrapolation of the plateau to the liquidus point would yield incorrect values for the impurity effects.

4.2 *Isotopic composition*

Isotopic effects are the largest source of uncertainty for the equilibrium-hydrogen and neon points. The normal variations in the isotopic composition of commercial gases, combined with a relatively high sensitivity of temperature to the isotopic composition, gives rise to variations in the hydrogen point spanning about 200 μK, and 400 μK in the neon point (Pavese 2005a). Because argon and oxygen are largely composed of a single isotope (> 99.6% abundance) and the atomic masses are greater, the isotopic effects for these points are probably below 20 μK (Tew 2008).

Table 4.1: The effect on T_f of various gaseous chemical impurities on the indicated pure substances (Pavese 2009[3]). The values are given in terms of the distribution coefficient, k_0, and the liquidus slope, m_L as μK.ppma^{-1} (for gasses equivalent to microkelvin per part-per-million by volume or amount of substance). Symbols: 0 indicates a zero effect, 0? indicates probable zero effect, - indicates effect not known.

Fixed-point substance								
Chemical impurity	***e*-Hydrogen**		**Neon**		**Oxygen**		**Argon**	
	k_0	m_L	k_0	m_L	k_0	m_L	k_0	m_L
He	0.21(14)	–11(2)		0	1.03(1)	1.5(5)		0?
H_2			0.53(20)	–7(3)		-		0
Ne	0.86(4)	–2.0(5)			0.98(1)	–1.0(5)		-
O_2		0		-			0.57(5)	–22(2.5)
N_2		0	0.47(13)	–8(2)	0.60(4)	–22(2.5)	0.52(4)	–24(2)
Ar		0?		0?	1.23(5)	13(2.5)		
CO		-		-		-	0.50(5)	–24(2.5)
F_2		-		-		-	0.80(4)*	–10(2)
CH_4		-		-	0.45(18)	–30(10)	0.42(5)	–28(2.5)
Kr		-		-	0.91(2)	–5(1)	1.11(5)	5(2.5)
Xe		-		-	0.85(4)*	–8(2)	0.88(4)	–6(2)

*** Note:** For F_2 in Ar and Xe in O_2, the reported liquidus slopes and solidus slopes are not consistent with each other (see Equations (2.14) and (2.15) and the text following the equations).

Hydrogen

The isotopic composition of commercially available 'tank' hydrogen varies from about 27 μmol D/mol ^{1}H to about 155 μmol D/mol ^{1}H, where D is deuterium (^{2}H). It has been established (Pavese and Tew (2000), Pavese *et al*. (2002)) that the discrepancies previously found at the e-H_2 triple point are mainly due to the variable deuterium content of the hydrogen used for its realization. The technical annex to the mise en pratique for the kelvin, therefore, specifies (BIPM 2006, Steur *et al*. 2005) that the ITS-90 temperature for the triple point of equilibrium hydrogen, 13.8033 K, is taken to refer to hydrogen with an isotopic ratio the same as that of standard light Antarctic precipitation (SLAP). SLAP and VSMOW (Vienna standard mean ocean water) are two standard reference materials (waters) widely distributed by the International Atomic Energy Agency for the standardization of isotopic analysis (Gonfiantini, 1978, see also Wise and Watters, 2005). The deuterium isotope ratio in SLAP is very close to the mean isotope ratio of commercially available hydrogen. Most hydrogen-isotope measurements are carried out with respect to the two reference materials, and reported as delta values with respect to VSMOW, which has an deuterium isotope ratio, [D]/[^{1}H] = 0.000 155 76. The deuterium isotope ratio in SLAP is defined in terms of deuterium isotope ratio of VSMOW, as (IUPAC 1994)[4]

$$\delta \mathrm{D}_{\mathrm{SLAP}} \equiv -428\ ‰, \tag{4.1}$$

where the symbol ‰ indicates permil (parts per thousand). Note that in molecular form, the isotopic ratio of hydrogen deuteride (HD) is approximately twice the ratio of atomic deuterium.

The isotopic correction for deuterium in the equilibrium-hydrogen triple point is

$$\Delta T_{\mathrm{iso}} = A_{\mathrm{D}}(\delta \mathrm{D}_{\mathrm{SLAP}} - \delta \mathrm{D}) \tag{4.2}$$

[3] Where Pavese reports both the solidus and liquidus slopes, the values of the liquidus slopes and the uncertainties given in Table 4.1 are calculated from the weighted average of the k_0 values, with the values and uncertainties infered from the values for the solidus and liquidus slopes (see Equations (2.14) and (2.15)).

[4] The mise en pratique for the kelvin specifies the composition in terms of the isotope ratio $R_{\mathrm{D,SLAP}}$ = [D]/[^{1}H] = 0.000 089 10. If composition measurements are reported as an isotopic ratio (see Section 2.4), R_{D}, the correction equation is $\Delta T_{\mathrm{iso}} = k_{\mathrm{D}}(R_{\mathrm{D,SLAP}} - R_{\mathrm{D}})$ with the isotope correction constant k_{D} = 5.42(31) μK per μmol D/mol ^{1}H.

where the current best measured value for A_D is 0.844(48) μK/ ‰ (Fellmuth *et al*, 2005b). The uncertainty in the isotope correction is

$$u^2\left(\Delta T_{\text{iso}}\right) = u^2\left(A_D\right)(\delta \text{D}_{\text{SLAP}} - \delta \text{D})^2 + A_D^2 u^2\left(\delta \text{D}\right). \tag{4.3}$$

The propagated uncertainty due to the uncertainty of A_D is less than 20 μK at the two extremes of the observed isotopic compositions. Isotopic analysis of the deuterium fraction may be obtained with standard uncertainties in the range 0.5 ‰ to 10 ‰, so typically contributes less than 8 μK uncertainty to the total.

If no isotopic analysis is available for the hydrogen, then the composition is assumed to lie in a rectangular distribution within ± 410 ‰ of the standard composition (4.1) based on the observed distribution of the composition of commercially available hydrogen. The resulting uncertainty due to the isotopic composition is, therefore, 200 μK.

Isotopic fractionation effects are expected to take place during melting, but no estimate of the magnitude of the effects is presently available.

Neon

Neon occurs naturally as three isotopes, ^{20}Ne, ^{21}Ne, and ^{22}Ne. The isotopic composition of atmospheric neon, which is normally taken to be the 'natural composition', has the isotopes in proportions of 90.48(3)%, 0.27(1)%, and 9.25(3)%, respectively (IUPAC 1997). Note, particularly, the large fraction of ^{22}Ne, which has a triple point temperature about 134 mK higher than that of neon of the natural composition and about 147 mK higher than that of ^{20}Ne (Furukawa 1972).

Recent research on the composition of commercially available neon (Pavese *et al*. 2005b, Pavese *et al* 2008) suggests that most commercial sources are enriched in ^{22}Ne by the equivalent of between 100 μK and 400 μK, with the composition strongly supplier dependent. Natural variations in the ^{21}Ne contribute to variations in the triple-point temperature of less than 5 μK, so are insignificant in comparison to the effect of ^{22}Ne.

In principle, the composition should be measured and corrected to the natural composition. However, at present this is impractical. Very few laboratories can provide accurate assays of the composition, in part because there is no convenient reference material for the calibration of mass spectrometers. There are also unresolved discrepancies between historical measurements (including atmospheric neon) and the more recent (and probably more accurate) measurements (see Pavese *et al* 2008).

For the moment, we adopt a literal interpretation of the definition of uncertainty: that it characterizes the range of values that can reasonably be attributed to the neon point. We assume that the independent samples measured by Pavese *et al*. (2005b) and Pavese *et al* (2008) are drawn from the full distribution of compositions of commercially available neon. We also assume that the neon used to define ITS-90 had a composition in the same range (so that no correction should be applied). The standard uncertainty in a realization of the neon point due to the isotopic composition is, therefore,

$$u_{\text{iso}} = 175\ \mu\text{K}. \tag{4.4}$$

Where expanded uncertainties are being calculated, a small number of effective degrees of freedom ($\nu = 10$) should be used. This recognizes the small number of independent samples of neon used to estimate the range of triple-point temperatures.

4.3 *Isomer equilibration* (e-H_2)

With the hydrogen point there is an additional concern with the composition in respect of the ortho-H_2 and para-H_2 forms, for which the triple points differ by about 148 mK (Pavese and Molinar 1992). At the triple point, the composition will very slowly evolve to towards the equilibrium composition (nearly 100% para-H_2). To reach the equilibrium in a reasonable time requires the addition of spin-conversion catalyst to the fixed-point cell. The approach to equilibrium follows an exponential decay depending on the amount, type, and activity of the catalyst (Fellmuth *et al*. 2005b). The total time for the equilibration process is normally in the range from 1 hour to 1 day. An equilibration period of about 10 time constants is required to ensure equilibration effects are below 10 μK.

4.4 *Strain and crystal defects*

Melting in all materials commences around grain boundaries, crystal defects, surfaces, and some impurity centres. These 'pre-melting' effects contribute to the rounding of the leading edge of the fixed-point plateaus. In particular, the high freezing velocity occurring as the fixed-point substance changes from the supercooled state, introduces large numbers of crystal defects into a large fraction of the sample. The effects of the defects can be minimized by refreezing (slowly) from a partially melted sample so that there are seeds for crystallization and supercooling is prevented (Wolber and Fellmuth 2008). Especially in the case of argon, this procedure reduces the rounding of the leading edge of the plateau.

There are also additional effects, perhaps due to the presence of solid and liquid distributed around the walls of the cell above the main body of the solid. These effects give rise to a non-linear plateau, but can be removed through appropriate heat treatment (Nakano *et al*. 2005a).

In the hydrogen point, the presence of the spin-conversion catalyst leads to a much longer and more pronounced pre-melting phase (Fellmuth *et al*. 2005b). The pre-melting behaviour is caused by the increase in the distortion of the crystal lattice of the hydrogen sample, by increasing the sample fraction in contact with a surface or boundary (Papon *et al*. 2002), or by the confinement of portions of hydrogen in a restricted geometry such as pores (Sakurai 1998, 1999, Nakano *et al*. 2005b). The extent of pre-melting is strongly dependent on the amount and type of catalyst (Steele 2002b, Nakano *et al*. 2003, 2005c). Depending on the amount of catalyst and the geometry of the cell, as much as the first 20% of data for an observed plateau may have to be discarded for the purpose of extrapolation to the liquidus point (see Section 4.7).

4.5 *Static thermal effects*

The fixed-point temperature is realized within the cell at the solid-liquid interface, normally some distance from the SPRT. Because the cryogenic substances have a very poor thermal conductivity, the combination of a background heat flux through the cell and the thermal resistance between the solid-liquid interface and the SPRT leads to a static temperature error. The error is minimized through careful attention to radiation shields and their control systems.

The magnitude of the required correction can be inferred as (Fellmuth *et al*. 1999, Pavese *et al*. 2003)

$$\Delta T_{\mathrm{st}} = -P_{\mathrm{st}} R_{\mathrm{thm}}\,, \tag{4.5}$$

where P_{st} is the background (static) heat flux and R_{thm} is the thermal resistance. The value of the thermal resistance is estimated by applying a small additional heat flux ΔP to the outside of the cell and observing the rise in the plateau temperature as measured by the SPRT:

$$R_{\mathrm{thm}} = \frac{\Delta T}{\Delta P}\,. \tag{4.6}$$

The thermal resistance is strongly dependent on the cell design and is dominated by the poor thermal conductance of the fluid phase and, therefore, on the fraction F of the sample melted. This means that the static error increases approximately linearly as the melted fraction increases. Values of the thermal resistance may vary over the range 0.1 ºC/W to 10 ºC/W with different F and cell design; i.e., orders of magnitude (Fellmuth *et al*. 1999).

If nearly isothermal conditions are realized, the background flux P_{st} can be estimated from the temperature drift $dT/d\tau$ before melting commences and the heat capacity, C, of the entire cell:

$$P_{\mathrm{st}} = C\, dT/d\tau\,, \tag{4.7}$$

where τ is time. The total magnitude of the static error can normally be kept below 30 μK. The uncertainty in the static temperature correction (4.5) is

$$u^2\left(\Delta T_{\mathrm{st}}\right) = u^2\left(P_{\mathrm{st}}\right) R_{\mathrm{thm}}^2 + P_{\mathrm{st}}^2 u^2\left(R_{\mathrm{thm}}\right), \tag{4.8}$$

where the uncertainties in the measurements of the heat flux and thermal resistance are those associated with the measurements (4.6) and (4.7).

4.6 *Dynamic thermal effects*

During the melting, after each heat pulse, a thermal transient is observed with a recovery time dependent on the cell design. An insufficient recovery period causes a dynamic temperature error. Because the temperature equilibration involves heat distributed throughout the cell, the thermal recovery may deviate significantly from a simple exponential law. Nevertheless, it is convenient to adopt a simple first-order model to characterize the minimum period required to attain thermal equilibrium with a time constant (Bonnier and Hermier 1982, Pavese *et al*. 2003)

$$\tau_0 = R_{\mathrm{thm}} C \,. \tag{4.9}$$

where the cell heat capacity C and thermal resistance R_{thm} are as determined in Section 4.5. Because of the differences in the thermal conductivities of solid and liquid, R_{thm} varies throughout the plateau. The minimum necessary recovery period τ_{min} for each pulse can be estimated roughly by the relation:

$$\tau_{\mathrm{min}} = \tau_0 \ln\left(\Delta T_{\mathrm{peak}} / \Delta T_{\mathrm{max}}\right), \tag{4.10}$$

where ΔT_{peak} is the peak overheating observed in response to the heat pulse, and ΔT_{max} is the maximum allowed dynamic temperature measurement error. Recovery times, τ_{min}, of up to 30 minutes (up to several hours in the case of neon) can be expected.

For the highest level of fixed-point realizations, ΔT_{max} should be kept below 20–30 μK. For this level of uncertainty, even longer time constants may come into play (Wolber and Fellmuth 2008). Especially in the case of neon, segregation during freezing may force the heat supplied to flow across the solid to the solid–liquid interface, which may require waiting times of several hours. The decay time of the measured temperature after the pulses have been applied should be measured and, if the calculated waiting times are considered too long, allowances must be made in the uncertainty budget.

4.7 *Determination of the liquidus point*

Because the cryogenic fixed points are realised as melting points, the fixed-point temperature should be determined by extrapolating the melting temperature to the liquidus temperature (at the end of the melt plateau). This may be done by fitting a function $T_{\mathrm{melt}}(F)$ or $T_{\mathrm{melt}}(1/F)$ to the experimental data (Felmuth *et al*. 2005c, Pavese and Molinar 1992), where F is the melted fraction. The fitting should typically be performed over the central part of the melt range, to ensure the liquidus temperature can be determined with the lowest possible uncertainty. For values of F close to 1, the poor thermal conductivity of the liquid causes the melting curves to become sensitive to the thermal surroundings. On the other hand, most physical effects influence the melting temperature at low F values, where the solid phase dominates. These effects include, for example, the influence of crystal defects and pre-melting effects due to the spin-conversion catalyst (for e-H_2 only). Thus, the choice of the F range used for fitting should be considered very carefully after taking into account the properties and behaviour of the specific fixed-point material.

Some care should also be exercised in the choice of the fitting function. The optimum function is usually different for different fixed-point substances and different fixed-point-cell designs. The hydrogen and oxygen points tend to have very flat plateaux over a wide range of F while the argon and neon points are rarely flat and usually require fitting and extrapolation. The choice of function should be guided by selecting a form that minimizes the standard deviation of the experimental data from the fit function and maximizes the repeatability of the liquidus-point temperature. Keep in mind that higher-order functions cause greater amplification of uncertainty with extrapolation.

In some cases, the melting curves may be sufficiently flat that detailed fitting is unnecessary. The value near 50% melted fraction is often an adequate estimate of the liquidus point, with a difference to the liquidus point lower than 20 μK (Pavese *et al*. 2003).

5. Metal Fixed Points (Hg, Ga, In, Sn, Zn, Al, Ag)

For most of the metal fixed points, the dominant source of uncertainty is impurities, as discussed in Section 2.3 (Mangum *et al*. 1999b). Additional guidelines on the realisation of the points may be found in (Mangum *et al*. 2000a).

Other significant influence effects include residual gas pressure (Section 2.1), hydrostatic pressure (Section 2.2), and stray thermal influences.

5.1 *Immersion and thermal effects*

In the most practical realization of the metal freezing points, the cell is cooled at a rate of about 3 W to 30 W so the system is not adiabatic and thermal equilibrium is not achieved. Thermal fluxes through the cell, insufficient immersion of the SPRT, and the propagation of thermal influences from outside the fixed-point cell all contribute to temperature errors that may be as large as several millikelvin (Batagelj *et al* 2005, Strouse 2005, Ilin 2003, Fahr and Rudtsch 2008).

Ideally, that part of the SPRT immersed in the fixed-point cell is surrounded by the solid–liquid interface. Non-uniform nucleation or large temperature gradients impressed on the cell lead to gaps in the interface though which thermal influences propagate (Ivanova and Ilin 2004, Fahr and Rudtsch 2008). In short cells, a similar effect occurs because the SPRT is insufficiently immersed. These two effects are minimised by ensuring that the furnace in which the cell is located is isothermal, and close to the fixed-point temperature. Ideally, the furnace should be isothermal over the length of the cell and some distance above the cell to ensure the SPRT is not conducting heat from the cell. If the space above the cell is not isothermal, achieving a satisfactory freeze can involve delicate tuning of the furnace (Ilin 2003). Finally, the transparent sheath of the SPRT provides a medium for exchange of infrared radiation.

Figure 5.1 shows an electrical-analogue model of an SPRT immersed in a fixed-point cell. The axial resistances model the thermal conductivity along the cell and SPRT, while the radial resistances model the thermal resistance between the SPRT and the fixed-point substance or the furnace. The resistances form a thermal transmission line so that the influence of temperature falls exponentially with distance. For a uniform furnace and a complete solid–liquid interface within the cell, the immersion profile seen by the SPRT will be

$$T(h) \approx T_{\mathrm{fp}} + \frac{dT}{dh}\left(h - h_0\right) + \left(T_{\mathrm{furnace}} - T_{\mathrm{fp}}\right)\exp\left(\frac{h_0 - h}{L}\right), \tag{5.1}$$

where h is the distance along the axis of the cell, h_0 is the location of the top of the liquid in the cell, the second term of (5.1) is due to the hydrostatic effect (Section 2.2), and the exponential term is due to poor immersion of the SPRT in the cell. The distance L is the $1/e$ attenuation length of the transmission line and is normally in the range 1–6 cm, depending on the fixed-point and the construction of the cell. The relatively short $1/e$ length and long immersion depth of most cells and furnaces ensures that thermal conduction and convection effects from ambient (room) temperature do not propagate along the thermometer to the cell (radiation effects are discussed below).

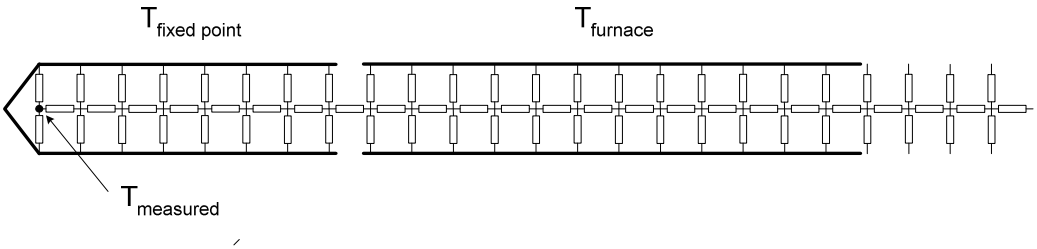

Figure 5.1: An electrical-analogue model of an SPRT immersed in a fixed-point cell and furnace.

The model suggests two approaches for evaluating the immersion conditions of the SPRT. In long cells, there is sufficient immersion to make the exponential term of (5.1) negligible. It is, therefore, possible to track the theoretical hydrostatic pressure dependence of the fixed-point temperature for several centimetres. Successful tracking of the hydrostatic dependence is only possible if (i) the immersion is sufficient and (ii) the solid–liquid interface surrounding the thermometer well is complete. Note that an exponential approach to the ideal immersion characteristic at lesser immersion, as described by (5.1), will be observed only if the furnace temperature near the top of the cell is uniform.

The uncertainty due to immersion and stray thermal effects can be estimated from the residual departures from the expected hydrostatic-pressure line (Strouse 2005, Quinn 1990):

$$u^2\left(\Delta T_{\text{thm}}\right) = \frac{1}{N-1}\sum_i \left(T(h_i) - T(h_0) - \frac{dT}{dh}\left(h_i - h_0\right)\right)^2 , \tag{5.2}$$

where N is the number of measurements of the immersion characteristic, and dT/dh is the hydrostatic pressure coefficient defined by ITS-90.

In short fixed-point cells it is not possible to achieve sufficient immersion to track the hydrostatic effect. The alternative test is carried out at full immersion with (5.1) replaced by

$$T_{\text{meas}} \approx T_{\text{fp}} + \frac{dT}{dh}\Delta h + \mu\left(T_{\text{furnace}} - T_{\text{fp}}\right). \tag{5.3}$$

Although this equation can be derived from (5.1) by using a fixed value for h, it is more general than (5.1) in that it also applies to systems where the furnace temperature is non-uniform and/or the solid-liquid interface is not complete; the term dependent on the furnace temperature is indicative of poor immersion or non-uniform nucleation of the freeze. The value for the appropriate correction can be determined by applying to the furnace a small, ~1 K, temperature oscillation with a period of at least 30 min while observing the plateau (Fahr and Rudtsch 2008). The amplitude of the observed fluctuations in the plateau temperature provides a direct measure of μ:

$$\mu = \frac{\Delta T_{\text{meas}}}{\Delta T_{\text{furnace}}} . \tag{5.4}$$

A correction for the effect,

$$\Delta T_{\text{thm}} = \mu(T_{\text{fp}} - T_{\text{furnace}}) , \tag{5.5}$$

is then applied, as well as the hydrostatic correction. Note that the value of μ varies throughout the melt or freeze of the cell (Fahr and Rudtsch 2008). The difference between the furnace temperature and the fixed-point temperature can be determined from the monitoring SPRT once the cell has stabilised after the freeze.

The uncertainty in the immersion correction is

$$u^2\left(\Delta T_{\text{thm}}\right) = u^2(\mu)\left(T_{\text{fp}} - T_{\text{furnace}}\right)^2 + \mu^2 u^2\left(T_{\text{fp}} - T_{\text{furnace}}\right). \tag{5.6}$$

Additional information on the thermal effects can be obtained by modelling (Batagelj, 2005) or by modifying the thermal properties of the cell and surrounds.

In the higher-temperature fixed points, (tin point upwards), the SPRT and cell are hot enough to generate significant blackbody radiation at short wavelengths. At near-infra-red wavelengths (< 3 μm in borosilicate glass, < 4 μm in fused silica) the sheath of the SPRT becomes transparent and provides a path for heat to leak from the fixed-point cell, causing the SPRT to be cool relative to the phase-transition interface. The effect ranges from about 1 mK or so near the zinc point (Berry 1966) to many tens of millikelvin at the silver point (Evans and Wood 1971). The effect can be reduced significantly either by sandblasting the outer surface of the SPRT sheath or by coating the outer surface of the sheath with colloidal graphite. At the aluminium and silver points, the effect is significant and both techniques are required to avoid errors of the order of 1 mK.

5.2 *Isotopic effects*

For an isotopic effect to be observable there must be a natural variation in the isotopic composition of the fixed-point substance. At present, the possibility of isotopic effects in the metal fixed points has been explored only for gallium and mercury, where it seems likely that the effects are at most a few tens of microkelvin, and probably less. There is no isotopic effect in aluminium because it exists as a single isotope. For all the metal fixed points, isotopic effects are currently assumed to be negligible.

Mercury

Mercury exists as 7 stable isotopes with mass numbers and nominal abundances (196, 0.15%), (198, 10.0%), (199, 16.9%), (200, 23.1%), (201 13.2%), (202, 29.9%), and (204, 6.9%) (IUPAC 1997). Natural isotopic compositions have δ^{198}Hg spanning a range of 10‰ with most within 5‰ (Hintelmann and Lu 2003).

Preliminary measurements of the temperature realised in mercury-triple-point cells with compositions spanning changes in δ^{198}Hg of 3‰ indicate that there were no discernable differences at the level of about 100 μK (Del Campo *et al* 2008).

Gallium

Gallium exists as two stable isotopes with mass numbers and nominal abundances (69, 60.1%) and (71, 39.9%) (IUPAC 1997). Natural variations in the abundances are very low with the standard deviation of δ^{69}Ga in 16 samples of about 1‰ (Gramlich and Machlan 1985), suggesting that any isotope effect will be very small. Measurements of the temperatures realised in three of the same samples spanning a range of 1‰ show no detectable differences at the level of about 20 μK (Mangum and Thornton 1979).

5.3 *Determination of the liquidus point*

For the freezing curves of the metallic fixed-point materials, the maximum observed temperature on the plateau should be taken as the best approximation of the liquidus temperature. The fixed points should be realised with inner and outer liquid-solid interfaces (Mangum *et al*. 2000a) and extend past the maximum by 10 % to 20 % of the fraction frozen, to establish clearly the value of the maximum and the resolution of its determination.

It should be kept in mind that the liquidus temperature depends on the degree to which the impurities in the liquid have been allowed to equilibrate and, as a minimum, the cell should be left molten overnight.

The observed liquidus point also depends on the process for initiation of the freeze, and the nucleation procedure should be tuned to achieve a rapid recovery from the supercool (Ivanova and Ilin 2004, Fahr and Rudtsch 2008). The observed variations in the liquidus point (non-repeatability) are attributable to a combination of thermal effects (Section 5.1) and impurity effects (Section 2.3), so no additional uncertainty should be added.

6. The SPRT

The ordinary long-stem SPRT with a water-triple-point resistance near 25 Ω is typically used from 83.8058 K (argon point) to 450 ºC or 660 ºC. The upper temperature limits arise from chemical or electrical breakdown of the insulating materials; 450 ºC for SPRTs with mica, and 660 ºC for 25 Ω SPRTs with quartz insulation. The main source of uncertainty in this temperature range is oxidation.

High-temperature SPRTs have quartz (fused-silica) insulation and a lower triple-point resistance to mitigate insulation breakdown effects in the temperature range 750 ºC to 960 ºC. The triple-point resistance is typically 0.25 Ω, but thermometers of 0.6 Ω and 2.5 Ω resistance are also used. The main contributions to uncertainty in this temperature range include long-term drift and insulation effects, which for 0.25 Ω thermometers may total several millikelvin at 960 ºC.

The preferred SPRT for the 24 K to 273 K range is a helium-filled capsule with a water-triple-point resistance near 25 Ω. The helium gas improves thermal contact between the platinum and its immediate surroundings while the capsule construction enables the use of longer and finer lead-wires to eliminate extraneous thermal conduction. Of the effects discussed here, only strain effects generally apply to capsule thermometers.

6.1 *Oxidation*

The chemical interactions between platinum and oxygen are extremely complex, with as many as a dozen possible oxides and allotropes. The formation of these phases depends on the partial pressure of oxygen, temperature, the presence of impurities in the platinum, and crystal size and orientation (Wang and Yeh 1998). Two of these oxidation states are of direct interest to platinum thermometry (Berry 1978, 1982a, 1982b), and without appropriate care, the effects can cause hysteresis errors of many tens of millikelvin.

For the purpose of the description here, we consider that platinum may exist in just three states: metallic platinum, a 2-dimensional or monolayer platinum oxide (PtO_2) on the surface of the wire, and 3-dimensional or multilayer platinum oxide (PtO_2 and PtO). The potential energies of these states are such that at room temperature the 3-d oxide is more stable than the 2-d oxide, which is in turn more stable than metallic platinum. However, there are energy barriers between these three states, with the result that the oxide states tend to occur over a narrow temperature range. Below 0 ºC, there is insufficient thermal energy (kT) to allow the 2-d oxide to form from the metallic state. Above 0 ºC the rate of formation of the 2-d oxide increases with temperature until about 380 ºC, when it begins to dissociate. Throughout the range, the rate of formation is slow; it is just detectable after 1 hour at 200 ºC and is still progressing after many tens of hours at 300 ºC. The 3-d oxide shows similar behaviour but is restricted to a temperature range from about 350 ºC to 560 ºC. These temperature ranges are approximate; as the partial pressure of the oxygen in the fill gas of the SPRT decreases, both the rates of oxidation and the dissociation temperatures decrease (Ancsin 2003).

Figure 6.1, from Berry (1982a, 1982b), shows the effect of oxidation on platinum SPRTs that are first heat treated at high temperature to dissociate all of the oxide, and then maintained at the indicated temperatures for 160 hours. The broader peaks in the curves of Figure 6.1, in the range 0 ºC to 350 ºC, betray the presence of the 2-d oxide. In the 100 º C to 350 º C, range the oxide has approached equilibrium concentration on the surface of the wire. Below 100 ºC, oxidation is still progressing slowly. As the equilibrium concentration is approached, the rate of oxidation decreases logarithmically, and it may take many days to reach some of the levels indicated in Figure 6.1. Because it is a surface effect, the relative resistance change is inversely proportional to the diameter of the platinum wire. It may give rise to as much as an 8 ppm increase in triple-point resistance for a 25 Ω SPRT, or, equivalently, as much as 5 mK error at 400 ºC. High-temperature SPRTs are less susceptible because of the larger diameter wire.

Prolonged exposure to temperatures in the range 350 ºC to 530 ºC (depending on partial pressure of oxygen) allows the PtO_2 to overcome the second potential barrier and diffuse into the platinum, forming the three-dimensional oxide. This oxide appears to be autocatalytic; i.e., once initiated the 3-d oxidation will proceed almost indefinitely. The narrower peaks in the 350 ºC to 450 ºC range of Figure 6.1 are characteristic of the effect. In extreme cases, resistance changes of more than 100 mK in 25 Ω SPRTs can occur. For this reason, SPRTs exhibiting a steady and relatively rapid upward drift in triple-point resistance with heat treatment at 450 ºC should be considered faulty. At temperatures above 450 ºC the platinum dioxide begins to dissociate and form platinum monoxide. By about 560 ºC (the exact temperatures depends on partial pressure of oxygen) the dissociation is complete, leaving metallic platinum. Heat treating the thermometers at 600 ºC or higher will cause the 3-d oxide to dissociate and should largely restore the SPRT. If the 3-d oxide has formed, extended heat treatment for very long periods (>>10 hours) may be required to restore stability.

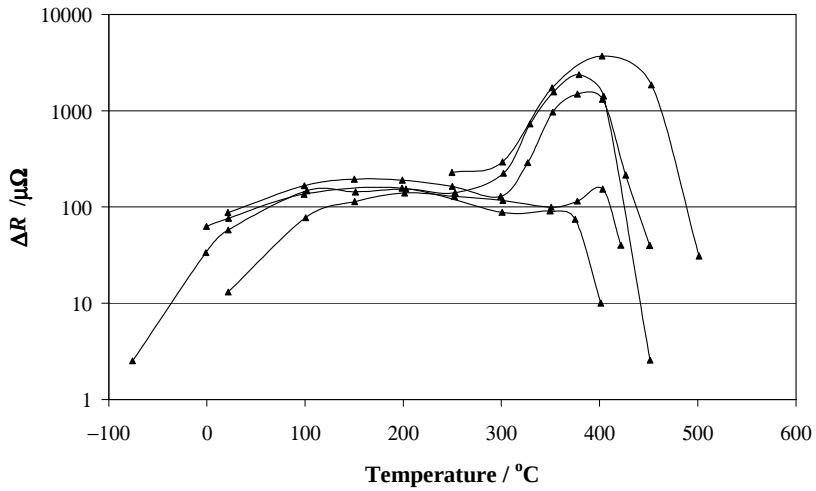

Figure 6.1: The increase in triple-point resistance observed in 25 Ω SPRTs following 160 hours exposure at the indicated temperatures (Berry 1982a, 1982b).

Because the rate of formation, the rate of dissociation, and the dissociation temperature of the oxides depend on the partial pressure of oxygen in the thermometer fill gas and the diameter of the wire, the magnitude of the effects vary amongst thermometers. In particular, since Berry discovered the effect, most thermometers have been manufactured with a relatively low partial pressure of oxygen to minimise the effects, and for the most part, the 3-d oxide state has been almost completely suppressed. Note that the presence of oxygen in the fill gas of a thermometer is essential for the stability of SPRTs. Indeed, metal-sheathed thermometers used at temperatures sufficient to oxidise the sheath material eventually become unstable when the partial pressure of oxygen is insufficient to prevent migration of metallic contaminants into the platinum (Zhao *et al*. 2003).

Berry (1982a) found that the effect of the 2-d oxide is equivalent to a low-conductivity semiconductor layer of PtO_2 about half of one atomic layer (~0.1 nm) in thickness. The resulting changes in the resistance of the SPRT are related according to

$$\frac{\Delta R(t)}{R_{\mathrm{H2O}}} = ZW\frac{\Delta R_{\mathrm{H2O,ox}}}{R_{\mathrm{H2O}}}, \tag{6.1}$$

where ΔR_{H2O} is the increase in the triple-point resistance due to oxidation, $\Delta R(t)$ is the increase in SPRT resistance at temperature t due to oxidation, and Z is a dimensionless parameter a little less than 1.0 and dependent on temperature and the relative electrical conductivities of the platinum oxide and platinum metal. The error in the resistance ratio calculated using a triple-point resistance measurement taken immediately after the measurement of $R(t)$, so that the SPRT is in the same oxidation state, is

$$\Delta W_{\mathrm{ox}} = (Z-1)W(t)\frac{\Delta R_{\mathrm{H2O,ox}}}{R_{\mathrm{H2O}}}. \tag{6.2}$$

Note that W decreases with oxidation since $Z < 1$. Berry found that the factor $(Z-1)W(t)$ was almost purely quadratic (actually almost linear):

$$(Z-1)W(t) \approx -1.33\times10^{-4}\,t - 9.53\times10^{-7}\,t^2 \tag{6.3}$$

with a relative uncertainty of about 5 %. Values of the factor are –0.023, –0.081, and –0.22 at 100 ºC, 230 ºC and 420 ºC respectively. Equations (6.1) and (6.2) show that the effect of oxidation is substantially reduced if the resistance ratio is calculated using the triple-point resistance of the SPRT in its oxidised state.

In order to avoid errors of several millikelvin due to 2d-oxidation effects it is necessary to manage the effects. There are two main options.

Scheme 1: *High accuracy measurements* (*incl. calibration at fixed points*)
For the highest accuracy in a temperature measurement, the resistance ratio should be calculated using the triple-point resistance taken immediately after the liquidus measurement at the fixed point. If SPRTs are allowed to

stay hot in the fixed point or cool slowly below 450 ºC, oxidation effects can change the resistance further. Similarly, 24 hours at room temperature will produce a detectable increase in the oxidation. All measurements for the Ga, In, Sn and Zn fixed points, in particular, should be measured this way. The uncertainty in the measured resistance ratio due to oxidation is then

$$u^2\left(W_{\mathrm{ox}}\right) = (1-Z)^2 W(t)^2 \frac{u^2\left(R_{\mathrm{H2O,ox}}\right)}{R_{\mathrm{H2O}}^2} + u^2\left((1-Z)^2 W(t)^2\right)\frac{\Delta R_{\mathrm{H2O,ox}}}{R_{\mathrm{H2O}}^2} \tag{6.4}$$

where $u(R_{\mathrm{H2O,ox}})$ is the uncertainty in the triple-point resistance due to oxidation, which can be estimated from the range of water-triple-point resistances observed during calibration. The relative uncertainty in the $(1 - Z)W$ term is small, less than 10^{-2}, so its contribution to the total uncertainty is usually negligible. An uncertainty of 2 ppm in triple-point resistance due to oxidation would yield an uncertainty of about 100 µK at 400 ºC. The effect scales approximately linearly with temperature, so the uncertainty would be about 25 µK at 100 ºC.

Scheme 2: *General-purpose measurements*
The procedure above requires a triple-point resistance measurement after each temperature measurement, which may be impractical in automated calibration systems, for example. If, instead, the resistance ratios are calculated using a triple-point resistance taken at any another time, when (6.1) does not apply, then the uncertainty in the calculated resistance ratio is

$$u^2\left(W_{\mathrm{ox}}\right) = (1+Z^2) W(t)^2 \frac{u^2\left(R_{\mathrm{H2O,ox}}\right)}{R_{\mathrm{H2O}}^2} \approx 2W(t)^2 \frac{u^2\left(R_{\mathrm{H2O,ox}}\right)}{R_{\mathrm{H2O}}^2}\,. \tag{6.5}$$

The range of triple-point-resistances observed when the SPRT is in typical use should be recorded. If the water-triple-point resistance, used to calculate the resistance ratio W for the unknown temperature, is the mean observed for the typical range of oxidation states, the factor of 2 can be omitted from (6.5). The range of values should be used to estimate the uncertainty, $u(R_{\mathrm{H2O,ox}})$. A 2 ppm uncertainty in the triple-point resistance gives rise to an uncertainty of 2.0 mK at 400 ºC. Note that the uncertainty in triple-point resistance due to oxidation, $u(R,\mathrm{ox})$, is a temperature-dependent characteristic of each SPRT.

There are also alternative calibration schemes for reducing the oxidation effect during the calibration; for example, by heat treating the SPRT before each fixed-point measurement and calculating the resistance ratios for the SPRT in an oxide-free state. This procedure has the advantage of enabling the use of a single value for the triple-point resistance, but the disadvantage is that oxidation of the SPRT during use will bias the measured temperature by up to 5 mK or more.

6.2 *Impurities*

In an ideal metal conductor, electrical resistance is caused by the scattering of electrons by thermally agitated platinum atoms. This leads to an electrical resistance increasing directly in proportion to temperature, and is the basis of metallic resistance thermometry. Additional scattering of electrons caused by impurities gives rise to additional electrical resistance and errors potentially ranging up to several tens of millikelvin.

Impurities lead to irreversible changes in the resistance-temperature dependence of SPRTs, and are the main cause of long-term drift. The impurities may originate in metal sheaths at temperatures above 450 ºC or diffuse through the silica and glass sheaths at higher temperatures. The effect of the impurities is to increase the resistance by an amount that, above 50 K, is almost constant with temperature (Berry 1963), i.e.

$$R(t) \approx R_{\mathrm{ideal}}(t) + \Delta R\,, \tag{6.6}$$

where $R_{\mathrm{ideal}}(t)$ is the $R(t)$ relation without impurities and ΔR is the shift induced by impurities. Equation (6.6) is a variation of Matthiessen's rule.

For thermometers used at temperatures below 450 ºC the long-term drift is usually very small, no more than 1 mK with many hundreds of hours of use (Berry 1962). Above 450 ºC the drift increases with increasing temperature and length of exposure reaching about 5 mK/100 hrs at the silver point (Berry 1966, Fellmuth *et al.* 2005a). Corrections can be applied using (6.6), but because the equation is approximate, and there are other causes of changes in the triple-point resistance, the uncertainties are a significant fraction of the correction. Ideally the SPRT should be recalibrated if the drift is significant.

6.3 *Vacancies and crystal defects*

Defects in the crystal lattice cause scattering of electrons and an increased resistance in the same manner as impurities. There are two causes for the creation of defects and vacancies. With sufficiently high temperatures (above 450 °C), the thermal agitation of the atoms may be sufficient for some atoms to jump out of position causing vacancies in the crystal lattice. At higher temperatures, more complex (higher energy) crystalline defects and vacancies may be created. At any temperature, the concentration of these thermal vacancies and defects rapidly reaches an equilibrium concentration causing an increased resistance of approximately (Berry 1966)

$$\Delta R \approx 1200 R_{\mathrm{H2O}} \exp\left(\frac{-E_{\mathrm{a}}}{kT}\right), \tag{6.7}$$

where E_{a} is the activation energy for the creation of the defects (~1.5 eV for simple vacancies). The effect becomes detectable at 500 °C (by quenching) and rises to many tens of millikelvin at 960 °C. The additional electrical resistance caused by the defects is an integral part of the $R(t)$ characteristic of the thermometer. However, if the thermometer is cooled too quickly, the vacancies and defects become "quenched in" and cause errors in the $R(t)$ characteristic at lower temperatures.

Defects can also be created by mechanical shock and vibration, with severe shock causing shifts as large as 100 mK. More typically, effects of the order of microkelvin accumulate each time an SPRT is knocked (Berry 1962). The most significant cause of defects is the cold drawing of the platinum wire prior to the manufacture of the SPRT. This necessitates extended annealing during manufacture of the SPRT to ensure stability. Mechanically created defects are associated with work hardening of the wire.

For temperatures below 300 ºC, the defects and vacancies have a similar effect to the impurities and lead to a temperature independent shift easily detectable as changes in the triple-point resistance (Equation (6.6)). Above 300 ºC, the thermal agitation of atoms may be enough to allow atoms to resettle in the lattice, restoring the vacancy and defect concentration to its equilibrium value. All defects anneal out according to an exponential law with a half-life, τ, dependent on the activation energy for the defect and temperature:

$$\tau = \tau_0 \exp\left(\frac{E_{\mathrm{a}}}{kT}\right), \tag{6.8}$$

where τ_0 is the time constant involved with the diffusion and equilibration process. Thus, the annealing of defects with high activation energies requires higher temperatures and longer annealing times. In principle, vacancies and crystal defects can be removed completely with sufficient annealing (Berry 1966, 1972, Berry and Lamarche 1970). However, for the highest-energy defects, such as caused by severe mechanical shock, the annealing temperatures may be beyond the material limit for most SPRTs. In these cases, the defect effects are practically irreversible.

Routine annealing at 450 °C for an hour or two will remove practically all low-energy defects and vacancies. SPRTs affected by severe shock or defects quenched in at high temperature (evident from triple-point resistance records) may require annealing at the highest operating temperature (up to 960 °C). To avoid quenching defects from high temperatures, Berry (1966) recommends SPRTs are cooled and annealed at decreasing temperatures in steps of 50 °C, with 10 to 20 minutes at each step. Once the thermometer has been cooled to 450 °C, it can be removed quickly (< 10 minutes) from the furnace to avoid oxidation effects.

For capsule thermometers, the upper temperature limit (typically 156 ºC) means these effects cannot be removed by annealing and are, therefore, practically indistinguishable from impurity effects. A valuable (high resolution) indicator of resistance shifts in capsule-type SPRTs is the residual resistance at liquid-helium temperature.

6.4 *Strain and hysteresis*

Strain on the platinum wires of SPRTs gives rise to three different types of deformation: elastic, plastic and anelastic (Berry 1983). Elastic strain occurs for small stresses, less than the yield point of the wire, and by definition, the wire fully recovers when the stress is removed. From work on platinum strain gauges it is known that electrical resistance increases when the wire is under tension and decreases when under compression. The combination of differential thermal expansion between the platinum wires and its insulating supports, and mechanical movements of the wire, therefore give rise to strain-gauge effects. These become apparent with cyclic excursions in temperature of more than several tens of degrees.

Plastic deformation occurs when the stresses exceed the yield point of the wire. Plastic deformation rarely happens with thermal effects, but commonly accompanies severe mechanical shock. It should never occur, therefore, during normal use of the SPRT. Plastic deformation tends to cause two effects: a dimensional change in the wire, and severe disruption to the crystalline lattice with the creation of defects. While some of the damage

will anneal out, the highest-energy defects and dimensional changes are practically permanent. Pure dimensional changes cause a change in R_{H2O} but not $W(t)$, whereas the high-energy defects have the same effect as impurities (Equation (6.6)).

Anelastic strain occurs at levels below the yield point, like elastic strain and in conjunction with elastic strain, but does not recover once the stress is removed. It also gives rise to hysteresis effects, but the SPRT can be restored by annealing. Berry (1983) describes this effect as similar to internal friction, so it is probably due to the creation of low-energy defects.

The magnitude of the hysteresis effects (elastic and anelastic deformation) is strongly influenced by the design of the SPRT and materials used in the construction of the SPRT, and ranges between 0.1 mK peak-to-peak to 1.8 mK peak-to-peak. Most SPRTs exhibit effects of the order of 0.3 mK peak-to-peak (0.1 mK uncertainty).

6.5 *Long-term drift and uncertainty*

Oxidation, impurities, and crystal defects all give rise to an increase in the triple-point resistance of an SPRT, and all may occur during the use of the SPRT. Because the three effects have a similar effect on the triple-point resistance, but have different propagation laws, increases in the triple-point resistance necessarily give rise to uncertainty (ambiguity). Control of cooling rates and careful handling can significantly reduce the ambiguity by eliminating thermally- and mechanically-induced defects. The remaining shifts may be separable according to operating temperature with oxidation effects occurring below 450 °C and impurity effects above 450 °C.

Long-term drift in SPRTs is evident from changes in the R_{H2O} values that cannot be removed by annealing. The shifts tend to be a mix of two types of change. Impurities and high-energy defects lead to changes in resistance that are well approximated by Matthiessen's rule (6.6). Note that downward drifts may be due to insufficient annealing during manufacture. Secondly, permanent dimensional changes, caused by plastic deformation, volatilisation of platinum, and changes incurred during an episode of 3d-oxidation, lead to a change in the triple-point resistance but not the $W(t)$ value (Berry 1966).

Ideally where thermometers exhibit significant drift, they should be recalibrated. Also, drift caused by impurities tends to accelerate with time, so excessive drift usually suggests replacement rather than recalibration. If necessary, corrections and uncertainties can be calculated by using the two cases (above) as bounds to determine a correction and uncertainty.

For a thermometer affected only by impurity-like effects according the Matthiessen's rule, the error in the thermometer reading using the latest annealed value of R_{H2O} is

$$\Delta W_{\text{drift}} = W - W_{\text{ideal}} \approx \frac{\Delta R_{\text{H2O}}}{R_{\text{H2O}}}(1-W)\,. \tag{6.9}$$

In the other case there is no change in the $W(t)$. Therefore, half of the value indicated by (6.9) should be used as a correction, and 1/3 of the value can be used as the standard uncertainty (assuming a rectangular distribution):

$$u^2(\Delta W_{\text{drift}}) = \frac{u^2(\Delta R_{\text{H2O,drift}})}{R_{\text{H2O}}^2}(1-W)^2\,. \tag{6.10}$$

If an SPRT affected by the impurity-like drift mechanisms is recalibrated, then the error in the interpolated value of reference resistance ratio is zero, since from (C.28) and (C.19)

$$\Delta W_{\text{r}} = \frac{\Delta R}{R_{\text{H2O}}}\left(1-\sum_{i=1}^{N} f_i(W)\right) = 0\,. \tag{6.11}$$

6.6 *Insulation and leakage effects*

There are two distinct effects causing electrical insulation or leakage effects in SPRTs: moisture in the SPRT fill gas, and insulation breakdown at high temperature. Capacitance or ac/dc effects, which may also be treated as a leakage effect, are generally due to faulty cables and ac-dc effects, as discussed in Section 8.2 (Resistance Measurement). Moisture and insulation breakdown effects cause the measured resistance to be low, so measurement configurations with the highest readings are generally the most correct.

Moisture effects

Berry (1966), and Zhang and Berry (1985), established that the insulation resistance of mica-insulated SPRTs deteriorates once the thermometer has been used above 450 ºC for an expended period. Marcarino and Dematteis (1999) subsequently demonstrated that the effect may be as large as 1 mK or more. The problem is caused by the release of water from the mica when the SPRT is exposed to high temperatures. Quartz insulated thermometers may also exhibit a moisture effect, although it is usually much smaller. The effect is greatest near 0 ºC, where the water condenses and possibly freezes on the internal surfaces of the SPRT. The effect decreases exponentially as the temperature moves away from 0 °C (Berry 1966). As the temperature decreases below 0 °C, the conductivity of the ice falls, while above 0 °C an increasing fraction of the water is vapour. At −38 ºC, the effect is very much reduced and by 200 ºC the effect is negligible.

SPRTs affected by moisture typically exhibit long (> 10 minutes) settling times, and sometimes instability, at the triple point of water. They will also exhibit hysteresis due to the migration of moisture within the sheath, which may be confused with oxidation effects. The effect may be sensitive to the operating frequency of the resistance bridge, so it is sometimes detectable by changing the frequency (current-reversal times for dc bridges).

The presence of moisture is measured by using dry ice to cool the upper end of the SPRT sheath, which condenses the moisture away from the electrically conducting elements of the SPRT. The observed change in the triple-point resistance typically ranges from undetectable for good quartz SPRTs to 100 μK or more for older mica-insulated SPRTs.

High-Temperature Breakdown

At sufficiently high temperatures, all of the insulating materials used in SPRTs show the thermistor-like decrease in electrical resistivity characteristic of large-band-gap semiconductors. The resistance decreases exponentially with temperature, causing significant effects in 25 Ω SPRTs at temperatures above 700 ºC and inducing errors as large as 40 mK at 960 ºC. Berry (1995) and earlier (Zhang and Berry 1985) investigated the effect and demonstrated a complex dependence on a variety of influence variables, including:

- The electrical operating conditions, including any ground and screen configuration of the measurement circuit, grounding or screening of components in the fixed-point furnace, any dc polarising voltage, and the time that the SPRT is subjected to the polarising voltage.
- The structure of the thermometer, including the insulator material, the geometry of the insulator material and the platinum winding, and contact between the platinum winding and the insulator.
- Thermal operating conditions including the temperature distribution along the thermometer sheath and the thermal history.

There were also peculiar effects, similar to the electrical charge and discharge of batteries, associated with the insulation (Berry 1995, Moiseeva 2005).

White *et al*. (2007) and Yamazawa *et al*. (2007a) showed that most of this complexity is explained by the influence of metal-semiconductor diodes (also known as Schottky-barrier or point-contact diodes) formed at the points of contact between the platinum and the silica insulators in the SPRT. The conductance of the silica insulation appears to be a combination of semiconductor behaviour, perhaps associated with the surface conductivity of the silica, and the small-signal resistance of the diodes:

$$S(T) = S_1 \exp\left(\frac{-E_g}{kT}\right) + S_2 T \exp\left(\frac{-q\phi_B}{kT}\right)\exp\left(\frac{qV}{kT}\right), \tag{6.12}$$

where S_1 and S_2 are constants, E_g is the energy band gap associated with the semiconductor characteristic (about 1.6 eV), $q\phi_B$ is the Schottky-barrier height associated with the diodes (about 3 eV), and V is any dc bias voltage across the diodes (a negative bias voltage reduces the conductance). At temperatures below 750 °C, the semiconductor contribution dominates the insulation behaviour and the various non-linear effects are not apparent. Above 750 °C the diode conductance begins to dominate and the various rectifying effects and susceptibility of the insulation resistance to dc bias voltage become apparent.

The conductance, S, in parallel with the sensing element leads to a decrease in measured SPRT resistance and a temperature error of

$$\Delta t \approx -S(t)R_0 \frac{\left(1 + At + Bt^2\right)^2}{A + 2Bt}, \tag{6.13}$$

where R_0 is the triple-point resistance of the SPRT, and A and B are derived from the approximation $R(T) \approx R_0(1 + At + Bt^2)$, where $A = 3.985 \times 10^{-3}$, $B = -5.85 \times 10^{-7}$. Note that the effect increases in proportion to the SPRT triple-point resistance.

Although (6.12) gives the temperature dependence of the effect, the magnitude is not so easily determined. In practice, the SPRT is far more complicated than a single conductance in parallel with $R(t)$. There are conductances distributed between each of the leads along the full length of the thermometer, each subject to different voltage and temperature profiles. Additionally, there are shunt resistances and dc voltages between the SPRT and the furnace. However, some general observations can be drawn that may enable its assessment.

Evans (1984) estimated the magnitude of both internal and external (through the sheath) leakage, and showed that guarding helps suppress some leakage resistance effects for several major models of thermometer. Berry (1995) also pointed out that external leakage effects (e.g., from the furnace) are significant, and proposed a model including the lead wires and the polarization effect (now recognised as due to the diodes). Berry (1995) showed that a dc offset of the correct polarity (the voltage V in (6.12)) applied to the measurement circuit or to conducting screens substantially reduces the shunt conductance (increases the resistance), and some resistance bridges have the facility for introducing the offset. This technique may yet prove to be a means for assessing the magnitude of the insulation resistance.

Measurements of the shunt resistance by many workers (e.g. Berry (1995), Yamazawa and Arai (2003, 2005), Moiseeva (2005)) suggest that typical values for a lumped shunt resistance for thermometers with quartz insulation are in the range 0.5 MΩ to 20 MΩ at 960°C, which produce leakage effects of 3 mK to 0.08 mK for a sensor with R_0 = 0.25 Ω. Note that this effect may increase or decrease following calibration, when the thermometer is in use, depending on the temperature profiles along the thermometer sheath. These observations suggest a standard uncertainty of the order of 1 mK at 960 °C of 0.25 Ω thermometers, with the uncertainty scaled according to (6.12) at lower temperatures, and scaled in proportion to the triple-point resistance of the SPRT (6.13).

For thermometers employing glass and/or mica insulation, the leakage conductance is much greater and becomes apparent at lower temperatures with errors of about 1 mK at 600 ºC. Yamazawa and Arai (2005) have evaluated the leakage resistance for Netsushin alumina-insulated thermometers.

7. Interpolation error and non-uniqueness

Ideally, the interpolating equations of ITS-90 should accommodate the real variations in the $W(t)$ relationship for different SPRTs. In practice, the functional form of the equations is insufficient to characterise the many complex physical effects that cause the variations, and hence the SPRT calibration equations are subject to interpolation error. The error, called non-uniqueness, is manifest as differences in the temperatures inferred using different thermometers or different equations. It may arise because more than one equation used (Type 1 non-uniqueness), more than one type of interpolating instrument is used (Type 2 non-uniqueness), or different instances of the designated interpolation instrument are used (Type 3 non-uniqueness - see Mangum *et al*. 1997).

In this section, we consider only Type 1 and Type 3 non-uniqueness in the SPRT subranges: Type 2 non-uniqueness contributes only between the e-H_2 point (13 K) and the Ne point (24 K) where the SPRT and the interpolating gas thermometer subranges overlap. Both Types 1 and 3 contribute up to 0.5 mK or more to uncertainty in the temperatures interpolated between fixed points. In most of the SPRT subranges of ITS-90 it is the largest source of uncertainty associated with the realisation of the scale.

Little is published on the various forms of non-uniqueness. The physical cause is presumed to be due to different crystal orientations, different grain sizes, and different impurities in different concentrations in the platinum wire, as well as variations in surface and vacancy effects. The general mathematical form of both types of non-uniqueness is known since they are forms of interpolation error (White and Saunders 2007):

$$\Delta W_{\mathrm{r}} = (W - W_1)(W - W_2)(...)(W - W_N)\,g(W)\,, \tag{7.1}$$

where $W_1 \ldots W_N$ are the measured resistance ratios at the fixed points and $g(W)$ is function of resistance ratio that may or may not be known depending on the type of non-uniqueness. It is not known whether there is any correlation between the two types of non-uniqueness; for the present they are assumed to be uncorrelated.

The definition of the uncertainty for non-uniqueness is problematic because of the multiple subranges and definitions, some of which are infrequently used, each of which gives rise to very different, typically non-normal distributions of temperatures. There is also a paucity of data in some subranges. To yield a consistent uncertainty characterising "the range of values that ITS-90 attributes to the temperature", the standard uncertainty assigned to non-uniqueness should be calculated as the standard deviation of the differences from the mean of all possible formulations of the scale (i.e., averaged over different SPRTs and different subranges).

7.1 *Type 1 non-uniqueness* (*Subrange inconsistency*)

Subrange inconsistency (SRI) arises from the difference between the interpolating equations for two different subranges and for the same SPRT. For example, the inconsistency between the water–zinc and water–aluminium subranges, expressed in terms of the difference in calculated reference resistance ratio, is

$$^{\mathrm{Al}}W_{\mathrm{r}}(W) - {}^{\mathrm{Zn}}W_{\mathrm{r}}(W) = (W - 1)(W - W_{\mathrm{Sn}})(W - W_{\mathrm{Zn}})c\,, \tag{7.2}$$

where the superscript indicates the subrange and c is the coefficient of $(W - 1)^3$ in the water–aluminium interpolating equation for the SPRT (Zhiru *et al*. 2002, White and Strouse 2008). SRI has two key features, both illustrated by (7.2). Firstly, it has a well-defined mathematical form determinable from the different interpolating equations and measured fixed-point resistance ratios. Secondly, it has zeros at the fixed points shared by the two subrange equations, which gives it the same form as Equation (7.1). There is also a tendency for the SRI to increase in proportion to ΔW^N where ΔW is the interval between adjacent fixed points, and N is the number of shared fixed points. This is also apparent in (7.2).

For temperatures between 420 ºC (zinc point) and 960 ºC (silver point), there are no overlapping equations and, therefore, there is no subrange inconsistency.

Between 0.01 ºC (water triple point) and 420 ºC (zinc point), the subrange inconsistency is described by 15 different equations arising from the overlap of the water–gallium, mercury–gallium, water–indium, water–tin, water–zinc, and water–aluminium subranges. Because of the ΔW^N scaling property, over most of the 0.01 ºC to 420 ºC range, the SRI is dominated by the difference between the water–zinc and water–aluminium subranges. There is good data for this subrange with studies by Mangum *et al*. (1990), Strouse (1992a), Moiseeva and Pokhodun (1992), and Ahmed (2005) and Ancsin (1996). The two most extensive studies are Zhiru *et al*. (2002), and White and Strouse (2008), who determined the subrange inconsistency for 65 and 50 thermometers, respectively. The maximum values for the SRI occur near 93.15 ºC where the two studies found standard uncertainties of 0.33 mK and 0.48 mK the latter result probably reflecting a wider range of SPRT models and manufacturers in the sample. Figure 7.1 gives the SRI uncertainty versus temperature, calculated according to

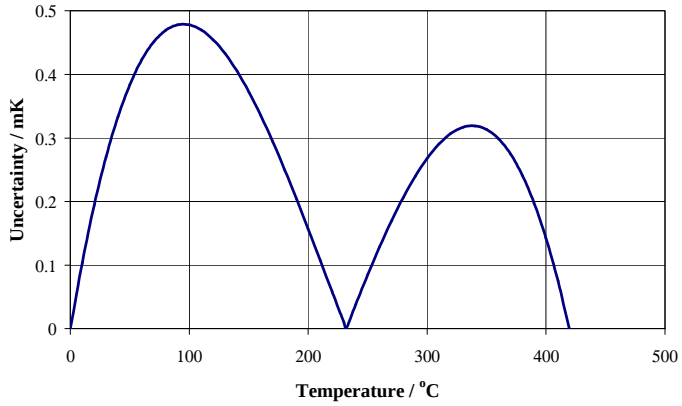

Figure 7.1: Uncertainty due to Type 1 non-uniqueness (subrange inconsistency) over the range 0 ºC to 420 ºC. The maxima occur at 93.15 ºC (W = 1.366 227) and 336.57 ºC (W = 2.274 97).

$$u_{Wr,\mathrm{SRI}} \approx 8.0\times10^{-6}\left|(W-1)(W-W_{\mathrm{Sn}})(W-W_{\mathrm{Zn}})\right|, \tag{7.3}$$

which is derived from the measurements of White and Strouse (2008). Note that the equation gives the uncertainty in resistance ratio as a function of resistance ratio, while Figure 7.1 has been scaled so that both axes are in terms of temperature.

For temperatures below 0.01 ºC, the SRI arises from the overlap of 5 different subranges between each of e-H_2, neon, oxygen, and argon points, and the water triple point. Recent data for these subranges comes from Meyer and Tew (2006), and Steele (2005), with very similar results. With the data from 18 thermometers, Meyer and Tew determined the uncertainties shown in Figure 7.2. Each curve in Figure 7.2 gives the uncertainty in temperature and is described by a polynomial of the form

$$u_{T,\mathrm{SRI},i} = \sum_{j=1}^{5} A_{ij}\,(T_{90}-T_0)^j\,. \tag{7.4}$$

where the coefficients A_{ij} and the constants T_0 are given in Table 7.1.

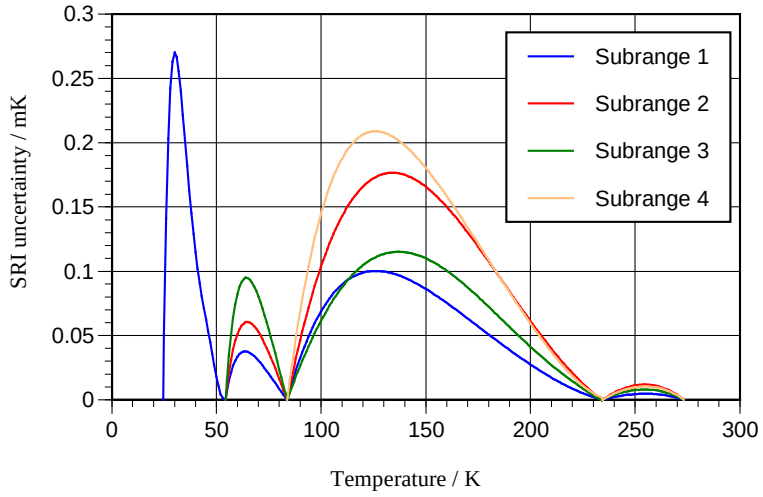

Figure 7.2: Uncertainty due to Type 1 non-uniqueness (subrange inconsistency) over the range 24 K to 273 K.

Table 7.1: Table of coefficients, A_{ij} and T_0, for the Equations (7.4) giving the uncertainty due to subrange inconsistency for temperatures below 273.16 K.

Interval		**24 K to 54 K**	**54 K to 84 K**	**84 K to 234 K**	**234 K to 273 K**
T_0		24.5561 K	54.3584 K	83.8058 K	234.3156 K
Subrange 1	A_{11}	1.22672×10^{-1}	1.03503×10^{-2}	5.93767×10^{-3}	4.29253×10^{-4}
	A_{12}	-1.88293×10^{-2}	-9.83657×10^{-4}	-1.19004×10^{-4}	-8.51144×10^{-6}
	A_{13}	1.16274×10^{-3}	4.04173×10^{-5}	9.79845×10^{-7}	-6.16575×10^{-8}
	A_{14}	-3.32079×10^{-5}	-8.84429×10^{-7}	-4.11701×10^{-9}	0
	A_{15}	3.61210×10^{-7}	8.18525×10^{-9}	7.43745×10^{-12}	0
Subrange 2	A_{21}	1.22672×10^{-1}	1.46965×10^{-2}	8.17935×10^{-3}	1.12123×10^{-3}
	A_{22}	-1.88293×10^{-2}	-1.22528×10^{-3}	-1.17448×10^{-4}	-2.41884×10^{-5}
	A_{23}	1.16274×10^{-3}	4.42159×10^{-5}	5.21656×10^{-7}	-1.18754×10^{-7}
	A_{24}	-3.32079×10^{-5}	-9.02157×10^{-7}	-6.27718×10^{-10}	0
	A_{25}	3.61210×10^{-7}	8.08877×10^{-9}	-3.52429×10^{-13}	0
Subrange 3	A_{31}		2.44661×10^{-2}	4.51632×10^{-3}	7.57190×10^{-4}
	A_{32}		-2.17672×10^{-3}	-4.24606×10^{-5}	-1.63114×10^{-5}
	A_{33}		8.41030×10^{-5}	-1.54105×10^{-7}	-8.05881×10^{-8}
	A_{34}		-1.78294×10^{-6}	2.65234×10^{-9}	0
	A_{35}		1.62720×10^{-8}	-7.17817×10^{-12}	0
Subrange 4	A_{41}			1.26290×10^{-2}	9.61622×10^{-4}
	A_{42}			-2.62539×10^{-4}	-1.95292×10^{-5}
	A_{43}			2.32229×10^{-6}	-1.27628×10^{-7}
	A_{44}			-1.07172×10^{-8}	0
	A_{45}			2.11043×10^{-11}	0

7.2 *Type 3 non-uniqueness*

Conventionally described simply as non-uniqueness, Type 3 non-uniqueness arises from the differences in the interpolated W_r values due to the use of different SPRTs over the same subrange. It has the form of (7.1) in that it exhibits zeros at all of the fixed points, but the $g(W)$ function is unknown. It is known that the non-uniqueness is made worse in the subranges where the fixed-point sensitivity coefficients amplify uncertainties (White and Saunders 2007). There have been several investigations of non-uniqueness at temperatures between 14 K and 273 K, e.g. Ward and Compton (1979), Head *et al*. (1997), and Hill and Steele (2003). Figure 7.3 shows the non-uniqueness for the temperature range between 14K and 273.16 K based on the data from Hill and Steele (2003). As with subrange inconsistency, Type 3 non-uniqueness scales approximately as ΔW^N in the intervals between adjacent fixed points.

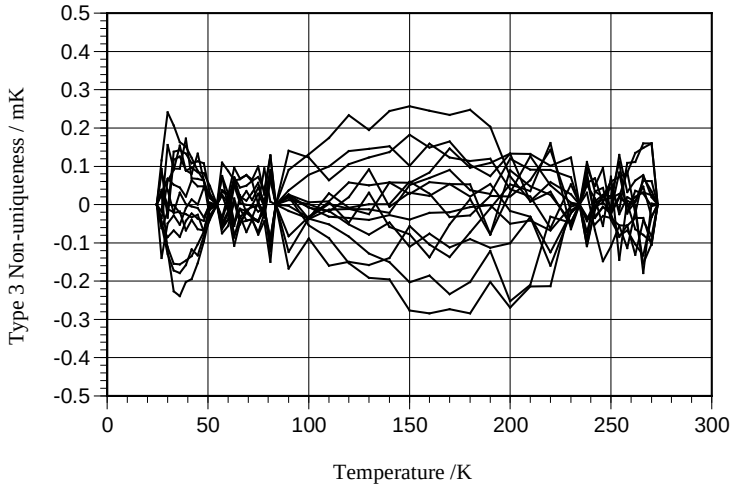

Figure 7.3: The non-uniqueness of ITS-90 between 24 K and 273.16 (from the data of Hill and Steele (2003)).

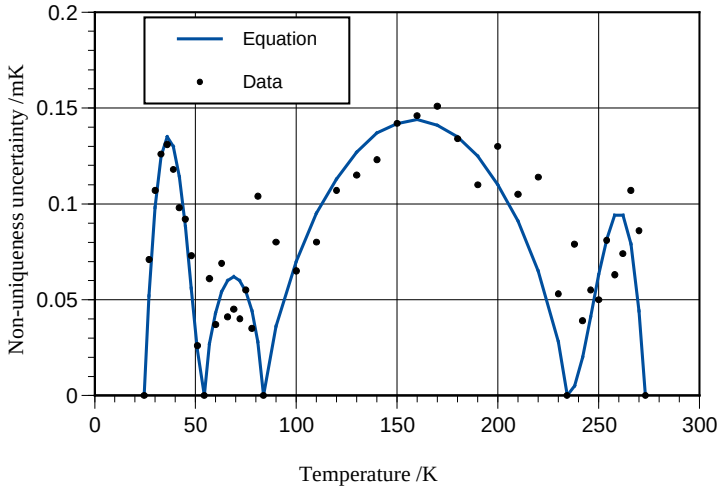

Figure 7.4: The measured uncertainty due to Type 3 non-uniqueness in the range 24.5561 K to 273.16 K and the functional approximation of Table 7.2.

Table 7.2: Uncertainty due to Type 3 non-uniqueness for intervals in the range 24K to 273.16 K.

Temperature range / K	Uncertainty / mK
24.5561 to 54.3584	$1.5\times10^{-4}(T-24.5561)(54.3584-T)^{1.5}$
54.3584 to 83.8058	$1.1\times10^{-3}(T-54.3584)^{0.75}(83.8058-T)^{0.75}$
83.8058 to 234.3156	$2.2\times10^{-4}(T-83.8058)^{0.75}(234.3156-T)^{0.75}$
234.3156 to 273.16	$1.1\times10^{-5}(T-234.3156)^{2}(273.16-T)$

Figure 7.4 shows the standard deviations versus temperature for the data of Figure 7.3 as well as functions fitted to the measured standard deviations. The functions are given in Table 7.2.

In the temperature range between 0 ºC and 962 ºC there is limited data on Type 3 non-uniqueness because of the problems with oxidation and drift of SPRTs. Most data is based on calibrations at redundant fixed points, e.g. Ancsin and Murdock (1990), Strouse (1992b), Furukawa and Strouse (2001), Ancsin (2004, 2006), which are summarised in Figure 7.5. In all cases, the uncertainties given in Figure 7.5 include uncertainties propagated from the calibrating fixed points, oxidation effects, resistance measurements, and non-uniformity of the comparison media. Thus, the lower values at any point are likely to be a better estimate of the contribution of the non-uniqueness.

The paucity of data makes the development of an equation for the uncertainty due to non-uniqueness problematic. Fellmuth *et al*. (2005a) applied a constant value of 0.6 mK to represent the uncertainty for this temperature range; however, that neglects the knowledge that the uncertainty should be zero at the fixed points. Figure 7.5 shows an improved approximation based on quadratic functions that pass near the lowest points in the interpolation intervals. The equations for the curves are given in Table 7.3.

Table 7.3: Approximate expressions for uncertainty due to Type 3 non-uniqueness above 0 ºC.

Temperature range	Uncertainty / mK
0.01 ºC to 231.928 ºC	$1.5\times10^{-5}t(231.928-t)$
231.928 ºC to 419.527 ºC	$3\times10^{-5}(419.527-t)(t-231.928)$
419.527 ºC to 660.323 ºC	$3\times10^{-5}(660.323-t)(t-419.527)$
660.323 ºC to 961.78 ºC	$4\times10^{-5}(961.78-t)(t-660.323)$

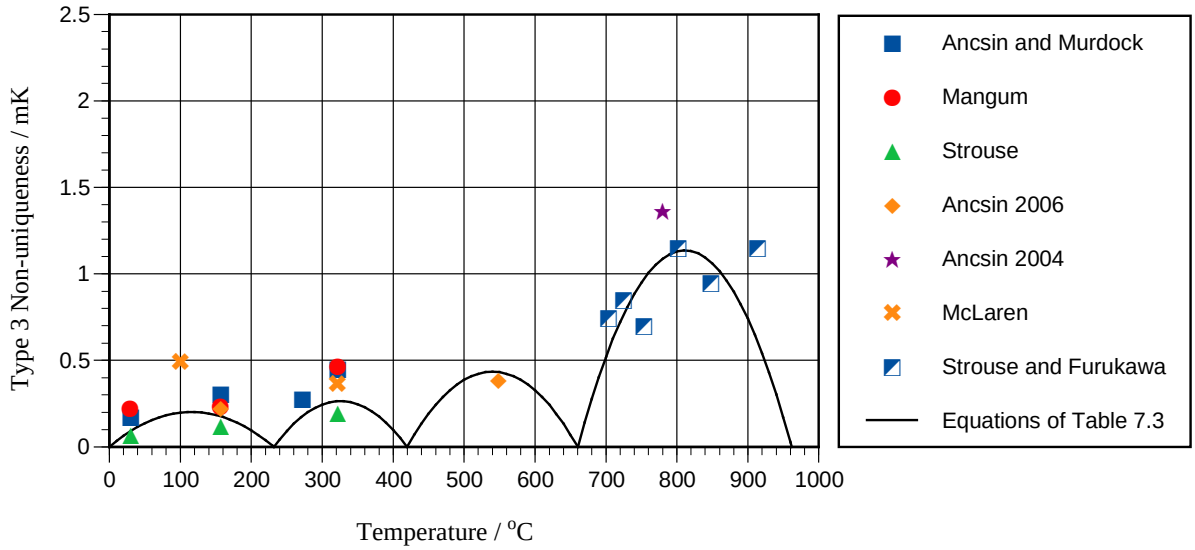

Figure 7.5: Summary of available data on Type 3 non-uniqueness of ITS-90 above 0 ºC. The data of Mangum and McLaren are from Hill and Woods (1992). The solid line shows the curves given by the polynomials of Table 7.3.

8. Resistance Measurement

Resistance measurements in platinum thermometry are usually made using automatic low-frequency resistance bridges. There are two basic types in common use that will be discussed here: ac bridges using a sinusoidal sensing current in the frequency range 10 Hz to 90 Hz, and the so-called dc bridges, which use a low-frequency square-wave (ac) sensing current in the range 0.01 Hz to 1 Hz. The bridges used for SPRT resistance measurements typically have a resolution of six to nine digits and a specified uncertainty in resistance ratio of between 2×10^{-8} and 5×10^{-6}, corresponding to equivalent uncertainties in temperature measurements ranging from about 5 μK to 2 mK, depending on the operating conditions. The bridges all employ a 4-terminal, or 4-terminal-coaxial, or guarded 4-terminal definition of resistance (Kibble and Rayner 1984) to reduce the effect of lead resistances and stray impedances. The major sources of uncertainty associated with the resistance measurements include the reference resistor value and its stability, and self-heating of the SPRT due to the sensing current. There are additional minor effects associated with the connecting cables and the resistance bridge itself.

8.1 *Reference Resistor*

Resistance Value and Temperature Coefficient

The two main contributions to the uncertainty in the value of the standard resistance can be evaluated using a simple model for the temperature dependence of the resistance:

$$R_S(t_{bath}) = R_S(t_{cal})\left[1+\beta(t_{bath}-t_{cal})\right], \tag{8.1}$$

where t_{bath} is the temperature of the oil or air bath used to maintain the resistor during use, t_{cal} is the temperature of the bath used to maintain the resistor when it was calibrated, and β is the temperature coefficient of the resistor. The temperature coefficient is normally expressed as the fractional change per degree; i.e.,

$$\beta = \frac{1}{R_S}\frac{dR_S}{dt}, \tag{8.2}$$

with typical values for good-quality resistors within the range $\pm 5 \times 10^{-6}$ /ºC.

If the resistor is not maintained at its calibration temperature, then a correction can be applied using (8.1). The cumulative uncertainty in the resistance value due to these terms is (for $\beta(t_{bath}-t_{cal}) << 1$)

$$u^2(R_S) = u^2(R_{S,cal}) + R_S^2\left[\beta^2 u^2(t_{bath}) + (t_{bath}-t_{cal})^2 u^2(\beta)\right], \tag{8.3}$$

where $u(R_{S,cal})$ is the calibration uncertainty as supplied by the electrical calibration laboratory, $u(t_{bath})$ is the uncertainty arising from fluctuations in the resistor-bath temperature, and $u(\beta)$ is the uncertainty in the temperature coefficient of the resistor. Where the t_{bath} and t_{cal} are nominally equal, the uncertainty in the temperature coefficient can usually be ignored.

Ac-dc differences

The calibration value for the standard resistor, $R_S(t_{cal})$, is nearly always the dc value. If the resistor is to be used with an ac resistance bridge, standard resistors with a low ac-dc difference should be used (Wilkins and Swan 1970) to minimise the additional uncertainty. For frequencies below 100 Hz, the dominant cause of ac-dc difference is the interaction of thermoelectric effects and the sensing current, which occurs with dc measurements only. There may be, additionally, contributions from stray inductance and capacitance, dielectric absorption, and eddy current effects. Some standard resistors exhibit relative ac-dc differences as large as 10^{-5}. With resistors of the Wilkins' design, the relative uncertainty due to ac-dc difference, $u(R_{S,ac\text{-}dc})$, is below 10^{-7}.

Power coefficient

In bridges based on dc current comparators (see for example McMartin and Kusters 1966), the current through the standard resistor changes with bridge reading. This causes variable power dissipation in the standard resistor and an error with a cubic dependence on the measured resistance ratio, X:

$$\Delta X_P = \frac{\Delta R}{R_S} = -I_0^2 R_S\left(\frac{R}{R_S}\right)^3\left(\frac{1}{R_S}\frac{\partial R_S}{\partial P}\right) = -I_0^2 R_S X^3\left(\frac{1}{R_S}\frac{\partial R_S}{\partial P}\right), \tag{8.4}$$

where P is the power dissipated in the standard resistor, and the term involving the derivative is the power coefficient. Electrical calibrations of standard resistors are normally carried out at a specified power. The power coefficient is the product of the temperature coefficient and the thermal resistance between the resistor windings and the environment, so good quality standard resistors are generally large bulky devices. The Wilkins' type resistors (Wilkins and Swan 1970) have a power coefficient of less than 4×10^{-6}/W. The error is typically no more than a few microkelvin, but can be more than 100 μK if a purpose-built standard resistor is not used. If sufficient time is allowed for the resistor to stabilise after current changes (tens of minutes), the effect is compensated by the self-heating correction for the SPRT.

Pressure coefficient

Some standard resistors, notably Thomas-type 1 Ω resistors, exhibit sensitivity to pressure. The effects arise from strain on the wire due to mechanical changes caused by pressure on air-filled cavities or other susceptible components in the resistors. For the Thomas-type resistors the effect is in the range 0.2 to 2.5 ppm per atmosphere. For typical daily variations in atmospheric pressure, the effects can be at the level of a few tenths of a ppm, and will influence high-resolution measurements. More significant are the changes in immersion depths in oil baths and changes in altitude, which can cause changes as large as 0.5 ppm. The pressure effect is generally linear and modelled as (Karlsson and Sørsdal (1995/96)):

$$R_S(p) = R_S(p_{cal})\left[1+\gamma(p-p_{cal})\right], \tag{8.5}$$

where γ is the pressure coefficient, and p_{cal} is the calibration pressure.

The total uncertainty in the standard resistance value is

$$u^2_{total}(R_S) = u^2(R_{S,cal}) + R_S^2\left[\beta^2 u^2(t_{bath}) + (t_{bath}-t_{cal})^2 u^2(\beta)\right] + u^2(R_{S,ac\text{-}dc}) + u^2(R_{S,power}) + u^2(R_{S,p}) . \tag{8.6}$$

The propagation of the various terms in (8.6) depends on the how the resistance-measurement results are used. Section 8.4 collates the various resistance measurements terms and describes the propagation of these uncertainties in detail. Witt (1998) gives a good summary of the limitations of standard resistors and methods for assessing their performance.

8.2 *Connecting cables and lead resistances*

Figure 8.1 shows a simplified equivalent circuit for the measurement of a 4-terminal resistance. The circuit includes the finite shunt resistance of the connecting cables. The model can also be used to characterise the input and output impedances of the bridge, hence the following nomenclature: R_{out} is the resistance shunting the current source I_0, and R_{in} is the resistance shunting the voltage measurement V_m. The equivalent circuit also includes the lead resistances R_L in each of the four leads to the measured resistance.

Analysis of Figure 8.1 shows that the error in the measured resistance ratio, X, (the bridge reading in resistance ratio) is well approximated by

$$\Delta X(t) = \frac{1}{R_S}\left(\frac{V_m}{I_0} - R(t)\right) \approx -\left(\frac{R(t)}{R_S}\right)^2 \frac{R_S}{R_{eff}} - \left(\frac{R(t)}{R_S}\right)\frac{R_L}{R_{eff}} = -X(t)^2\frac{R_S}{R_{eff}} - X(t)\frac{R_L}{R_{eff}} , \tag{8.7}$$

where

$$R_{eff} = \frac{R_{out}R_{in}}{R_{out}+R_{in}} .$$

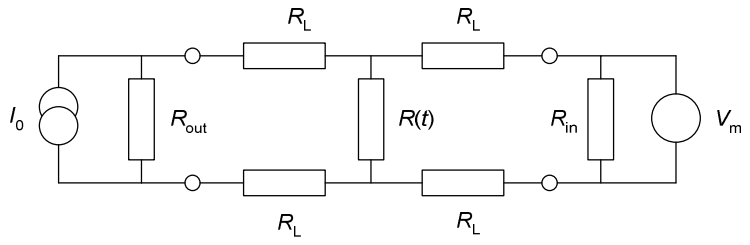

Figure 8.1: The equivalent circuit for a 4-terminal resistance measurement.

Thus, the finite resistances, R_{out} and R_{in}, give rise to an error proportional to the square of the resistance ratio. With care, cable shunt resistances can normally be maintained at greater than 10^{10} Ω, ensuring the coefficient R_S/R_{eff} is well below 10^{-8}. With poor or very long cables, the coefficient can be as large as 10^{-6} or more. In particular, significant effects can be observed in unscreened cables immersed in oil (the standard resistor bath), and with some coloured PVC cables. With ac bridges, dielectric loss in the cables gives rise to a similar error that increases as the square of the resistance, as described by (8.7), and increases linearly with frequency. Dielectric loss can be a major problem in low temperature measurements where many meters of lead wire is used for thermal anchoring. Operating an ac bridge at low frequencies or using a dc bridge can significantly reduce the effects. The effects of lead resistances are usually negligible in comparison to the effects of the finite cable shunt resistance since $R_L \le R_S$ in most resistance measurements.

In ac bridges, the measurements can also be affected by the stray capacitance and inductance of the connecting cables. Any capacitance in parallel with $R(t)$ (Figure 8.1) causes the impedance 'seen' by the resistance bridge to be

$$Z(t) = \frac{R(t)}{1+\omega^2 R(t)^2 C^2} - \frac{j\omega R(t) C}{1+\omega^2 R(t)^2 C^2}, \tag{8.8}$$

where $\omega = 2\pi f$ is the angular frequency, C is the cable capacitance (about 100 pF/m for coaxial and twisted pair cable), and $j = \sqrt{-1}$ represents a 90º phase shift. The real part of (8.8) is the resistance seen by an ideal ac thermometry bridge; the imaginary part contributes to the quadrature component of the bridge signal, which must be balanced or rejected by the bridge. The real part of (8.8) contributes a resistance ratio error with a cubic dependence on the measured resistance ratio:

$$\Delta X(t) = \frac{\mathrm{Re}\left(Z(t)\right) - R(t)}{R_S} \approx -\omega^2 C^2 R_S^2 \left(\frac{R(t)}{R_S}\right)^3 = -\omega^2 C^2 R_S^2 X(t)^3 . \tag{8.9}$$

For a bridge with a 100 Ω standard resistor operating at 100 Hz, and measuring an SPRT with relatively short coaxial leads (a pair of 3 m cables, C = 600 pF), the coefficient of $X(t)^3$ is about 10^{-9} (about 1 μK for a 25 Ω SPRT), so the effect is usually negligible. However, because of the quadratic dependence on capacitance, in measurement systems with multiplexers and long leads, the capacitance may overload the quadrature-balance capability of the bridge or lead to relative errors in resistance ratio as large as 10^{-4} (many millikelvin).

AC bridges used at low temperatures may also be affected by the self-inductance of the long high-resistance lead wires required to prevent unwanted thermal conduction in cryogenic systems. In principle, the measured resistance is independent of the inductance (unlike the case for capacitance). However, the large quadrature signal can overload the bridge leading to excessive noise.

For dc resistance bridges the effect of stray capacitance is complicated by the many harmonics in the 'square-wave' sensing current, but normally below the limit of detection. Where detectable, it is apparent with changes in the current-reversal times and settling times (Zhang and Berry 1985).

In systems with short leads, most cable effects can be treated as fault conditions and reduced to negligible levels with care, and hence the application of corrections and consideration of the uncertainties due to cable effects is not usually necessary.

8.3 *The resistance bridge*

Some of the sources of error within thermometry bridges and bridge calibration methods are summarized in White (2003b). Rudtsch *et al*. (2005), Strouse and Hill (2003), and White (1996) give additional information on typical performance of some resistance bridges. The sources of error in bridges include noise, large scale or 'integral' non-linearities, and short-range or 'differential' non-linearities.

The resolution of a bridge is determined by a combination of the thermal noise generated in all resistances and amplifiers, and quantisation error due to the conversion of the signal to a digital reading. The resolution is readily measured as the standard deviation, $u(X_{noise})$, when measuring a single stable resistance, and can be reduced by decreasing the operating bandwidth of the bridge or, equivalently, increasing the measurement time or averaging results. In high-quality bridges, standard deviations in resistance ratio below 10^{-8} (~10 μK) are readily obtainable.

Additional noise in the resistance measurement may arise from electromagnetic interference (EMI). In the high-temperature fixed points, electrical noise coupled from ac power supplies and controllers can introduce noise at the level of a millikelvin (many times higher than the thermal noise in the bridge). A second source of EMI is electric motors close to the measurement circuit. These include stirrer motors for calibration and standard resistor baths. A more insidious source of noise is other ac resistance bridges operating nearby on the same

carrier frequency. In a bridge with resolution limited by thermal noise, the standard deviation of measurements will change as the square root of the bandwidth or measurement time. If EMI due to ac machinery is present then often the standard deviation changes more rapidly.

Large-scale or integral non-linearities (INL) are those that change slowly over a wide range of bridge readings (see Figure 8.2). These effects tend to be caused by finite input and output impedances, power coefficients, finite gains, and stray capacitance and resistance of sub-circuits of the bridge. They, therefore, tend to have correction equations with terms ranging up to a quadratic or cubic dependence on bridge reading, much like (8.4), (8.7) and (8.9):

$$\Delta X_{\mathrm{INL}} = A_0 + A_1 X + A_2 X^2 + A_3 X^3 , \tag{8.10}$$

where A_1, A_2, … are coefficients determined during the calibration of the bridge. The uncertainty due to INL, $u(X_{\mathrm{INL}})$, may be the uncertainty in the INL correction or the uncertainty due to INL where no correction is applied.

With many bridges, the INL effects are below the manufacturers' accuracy specification and, therefore, less significant than many other sources of uncertainty. INL errors larger than the bridge manufacturer's specification are usually indicative of a faulty sub-circuit within the bridge or poor adjustment. Additionally, because ITS-90 is defined in terms of resistance ratio, only the non-linear bridge errors (offsets, quadratic, and cubic terms) propagate and affect the temperature measurement. Further, if the same bridge is used for the calibration and use of an SPRT, then the SPRT interpolating equations largely correct the INL errors of the bridge (see Section C.3). In such cases the INL correction and uncertainty can be omitted from the uncertainty analysis.

Differential non-linearities (DNL) are short-range errors commonly caused by errors in the transformer windings or analogue-to-digital converters in the bridge. The errors are typically different for every possible reading and too complex to measure, model and correct (see Figure 8.2). As with integral non-linearities, the effects tend to be below the manufacturers' specifications, but can increase with time and mechanical vibration as transformer cores lose magnetic permeability, and ADC circuits drift out of adjustment. DNL error is the dominant source of uncertainty in resistance measurements for high resolution or differential measurements (e.g., fixed-point comparisons and self-heating measurements). The magnitude of the resulting uncertainty can be inferred from the standard deviation of residual error in the calibration curves for bridges.

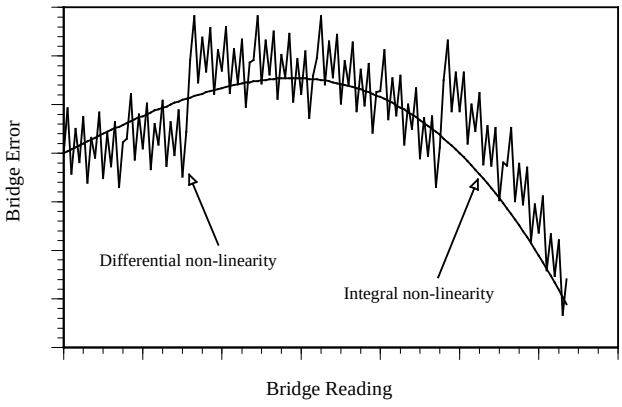

Figure 8.2: Graphical representation of the non-linearity of a resistance bridge including integral non-linearity (INL) and differential non-linearity (DNL). The smooth curve shows the INL only. The jagged curve is the sum of the INL and DNL.

Overall the uncertainty in bridge readings can be modelled as

$$u^2\left(X_{\mathrm{bridge}}\right) = u^2\left(X_{\mathrm{INL}}\right) + u^2\left(X_{\mathrm{DNL}}\right) + u^2\left(X_{\mathrm{noise}}\right). \tag{8.11}$$

The relative magnitude of the various components in (8.11) depends on the bridge architecture. In bridges using voltage or current dividers the DNL errors often dominate and are similar for every reading. The noise term tends to be smaller but varies with the sensing current (White 2003). Experience suggests that for a bridge in good working order (about 1 in 6 bridges are not, see White (1996)) the uncertainties in the INL and DNL are similar in magnitude and less than half the manufacturer's specified accuracy. In bridges, or resistance meters using integrating or sigma-delta analogue-to-digital converters, the DNL errors are usually insignificant and INL

errors dominate. The values for the various uncertainty terms may depend on the bridge operating conditions so the bridge should be calibrated and the uncertainties assessed under the conditions in which it is to be used.

In the propagation of the various terms of (8.11) it should be kept in mind that the INL errors are the same over a wide range of readings, the DNL errors are random for different readings but the same over time, and noise effects are purely random.

8.4 *Self-heating*

The measurement of resistance necessarily involves passing a current through the resistor and, therefore, heating of the resistor. For the small temperature changes typical of thermometry, the effect generally obeys Fourier's law: the temperature rise is directly proportional to the power dissipated. For new or unusual measurements, in the low-temperature regime, or where convection may occur, Fourier's' law should be confirmed. A simple model (Batagelj *et al*., 2003) shows the temperature of the sensor is

$$T(I) = T(I=0) + I^2 R(t)(r_{\text{int}} + r_{\text{ext}}), \tag{8.12}$$

where I is the rms sensing current, $R(t)$ is the resistance of the SPRT, and r_{int} and r_{ext} are the internal and external components, respectively, of the thermal resistance between the SPRT and its surroundings. The two thermal resistances are strongly dependent on the construction of the SPRT, particularly the length, diameter and the geometry of the sensor winding, and the fill gas used for the thermometer. For a 25 Ω SPRT at the triple point of water the temperature rise is in the range 0.3 mK/mA^2 to 7 mK/mA^2.

While the internal component of the thermal resistance is a constant at a given temperature, the external component is dependent on the SPRT surroundings. For example, this leads to about a 0.1 mK variation in self heating in a water-triple-point measurement due to the variation in the thickness of the water film surrounding the thermometer well, and several tenths of millikelvin variation between cells. Similarly, the forced convection, heat capacity and viscosity of the fluid influence the self-heating in a stirred calibration bath (Batagelj *et al*., 2003).

For the highest accuracy measurements, corrections should be applied by measuring at two currents, I_1 and I_2, and extrapolating to zero current. In order to make the correction by this method it is necessary for the measured temperature to be stable. Because of the small temperature changes and the linearity of the SPRT, the correction can be done in terms of the SPRT resistance, $R(I)$, or bridge reading (resistance ratio), $X(I)$:

$$\begin{aligned} X(0) &= X(I_1) + \Delta X_{\text{sh}} = X(I_1) - \frac{I_1^2}{I_2^2 - I_1^2}\left(X(I_2) - X(I_1)\right) \\ &= \frac{I_2^2}{I_2^2 - I_1^2} X(I_1) - \frac{I_1^2}{I_2^2 - I_1^2} X(I_2). \end{aligned} \tag{8.13}$$

Note that we have defined the self-heating correction ΔX_{sh} to be that applied to the I_1 reading. Differentiation of this equation leads to the propagation-of-error equation

$$dX(0) = \frac{I_2^2}{I_2^2 - I_1^2} dX(I_1) - \frac{I_1^2}{I_2^2 - I_1^2} dX(I_2) - \frac{2I_2^2}{\left(I_2^2 - I_1^2\right)}\left[\frac{I_1^2\left(X(I_2) - X(I_1)\right)}{\left(I_2^2 - I_1^2\right)}\right]\left(\frac{dI_1}{I_1} - \frac{dI_2}{I_2}\right). \tag{8.14}$$

This equation has two pairs of terms, one pair for the errors in bridge ratios, and one pair for the errors in the sensing currents. We will consider these separately.

Uncertainty in sensing currents

There are three observations that can be drawn from (8.14). Firstly, the error due to the sensing-current error is proportional to the self-heating correction (the term in square brackets). Secondly, there is no error in the measured zero-current bridge reading if the relative errors in the currents are the same; i.e., if $\Delta I_1/I_1 = \Delta I_2/I_2$, so that the current ratio is correct. Finally, the relative uncertainty in the self-heating correction is approximately

$$\frac{u\left(X_{\text{sh},I}\right)}{\Delta X_{\text{sh},I}} \approx \frac{2\sqrt{2}I_2^2}{\left(I_2^2 - I_1^2\right)^2}\left(\frac{u(I)}{I}\right). \tag{8.15}$$

For $I_2 = \sqrt{2} I_1$, and 1% uncertainties in the sensing currents, the propagated uncertainty in the self-heating correction is 5.6% of the correction (about 80 μK uncertainty for a SPRT with 1.4 mK self heating at I_1). The uncertainties in the sensing-current ratios typically vary between about 0.1% and 1%, but can be as large as several percent for some current ratios. Often the 1:√2 current ratios are the most accurate. In measurements requiring high resolution, such as fixed-point comparisons, it is essential to measure and confirm the current ratios.

For measurements of SPRT resistance ratio, *W*, there is a small reduction in uncertainty if the same bridge and the same sensing currents are used for the two resistance measurements:

$$u^2\left(W_{\mathrm{sh},I}\right) = \frac{8I_2^4}{\left(I_2^2 - I_1^2\right)^2}\left(\frac{u^2(I)}{I^2}\right)\frac{1}{X_{\mathrm{H2O}}^2}\left(\Delta X_{\mathrm{sh}} - W\Delta X_{\mathrm{sh,H2O}}\right)^2 . \tag{8.16}$$

Where a single bridge and the same sensing currents are used for all resistance measurements, the SPRT interpolation process interpolates between the errors in the self-heating corrections, further reducing the effect of the sensing current mismatch (see (C.28) and accompanying discussion):

$$u_{\mathrm{sh},I}^2(W) = \frac{8I_2^4}{\left(I_2^2 - I_1^2\right)^2}\left(\frac{u_I^2}{I^2}\right)\frac{1}{X_{\mathrm{H2O}}^2}\left(\Delta X_{\mathrm{sh}} - \sum_{i=1}^{N} f_i(W)\Delta X_{\mathrm{sh},i}\right)^2 . \tag{8.17}$$

Propagated uncertainty in bridge readings

The propagation of error equation for the zero-current bridge reading, including terms due to the bridge errors is, from (8.14),

$$dX(0) = \frac{I_2^2}{I_2^2 - I_1^2}\left(dX_{\mathrm{INL}} + dX_{1,\mathrm{DNL}} + dX_{1,\mathrm{noise}}\right) - \frac{I_1^2}{I_2^2 - I_1^2}\left(dX_{\mathrm{INL}} + dX_{2,\mathrm{DNL}} + dX_{2,\mathrm{noise}}\right). \tag{8.18}$$

Note that the INL error is the same for the two readings, because the two readings are very close, while the DNL error and noise contributions are assumed to be independent. Thus, the sensitivity coefficient for the INL errors is 1, while the sensitivity coefficients for the other terms are functions of the sensing currents:

$$u^2\left(X(0)\right) = u^2\left(X_{\mathrm{INL}}\right) + \frac{\left(I_2^4 + I_1^4\right)}{\left(I_2^2 - I_1^2\right)^2}u^2\left(X_{\mathrm{DNL}}\right) + + \frac{I_2^4}{I_2^2 - I_1^2}u^2\left(X_{1,\mathrm{noise}}\right) + \frac{I_1^4}{I_2^2 - I_1^2}u^2\left(X_{2,\mathrm{noise}}\right). \tag{8.19}$$

Note too that the self-heating correction involves extrapolation to zero current, and with extrapolation, there is usually an amplification of uncorrelated uncertainties. In this case, the amplifying factor for the uncertainties is $\left(I_2^4 + I_1^4\right)^{1/2} \Big/ \left(I_2^2 - I_1^2\right)$.

Total uncertainty in resistance measurements

In principle, the extrapolation to zero current ((8.13) and (8.18)) should be carried out in terms of the measured resistance rather than bridge reading, and errors in each resistance measurement propagated according to $dR = R_{\mathrm{s}}dX + XdR_{\mathrm{s}}$ (i.e., (8.18) should be in terms of resistance and include the errors due to the standard resistor). However, with the exception of the bath stability term of (8.3), all of the terms arising from the standard resistor are the same for each bridge reading and combine in the same way as the INL error terms of (8.19). Hence the total uncertainty in a measured zero-current resistance due to the standard resistor, bridge effects, and the match of the sensing currents is

$$u^2(R_{\text{meas}}) = X^2\left(u^2(R_{\text{S,cal}}) + R_{\text{S}}^2(t_{\text{bath}} - t_{\text{cal}})^2 u^2(\beta) + u^2(R_{\text{S,ac-dc}}) + u^2(R_{\text{S,power}}) + u^2(R_{\text{S},p})\right) + \frac{\left(I_2^4 + I_1^4\right)}{\left(I_2^2 - I_1^2\right)^2} R_{\text{S}}^2 X^2 \beta^2 u^2\left(t_{\text{bath}}\right)$$
$$+ R_{\text{S}}^2 u^2(X_{\text{INL}}) + \frac{R_{\text{S}}^2}{\left(I_2^2 - I_1^2\right)^2}\left[\left(I_2^4 + I_1^4\right)u^2(X_{\text{DNL}}) + I_2^4 u^2(X_{1,\text{noise}}) + I_1^4 u^2(X_{2,\text{noise}})\right]$$
$$+ 4R_{\text{S}}^2 \Delta X_{\text{sh}}^2 \frac{I_2^4}{\left(I_2^2 - I_1^2\right)^2}\left(\frac{u^2(I_1)}{I_1^2} + \frac{u^2(I_2)}{I_2^2}\right). \tag{8.20}$$

When calculating a resistance ratio from two such resistance measurements made with the same standard resistor, all but the bath stability term associated with the standard resistor cancel (see equation (C.25)). The resulting uncertainty in a measured resistance ratio is

$$u^2\left(W_{\text{meas}}\right) = \frac{\left(1+W^2\right)}{X_{\text{H2O}}^2}\left[u^2\left(X_{\text{INL}}\right) + \frac{\left(I_2^4 + I_1^4\right)}{\left(I_2^2 - I_1^2\right)^2}\left(X^2\beta^2 u^2\left(t_{\text{bath}}\right) + u^2\left(X_{\text{DNL}}\right) + u^2\left(X_{\text{noise}}\right)\right)\right] \tag{8.21}$$
$$+ \frac{\left(\Delta X_{\text{sh}} - W\Delta X_{\text{sh,H2O}}\right)^2}{X_{\text{H2O}}^2} \frac{8I_2^4}{\left(I_2^2 - I_1^2\right)^2}\left(\frac{u^2(I)}{I^2}\right).$$

Note that we have ignored the correlation in the two INL terms (which is likely if W is close to 1), and assumed the bridge noise and sensing current uncertainties are the same for all measurements. Equation (8.20) is usually dominated by the terms due to the bath instability and bridge DNL and is not correlated, therefore, with similar terms for other resistance ratios; it propagates according to (C.14).

9. Total Uncertainty in SPRT Measurements

The many interpolating equations of the ITS-90 greatly complicate the propagation of uncertainty for temperatures measured using SPRTs. The complications arise from the variety of subranges, the option to use either single or multiple triple-point-of-water measurements, possibly with different water-triple-point cells, and the options for the use of different resistance bridges or standard resistors for different resistance measurements. In principle, each of these possibilities results in a different equation for total uncertainty. The complexity of ITS-90 is such that **it is generally impractical to obtain correct mathematical expressions for total uncertainty without some supporting mathematics.** This section covers in detail most of the cases routinely met during calibration and application of SPRTs. For cases not covered here, the reader is referred to Appendix C, which provides the mathematical background for the development of the uncertainty expressions.

The equations for total uncertainty given below are detailed, and include and propagate all of the uncertainty terms identified in previous sections. While this detail may seem excessive, it is expected that the uncertainty analyst will rapidly learn which terms of the equations are insignificant in the user's applications and can be safely neglected.

Some sections below also provide graphs giving numerical values for some of the uncertainty contributions and the total uncertainty. The values in these graphs are purely indicative, and are given only to illustrate the approximate magnitude and temperature dependence of the various contributions. Users are expected to determine uncertainties appropriate to their measurements and use these in the equations.

Although the equations below identify each contribution to the total uncertainty, it is not essential that distinct values of uncertainty are determined for each source of uncertainty; usually it is sufficient that all terms have been identified and considered. In some cases, experiments can be designed to assess the collected contribution of several terms (e.g., Nguyen and Ballico 2008). If distinct values are required for each contribution, it is also possible to use ANOVA techniques to determine values for the individual terms contributing to a Type A uncertainty (Filipe 2008).

Appendix A gives values for the range of some of the contributions to the uncertainty in fixed-point measurements. These values are also indicative. Most of the ranges encompass the uncertainties reported from recent measurement comparisons[5], as well as the expected extremes determined from the application of the models given in previous sections.

9.1 *The fixed-point sensitivity coefficients*

Many of the effects discussed in previous sections influence the calibration of SPRTs at the fixed points. Through the SPRT interpolating equations, these effects propagate to temperatures between the fixed points. The relationship between the fixed-point errors (or uncertainties) and errors (or uncertainties) at other temperatures are described by the fixed-point sensitivity coefficients.

The ITS-90 specifies the mathematical relationship between measured SPRT resistance and temperature. This follows a three-step process converting measured resistance first to resistance ratio, then reference resistance ratio, and finally to temperature: $R \rightarrow W \rightarrow W_r \rightarrow T_{90}$. The step $W \rightarrow W_r$ is the most complicated since it is an interpolation and is different for all of the ITS-90 subranges. Figure 9.1 shows graphically the interpolation process for two SPRT calibrations over the water–aluminium subrange. Note the mapping from $W \rightarrow W_r$.

The solid curve of Figure 9.1 passes through all four marked points. For the second curve (dotted), a small error has been introduced into the measured zinc-point value, W_{Zn}. The new curve passes through the new zinc point but continues to pass through the other, original calibration points. The difference between the two curves is the fixed-point sensitivity coefficient for the zinc point for this subrange. It shows how an error in the zinc-point measurement propagates to W_r values, and hence to temperatures, in between the fixed points. Such sensitivity coefficients occur repeatedly in SPRT uncertainty analysis. Therefore, to simplify the various mathematical expressions for total uncertainty we will represent the sensitivity coefficients simply as functions of W using a lower case f, for example $f_{Zn}(W)$; the subscript identifies the fixed point, and the subrange is usually apparent from the context.

Appendix C provides a detailed explanation of the derivation and mathematical properties of the sensitivity coefficients. This appendix also includes a tutorial introduction to the ITS-90 interpolating equations and some methods for reducing uncertainty. Approximate expressions for the sensitivity coefficients for all of the SPRT subranges are given in Appendix D, along with two methods for calculating the functions.

---

[5] For comparisons involving the water triple point, see Stock and Solve (2006), Renaot *et al*. (2005).
For comparisons involving low temperature fixed points (< 0 °C) and SPRTs, see Steele *et al*. (2002a), Fellmuth *et al*. (1999, 2003b), Head *et al*. (1997), Pavese *et al*. (1984).
For comparisons involving high-temperature fixed points (> 0 °C) and SPRTs, see Mangum (2002b), Nubbemeyer and Fischer (2002).

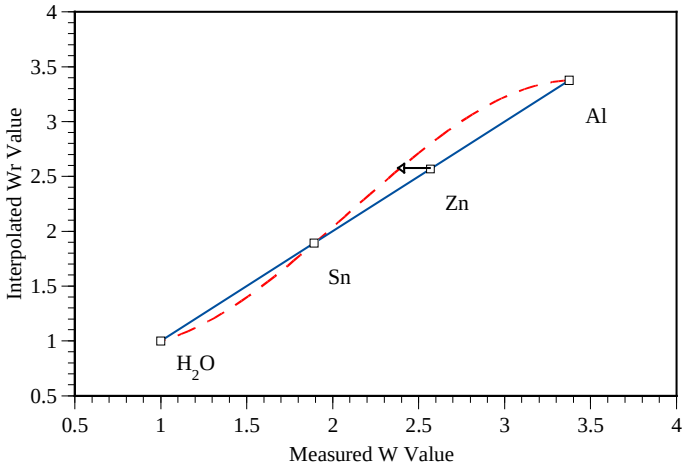

Figure 9.1: The influence of an error in a fixed-point measurement. The solid line shows an interpolation between the measured W values and the W_r values. The dotted line shows the effect of a small error in the measured W_{Zn} value. The difference in the two curves is the $f_{Zn}(W)$ sensitivity coefficient for the water-aluminium subrange.

9.2 *Methods for calculating total uncertainty*

Historically, to address the complexity of the ITS-90 equations, there have been a large number of different approaches for calculating total uncertainty. These can be catalogued into four basic methods.

Numerical analysis

This involves repeated numerical solution of the interpolating equations with the measurement results varied according to their uncertainties. This was the approach adopted during the development of the ITS-90. In recent years it has become more accessible with the advent of software applications that carry out Monte Carlo analysis (e.g. @Risk®) or propagate uncertainty (e.g. Maple®). The analyst must follow the exact procedure followed for the calculation of the temperature; departures and simplifications may inadvertently invoke assumptions about the nature of correlations and may lead to incorrect results. The equations given here and in Appendix C provide a guide.

Direct algebraic application of the ISO Guide

This is the conventional algebraic approach and there are a number of published examples including Sadli *et al* (1998), and Palenčár *et al*. (2000). The approach has the appeal of simple principles but is suitable for simple cases only. It quickly becomes cumbersome when applied to complex subranges, and when the effects of correlations between water-triple-point terms are included.

Mixed Numerical and algebraic approaches

It is often convenient to use numerical analysis to determine the fixed-point sensitivity coefficients, and then use algebra to guide the calculation of total uncertainty. Meyer and Ripple (2006) give an example treating six different cases combining variations in the treatment of the SPRT and the instruments used. Again, care is required to follow the exact procedure used for the calculation of the temperature in order to avoid errors.

Application of the ISO guide via interpolation theory

An alternative algebraic approach to uncertainty analysis involves rewriting the SPRT interpolation equations in terms of a set of interpolating functions, which are also the fixed-point sensitivity coefficients (White and Saunders (2000, 2007), and White (2001)). With modest effort, the approach rapidly becomes intuitive and greatly simplifies the equations for total uncertainty. This was the approach used in the development of the equations given below. Appendix C and White and Saunders (2007) provide the mathematical background.

9.3 *Uncertainty in SPRT resistance at the triple point of water (reported value)*

The main purpose of the triple-point-resistance value reported on a calibration certificate is to enable users of the SPRT to assess the stability of the SPRT and detect major changes that may have occurred through shipping, or to detect damage that may have occurred during use. For this purpose, it is best if the SPRT is in its most reproducible state.

Assumption:

- The SPRT is well annealed and heat-treated so that it is strain-, vacancy-, and oxide-free. The value of the triple-point resistance in this state may be different from that used for the calculation of resistance ratios or temperature.

There are three steps to calculating the triple-point resistance.

Step 1: correct the measured bridge ratio for the bridge INL errors (Sec. 8.3) and the self-heating effect (Sec. 8.4):

$$X_{\mathrm{corr}}(t) = X_{\mathrm{meas}}(t) + \Delta X_{\mathrm{INL}} + \Delta X_{\mathrm{sh}} \,. \tag{9.1}$$

Step 2: multiply the corrected bridge reading by the value of the standard resistor (Sec. 8.1):

$$R_{\mathrm{meas}}(t) = R_{\mathrm{S}}(t_{\mathrm{cal}})\left[1+\beta(t_{\mathrm{bath}}-t_{\mathrm{cal}})\right]\left[X_{\mathrm{meas}}(t) + \Delta X_{\mathrm{INL}} + \Delta X_{\mathrm{sh}}\right]. \tag{9.2}$$

Step 3: apply the various corrections for errors in the realisation of the water triple point:

$$R_{\mathrm{H2O,\,report}} = R_{\mathrm{meas}}(t) + R_{\mathrm{H2O}}\frac{dW_1}{dt}\left(\Delta t_{\mathrm{hyd}} + \Delta t_p + \Delta t_{\mathrm{imp}} + \Delta t_{\mathrm{liq}} + \Delta t_{\mathrm{iso}} + \Delta t_{\mathrm{ther}} + \Delta t_{\mathrm{dyn}}\right). \tag{9.3}$$

Note that there are no corrections for SPRT effects (oxidation, strain, vacancies, contamination, and insulation leakage) because the SPRT is assumed to be in its most well defined state. Uncertainties associated with these effects characterise departures from this state when the SPRT is later used to measure a temperature.

The total uncertainty in the zero-current water-triple-point resistance, determined using sensing currents of I_1 and I_2, is

$$\begin{aligned} u^2(R_{\mathrm{H2O}}) = {} & \left(R_{\mathrm{H2O}}\frac{dW_{\mathrm{H2O}}}{dt}\right)^2\left[u^2(\Delta t_{\mathrm{hyd}}) + u^2(\Delta t_p) + u^2(\Delta t_{\mathrm{imp}}) + u^2(\Delta t_{\mathrm{liq}}) + u^2(\Delta t_{\mathrm{iso}}) + u^2(\Delta t_{\mathrm{ther}}) + u^2(\Delta t_{\mathrm{dyn}})\right] \\ & + X_{\mathrm{H2O}}^2\left(u^2(R_{\mathrm{S,cal}}) + R_{\mathrm{S}}^2(t_{\mathrm{bath}}-t_{\mathrm{cal}})^2u^2(\beta) + u^2(R_{\mathrm{S,ac\text{-}dc}}) + u^2(R_{\mathrm{S,power}}) + u^2(R_{\mathrm{S},p})\right) + R_{\mathrm{S}}^2u^2(\Delta X_{\mathrm{INL}}) \\ & + \frac{R_{\mathrm{S}}^2}{\left(I_2^2-I_1^2\right)^2}\left[\left(I_2^4+I_1^4\right)\left(u^2(\Delta X_{\mathrm{DNL}}) + X^2\beta^2u^2(t_{\mathrm{bath}})\right) + I_2^4u^2(X_{1,\mathrm{noise}}) + I_1^4u^2(X_{2,\mathrm{noise}})\right] \\ & + 8R_{\mathrm{S}}^2\Delta X_{\mathrm{sh}}^2\frac{I_2^4}{\left(I_2^2-I_1^2\right)^2}\left(\frac{u^2(I)}{I^2}\right), \end{aligned} \tag{9.4}$$

where the first line follows from (9.3), and the remaining lines follow from (8.20).

9.4 *Uncertainty in SPRT resistance ratio at fixed points*

In general, when measuring the resistance at the gallium, indium, tin, or zinc points, it is not possible to keep the SPRT in an oxide-free state (Section 6.1).

Assumptions:

- For fixed-point measurements other than the water triple point, the SPRT was initially well annealed. During exposure at the fixed-point temperature, the SPRT's oxidation state may have changed, and at higher temperatures, the vacancy concentration has been allowed to come to equilibrium.
- For water-triple-point measurements, the SPRT is in the same oxidation state as for the corresponding fixed-point measurement.
- For temperatures above room temperature and below 450 °C, the SPRT is cooled relatively quickly (<10 minutes) to room temperature to prevent further oxidation.
- If used at temperatures above 450 ºC, the SPRT is cooled sufficiently slowly (hours) to 450 °C to restore the low-temperature vacancy concentration, and then cooled relatively quickly (<10 minutes) to room temperature to prevent oxidation.

- The same standard resistor and resistance bridge are used for both measurements, and the standard resistor is at the same nominal temperature for both resistance measurements.

The steps followed are as for Section 9.3 except that the SPRT may be in a different oxidation state. Effects expected to cancel in the resistance ratio (according to the assumptions) are omitted.

The total uncertainty in the fixed-point resistance ratio is

$$u^2(W_i) = \frac{1}{R_{\mathrm{H2O}}^2}\left(u^2(R_i) + W_i^2 u^2(R_{i,\mathrm{H2O}}) + (1-Z)^2 W^2 u^2(R_{\mathrm{H2O,ox}})\right), \tag{9.5}$$

where the index i corresponds to the fixed points other than water, $u(R_{\mathrm{H2O,ox}})$ is the uncertainty in the SPRT-triple-point resistance due to variations in its oxidation state (from Equation (6.4), applies to Ga, In, Sn, and Zn points only), and

$$\begin{aligned} u^2(R_i) = {} & \left(R_i \frac{dW_i}{dt}\right)^2 \left[u^2(\Delta t_{\mathrm{hyd},i}) + u^2(\Delta t_{p,i}) + u^2(\Delta t_{\mathrm{imp},i}) + u^2(\Delta t_{\mathrm{liq},i}) + u^2(\Delta t_{\mathrm{iso},i}) + u^2(\Delta t_{\mathrm{ther},i}) + u^2(\Delta t_{\mathrm{dyn},i})\right] \\ & + R_S^2 u^2(\Delta X_{\mathrm{INL}}) + \frac{R_S^2}{\left(I_2^2 - I_1^2\right)^2}\left[\left(I_2^4 + I_1^4\right)\left(u^2(\Delta X_{\mathrm{DNL}}) + X^2\beta^2 u^2(t_{\mathrm{bath}})\right) + I_2^4 u^2(X_{1,\mathrm{noise}}) + I_1^4 u^2(X_{2,\mathrm{noise}})\right] \\ & + 8R_S^2 \Delta X_{\mathrm{sh},i}^2 \frac{I_2^4}{\left(I_2^2 - I_1^2\right)^2}\left(\frac{u^2(I)}{I^2}\right) \end{aligned} \tag{9.6}$$

is the uncertainty in the SPRT resistance value for each fixed point. The value of $u(R_{\mathrm{i,\,H2O}})$ is also given by (9.6) with values appropriate for the triple point of water (i = 1).

9.5 *An approximate expression for total uncertainty in interpolated resistance ratio, W_r*

Once the uncertainties in the resistance ratios have been calculated, it might seem that the next logical step is to combine the uncertainties in the fixed-point-resistance ratios to obtain the uncertainty in interpolated reference resistance ratio. However, as shown in Appendix C, directly combining the uncertainties in the resistance ratios $u(W_i)$ neglects correlations due to shared triple-point-resistance values or a common triple-point-of-water cell, and usually leads to a slight overestimate of the uncertainty for some W values. Nevertheless, so long as the uncertainties associated with the triple point of water are small, the approximation is very good. The approximation is especially convenient where the $u(W_i)$ values are reported on calibration certificates.

Assumptions:

- The uncertainties due to the water triple point are negligible, i.e. $u^2(R_i) >> W_i^2 u^2(R_{\mathrm{H2O}})$ in (9.5).
- The uncertainties due to resistance measurements are negligible.

The uncertainty in the interpolated reference resistance ratio is approximately

$$u^2(W_r) \approx u^2(W) + \sum_{i=2}^{N} f_i^2(W) u^2(W_i), \tag{9.7}$$

where $u(W)$ is the uncertainty in the resistance ratio for the unknown temperature, $u(W_i)$ are the uncertainties in the fixed-point resistance ratios from (9.5), and the $f_i(W)$ functions are the fixed-point sensitivity coefficients described in Appendix C and given in Appendix D.

The $u(W)$ term of (9.7) accounts for the uncertainties arising from the use of the SPRT to measure an unknown temperature. It must include any uncertainties associated with changes of SPRT state, such as oxidation, vacancy, and contamination effects, in addition to others associated with the measurement of resistance, the triple-point measurement, and the thermal conditions defining the unknown temperature.

Figures 9.2 and 9.3 compare the uncertainty calculated according to this approximation with the exact expressions given later in Sections 9.6 to 9.10. The calculations assume an uncertainty in the realisation of the water triple point of 0.1 mK, and an uncertainty in the resistance measurements of 5 μΩ. Note that the uncertainty values given in all figures in this section are indicative only; actual values may be greater or smaller depending on practice.

Figures 9.2 and 9.3 show that the approximation is very good at low temperatures, especially below 84 K, (9.7) where the W values that weight the water-triple-point uncertainties are small (see (9.5)). The approximation is also good for cases where the SPRT is used outside the calibration laboratory where the user does not have access to the same triple-point-of-water cell (the exact 'for client' curves of Figures 9.2 and 9.3). Where the SPRT is used 'in-house' so the user has access to the same triple-point-of-water cell, it may be better to use the exact 'in-house' expressions calculated in the sections below.

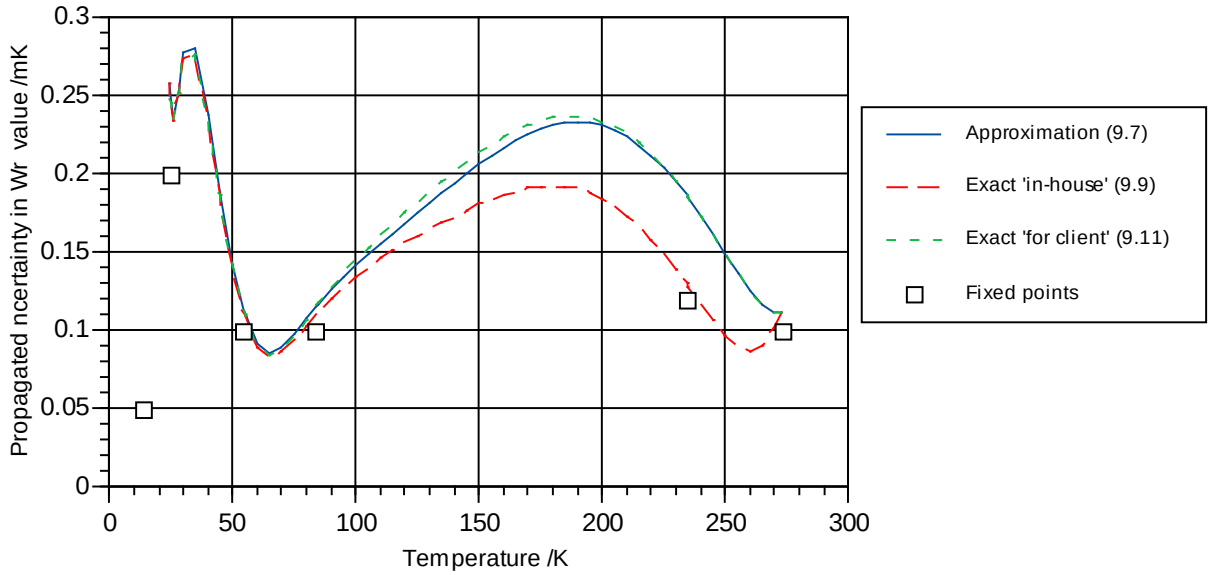

Figure 9.2: The propagated calibration uncertainty for the neon-water subrange, according to the different equations. The fixed-point uncertainties, as shown by the marked points, are indicative only. It is assumed that $u(W)$, the uncertainty in the W value in use, is zero.

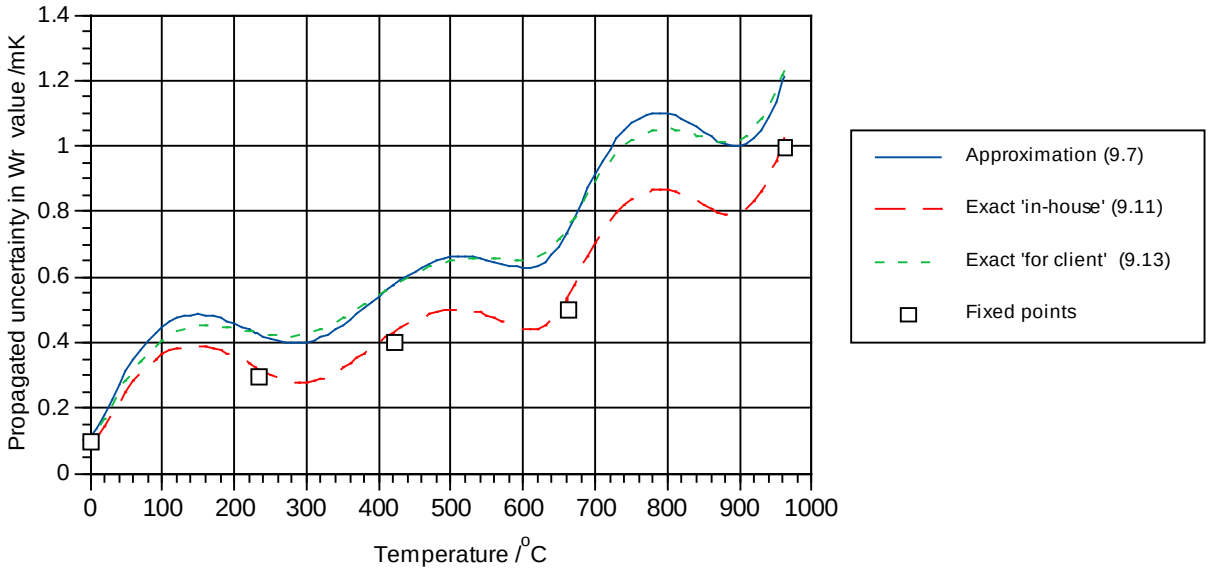

Figure 9.3: The propagated calibration uncertainty for the water-silver subrange, according to the different equations. The uncertainties for the fixed points, as shown by the marked points, are indicative only. It is assumed that $u(W)$, the uncertainty in the W value in use, is zero.

9.6 *Total uncertainty in measured temperature*

Once the uncertainty in the interpolated resistance ratio is calculated, the total uncertainty in the measured temperature is then given by

$$u^2_{\text{total}}(T) = \left(\frac{dT}{dW}\right)^2 \left[u^2(W_{\text{r}}) + u^2(\Delta W_{\text{SRI}}) + u^2(\Delta W_{\text{NU}})\right], \tag{9.8}$$

where $u(\Delta W_{\text{SRI}})$ and $u(\Delta W_{\text{NU}})$ are the uncertainties due to Type 1 (subrange inconsistency) and Type 3 non-uniqueness, as described in Section 7. The examples of Sections 9.7 and 9.8 below indicate the total uncertainty including these terms. Note that some of the expressions for the non-uniqueness in Section 7 give the uncertainty in temperature, so already include the dT/dW factor.

9.7 *Total uncertainty for capsule SPRTs used 'in-house'*

This example illustrates a measurement achieving the lowest practical calibration uncertainty for temperatures below 0 ºC.

Capsule SPRTs are generally used only below 0 ºC. This means that the SPRT triple-point resistance is extremely stable and it is possible to use a single water-triple-point resistance value for all calculations. This example treats this case. It is typical where the calibrated SPRT is used 'in-house' by the calibrating laboratory with the same value of triple-point resistance, and with the same resistance bridge and standard resistor as used for calibration of the SPRT.

Assumptions:

- Uncertainty due to SPRT oxidation (Section 6.1) is zero.
- Uncertainty due to SPRT vacancy and contamination effects (Section 6.2) is zero.
- The same resistance bridge and standard resistor are used for all measurements so that effects of standard resistor value (Section 8.1), cable effects, standard resistor power dissipation (Section 8.1), bridge INL error (Section 8.3), and sensing-current ratio errors can all be neglected.
- The same water-triple-point resistance is used for all calculations of resistance ratio.
- The uncertainties contributing to non-repeatability of measurements, i.e., resistance bath instability, bridge noise, and differential non-linearity, are all uncorrelated.
- The measurement at the unknown temperature is corrected for self-heating, and the uncertainty due to the sensing-current-ratio is negligible (8.15).

The total uncertainty in the interpolated W_{r} values is, from (C.22),

$$u^2_{\text{total}}(W_{\text{r}}) = \frac{1}{R^2_{\text{H2O}}}\left(u^2(R) + \sum_{i=1}^{N} u^2(R_i)\, f_i^{\,2}(W)\right), \tag{9.9}$$

where $u(R_i)$ collects all of the uncertainty terms associated with each of the calibrating fixed points including the triple point of water ($i = 1$):

$$\begin{aligned} u^2(R_i) = {} & \left(R_i \frac{dW_i}{dT}\right)^2 \left[u^2(\Delta t_{\text{hyd},i}) + u^2(\Delta t_{p,i}) + u^2(\Delta t_{\text{imp},i}) + u^2(\Delta t_{\text{liq},i}) + u^2(\Delta t_{\text{iso},i}) + u^2(\Delta t_{\text{ther},i}) + u^2(\Delta t_{\text{dyn},i})\right] \\ & + \frac{R_{\text{S}}^2}{\left(I_2^2 - I_1^2\right)^2}\left[\left(I_2^4 + I_1^4\right)\left(u^2(X_{\text{DNL}}) + X^2\beta^2 u^2(t_{\text{bath}})\right) + I_2^4 u^2(X_{1,\text{noise}}) + I_1^4 u^2(X_{2,\text{noise}})\right], \end{aligned} \tag{9.10}$$

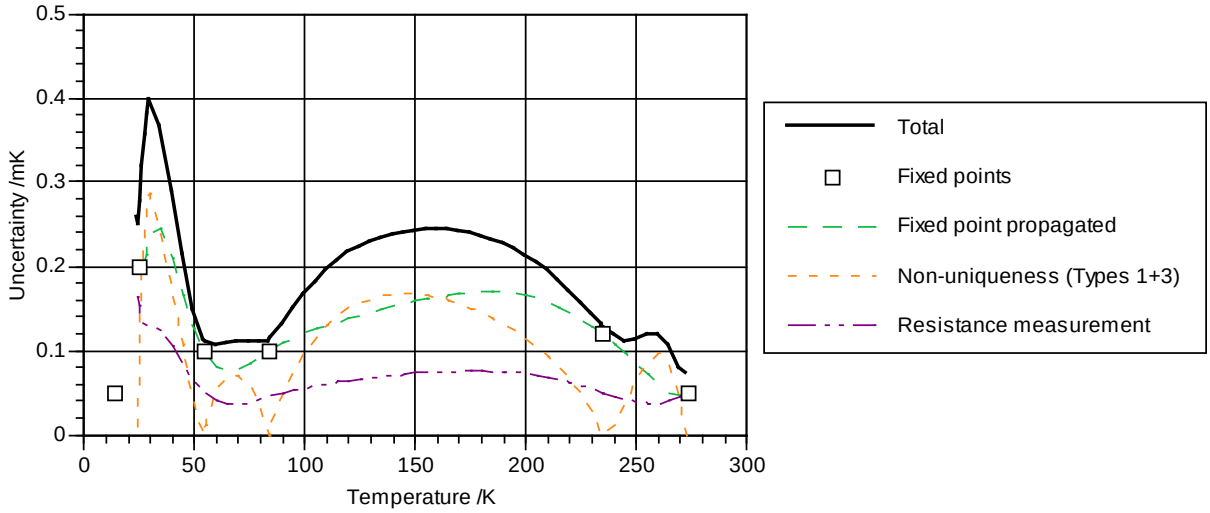

Figure 9.4: The contributions to the total calibration uncertainty for a 25 Ω capsule SPRT used 'in-house'. The calculated value includes the effects of non-uniqueness, the fixed point uncertainties are as indicated, the uncertainty in the resistance measurements is 5 μΩ, and the in-use uncertainty $u(R)$ is assumed to be zero.

The uncertainty $u(R)$ in (9.9) collects all of the terms associated with the measurement at the unknown temperature. This will include the resistance measurement terms of (9.10), terms associated with the realisation of the temperature, and terms characterising the thermal connection between the SPRT and the temperature of interest. The total uncertainty in a measured temperature is obtained using (9.8).

A numerical example of (9.9) for total uncertainty propagated from the fixed-point measurements is shown in Figure 9.4. This figure plots an example of the total propagated calibration uncertainty, including non-uniqueness, for this case. For the purpose of drawing the figure, $u(R)$ is set to zero.

9.8 *Total uncertainty for capsule SPRTs used outside the calibration laboratory*

This example is similar to the example above except that the calibrated SPRT is used by a 'client' to make measurements using a different water-triple-point cell and a different resistance bridge. The consequence of this change is that the uncertainties associated with the water-triple-point measurements propagate according to (C.23) instead of (C.22). In most applications, the procedure of Section 9.5 provides a very good approximation to this procedure (see Figure 9.2).

Assumptions:

- Uncertainty due to SPRT oxidation (Section 6.1) is zero.
- Uncertainty due to SPRT vacancy and contamination effects (Section 6.2) is zero.
- The client and calibration laboratory use different triple-point-of-water cells and resistance bridges.
- The same resistance bridge and standard resistor are used for all measurements in the calibration laboratory.
- The same resistance bridge and standard resistor are used by the user of the SPRT for all measurements of R and R_{H2O}.
- The uncertainties contributing to non-repeatability of measurements, i.e., resistance bath instability, bridge noise and differential non-linearity are all uncorrelated.
- The sensing-current ratio errors can be neglected in all self-heating corrections.
- The measurement at the unknown temperature is corrected for self-heating, and the uncertainty due to the sensing-current-ratio is negligible (8.15).

The total uncertainty in the interpolated W_{r} values is

$$u^2_{\mathrm{total}}(W_{\mathrm{r}}) = \frac{1}{R^2_{\mathrm{H2O}}}\Big[u^2(R) + W^2u^2(R_{\mathrm{H2O,client}}) + R^2_{\mathrm{S,client}}u^2(X_{\mathrm{INL,client}}) + R^2_{\mathrm{S,cal}}u^2(X_{\mathrm{INL,cal}}) + u^2(R_{\mathrm{H2O,cal}})\big(W - f_{\mathrm{H2O}}(W)\big)^2 + \sum_{i=2}^{N} u^2(R_i)\, f_i^2(W)\Big], \tag{9.11}$$

where $u(R_i)$ and $u(R_{\mathrm{H2O,cal}})$ collect the fixed-point uncertainty terms for the calibration laboratory:

$$u^2(R_i) = \left(R_i \frac{dW_i}{dt}\right)^2 \left[u^2(\Delta t_{\mathrm{hyd},i}) + u^2(\Delta t_{p,i}) + u^2(\Delta t_{\mathrm{imp},i}) + u^2(\Delta t_{\mathrm{liq},i}) + u^2(\Delta t_{\mathrm{iso},i}) + u^2(\Delta t_{\mathrm{ther},i}) + u^2(\Delta t_{\mathrm{dyn},i})\right] + \frac{R_S^2}{\left(I_2^2 - I_1^2\right)^2}\left[\left(I_2^4 + I_1^4\right)\left(u^2(X_{\mathrm{DNL}}) + X^2\beta^2 u^2(t_{\mathrm{bath}})\right) + I_2^4 u^2(X_{1,\mathrm{noise}}) + I_1^4 u^2(X_{2,\mathrm{noise}})\right]. \quad (9.12)$$

The uncertainty $u(R_{\mathrm{H2O,client}})$ is the same as (9.12) except that all of the terms are evaluated for the client's measurement. The uncertainty $u(R)$ in (9.11) collects all of the terms associated with the client's measurement at the unknown temperature. This includes the resistance-measurement terms of (9.12), terms associated with the realisation of the temperature, and terms characterising the thermal connection between the SPRT and the temperature of interest. The total uncertainty in a measured temperature is obtained using (9.8). Figure 9.4 includes a curve showing the total calibration uncertainty propagated for this case.

9.9 *Total uncertainty for long-stem SPRTs used 'in-house'*

This example applies to long-stem SPRTs used above 0 ºC, and gives an indication of the least uncertainty obtainable in these subranges. In this case, oxidation effects must be considered, and this means that multiple triple-point-resistance measurements must be made. The uncertainty is minimised by using the same triple point of water cell. In most applications, the procedure of Section 9.5 provides a very good approximation to this procedure (see Figure 9.3).

Assumptions:

- Uncertainty due to SPRT oxidation (Section 6.1) is **not** zero. The oxidation effects are minimised by measuring the water-triple-point resistance immediately after measurements at higher temperatures. Each of the contributing uncertainties due to oxidation are assumed to be uncorrelated.
- Uncertainty due to SPRT vacancy, contamination, and electrical leakage effects (Section 6) during calibration is zero.
- The same resistance bridge and standard resistor are used for all measurements.
- The same triple-point-of-water cell is used for all measurements.
- The uncertainties contributing to non-repeatability of measurements, i.e., resistance bath instability, bridge noise, and differential non-linearity are all uncorrelated.
- The sensing-current-ratio errors can be neglected in all self-heating corrections.
- The measurement at the unknown temperature is corrected for self-heating (so (8.17) applies).

This equation is complicated because the uncertainties associated with the realisation of the triple point of water propagate according to (C.22), while the measurements of the SPRT resistance at the triple point of water propagate according to (C.23). The total uncertainty in the interpolated W_r values is

$$u^2_{\mathrm{total}}(W_r) = \frac{1}{R^2_{\mathrm{H2O}}}\left[u^2(R) + W^2 u^2(R_{\mathrm{meas}}) + (1-Z)^2 W^2 u^2(R_{\mathrm{H2O,ox}}) + \sum_{i=1}^{N} u^2(R_i) f_i^2(W) + u^2(R_{\mathrm{meas}}) \sum_{i=2}^{N} \left(1 + W_i^2\right) f_i^2(W) + \sum_{i=2}^{N} (1-Z_i)^2 W_i^2 f_i^2(W) u^2(R_{\mathrm{ox},i})\right], \quad (9.13)$$

where the first line collates uncertainties arising from the use of the SPRT at the unknown temperature including contribution due to changes in oxidation, vacancy effects, impurity effects and electrical insulation breakdown, and the second line collates uncertainties associated with the calibration at the fixed points, $u(R_i)$ collects the uncertainties associated with the realisation of the fixed points:

$$u^2(R_i) = \left(R_i \frac{dW_i}{dt}\right)^2 \left[u^2(\Delta t_{\mathrm{hyd},i}) + u^2(\Delta t_{p,i}) + u^2(\Delta t_{\mathrm{imp},i}) + u^2(\Delta t_{\mathrm{liq},i}) + u^2(\Delta t_{\mathrm{iso},i}) + u^2(\Delta t_{\mathrm{ther},i}) + u^2(\Delta t_{\mathrm{dyn},i})\right], \quad (9.14)$$

and $u(R_{\mathrm{meas}})$ collects the uncertainties associated with each of the resistance measurements:

$$u^2(R_{\text{meas}}) = R_S^2 \frac{\left(I_2^4 + I_1^4\right)}{\left(I_2^2 - I_1^2\right)^2}\left(u^2(X_{\text{DNL}}) + X_i^2 \beta^2 u^2(t_{\text{bath}}) + u^2(X_{\text{noise}})\right), \qquad (9.15)$$

and $u(R_{ox})$ is the uncertainty due to the unknown oxidation state of the SPRT (Section 6.1).

The total uncertainty in a measured temperature is obtained using (9.8). Figure 9.5 plots an example of the total propagated calibration uncertainty for this case. Over a large fraction of the range the uncertainty is dominated by the non-uniqueness.

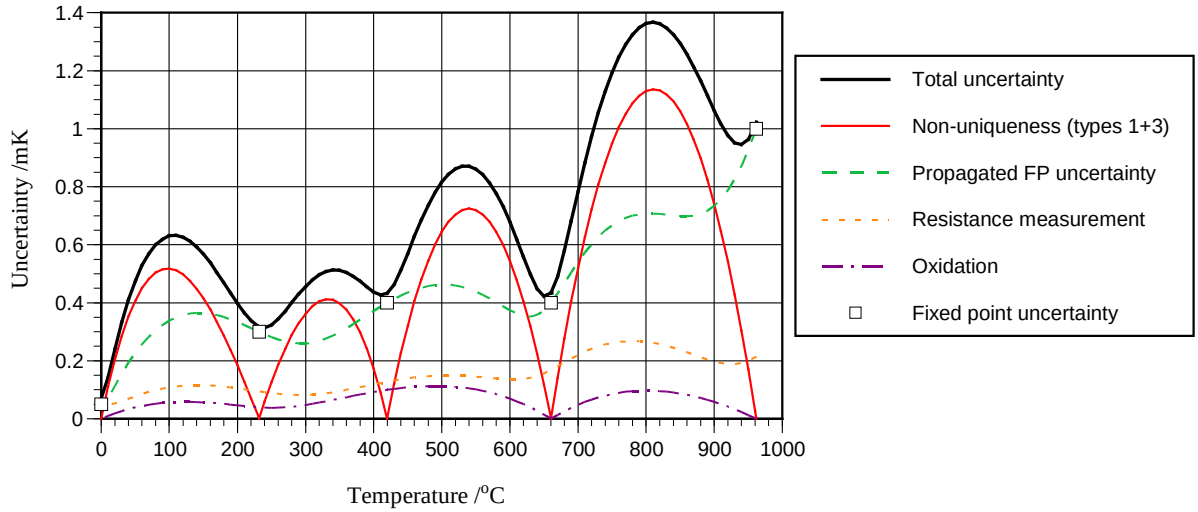

Figure 9.5: Contributions to total uncertainty for a long-stem SPRT calibrated over the water–silver subrange. It is assumed that the thermometer is to be used 'in-house'. The calculated value includes the effects of non-uniqueness, the fixed-point uncertainties are as indicated, and the uncertainty in the resistance measurements is 5 μΩ. Contributions due to the uncertainty in use, $u(R)$, instability of the SPRT, and insulation breakdown have been omitted.

9.10 *Total uncertainty for long-stem SPRTs used in a calibration bath*

This example demonstrates the calculation of total uncertainty in measured temperature, and the increase in uncertainty that may accompany oxidation effects.

Specifically, we consider a long-stem SPRT used in a calibration bath over the range 0 to 550 °C.

Assumptions:

- Uncertainty due to SPRT oxidation (Section 6.1) is **not** zero. During calibration, the oxidation effects were minimised by measuring the water-triple-point resistance immediately after the fixed-point measurements at higher temperatures. However, during use in the calibration bath, the oxidation state of the SPRT varies with the exposure to different temperatures. Subsidiary experiments show that the water-triple-point resistance increases by up to 80 μΩ depending on the oxidation state. Accordingly, the value of R_{H2O} used to calculate the resistance ratio during use is 40 μΩ higher than the value reported in the calibration certificate. Based on a rectangular distribution, the value assigned to the uncertainty in R_{H2O} to account for the variable oxidation state, $u(R_{ox})$, is 25 μΩ.
- Uncertainty due to SPRT vacancy, contamination, and electrical leakage effects (Section 6) during calibration is zero.
- The same resistance bridge, standard resistor, and triple-point-of-water cell were used for all calibration measurements.
- The user (client) uses a different water-triple-point cell with a standard uncertainty associated with the realisation of the triple point of 0.1 mK.
- The user uses the same bridge for measurement of the triple-point resistance and SPRT resistance in the calibration bath. The bridge is a 7-digit bridge with an uncertainty of 0.5×10^{-7} in resistance ratio and is used with the same 100 Ω standard resistor for all measurements.
- The uncertainty due to the instability and non-uniformity of the calibration bath is $u(T)$ and equal to the quadrature sum of 0.5 mK and $5 \times 10^{-5} t$.

- The SPRT is operated at 0.5 mA to minimise the self-heating, a constant temperature correction is applied, and uncertainty of 0.2 mK is included to account for the variations in self heating at different temperatures.

This equation is again complicated because the uncertainties associated with the realisation of the triple point of water propagate according to (C.22), while the measurements of the SPRT resistance at the triple point of water propagate according to (C.23). The oxidation effects are also different for the in-use measurements (6.5) and the calibration measurements (6.4). The total uncertainty in the interpolated W_r values is

$$\begin{aligned} u^2(W_r) = \frac{1}{R_{H2O}^2}\Big[& u^2(R) + W^2 u^2(R_{H2O,client}) + R_{S,client}^2 u^2(X_{INL,client}) + W^2 u^2(R_{H2O,ox}) \\ & + R_{S,cal}^2 u^2(X_{INL,cal}) + \sum_{i=2}^{N} u^2(R_i) f_i^2(W) + u^2(R_{H2O,cal})\left(W - f_{H2O}^2(W)\right)^2 \\ & + u^2(R_{meas}) \sum_{i=2}^{N} \left(1 + W_i^2\right) f_i^2(W) + \sum_{i=2}^{N} \left(1 - Z_i\right)^2 W_i^2 f_i^2(W) u^2(R_{H2O,ox}) \Big]. \end{aligned} \quad (9.16)$$

where the first line collates all of the contributions associated with the use of the SPRT including changes in oxidation ,vacancy and impurity concentration , and electrical breakdown, while the second and third line collate the contributions arising from the calibration, $u(R_i)$, collects the uncertainties associated with the realisation of the fixed points:

$$u^2(R_i) = \left(R_i \frac{dW_i}{dt}\right)^2 \left[u^2(\Delta t_{hyd,i}) + u^2(\Delta t_{p,i}) + u^2(\Delta t_{imp,i}) + u^2(\Delta t_{liq,i}) + u^2(\Delta t_{iso,i}) + u^2(\Delta t_{ther,i}) + u^2(\Delta t_{dyn,i})\right] \quad (9.17)$$

$u(R_{meas})$ collects the uncertainties associated with each of the resistance measurements carried out during the calibration,

$$u^2(R_{meas}) = R_S^2 \frac{\left(I_2^4 + I_1^4\right)}{\left(I_2^2 - I_1^2\right)^2}\left(u^2(X_{DNL}) + X_i^2 \beta^2 u^2(t_{bath}) + u^2(X_{noise})\right), \quad (9.18)$$

and $u(R_{H2O,ox})$ is the uncertainty due to the unknown oxidation state of the SPRT (Section 6.1). The first two terms of (9.16) include the uncertainty in the user's realisation of the temperature (stability and uniformity of the calibration bath), the resistance measurements, the realisation of the triple point, and the oxidation state of the SPRT. Figure 9.6 summarises the various contributions for the numerical example.

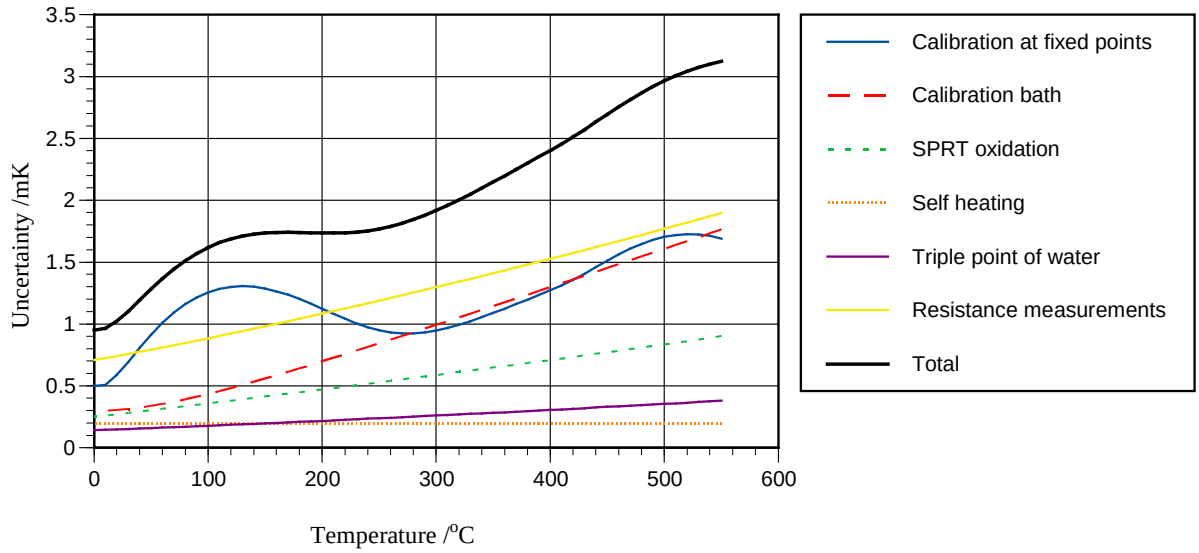

Figure 9.6: A numerical example for the total uncertainty for an SPRT used in a calibration bath.

9.11 *Total uncertainty in fixed-point comparisons*

This example illustrates the high accuracy obtainable in differential temperature measurements using a SPRT. Generally, the most demanding examples are for fixed-point comparisons, where, in the case of the triple point of water, the resolution may be of the order of a few microkelvin, and total uncertainties in the temperature differences are perhaps as low as 10 μK. The low uncertainties are possible only by using the same equipment and procedures for the two measurements so that many of the errors cancel.

Assumptions:

- The same resistance bridge and standard resistor are used for all resistance measurements.
- The same SPRT in (as near as practical) the same oxidation and vacancy state, and without any measurable moisture effects, is used for all measurements (see Section 6).
- The SPRT is used with the same pair of sensing currents to ensure the self-heating in the two fixed points is similar.

First, we note that the $f_i(W)$ functions take the value 1.0 for the fixed point for which they are named and zero for all other fixed points. Thus, if a temperature is measured using a reference cell at the *i*th fixed point, the propagation-of-error Equation (C.11) simplifies to

$$dW_{\mathrm{r}} = \frac{1}{R_{\mathrm{H2O}}}\left(dR - W dR_{\mathrm{H2O}} - dR_i + W_i dR_{\mathrm{H2O},i}\right). \tag{9.19}$$

This equation (and hence the equation for total uncertainty) is simplified by using the same water-triple-point value for all W calculations, and hence the difference in the interpolated reference resistance ratio for the two measurements is

$$dW_{\mathrm{r}} = \frac{1}{R_{\mathrm{H2O}}}(dR - dR_i), \tag{9.20}$$

so the calculation can be carried out in terms of the difference in SPRT resistance. The temperature difference between the two cells is

$$\Delta t = t - t_i = \left(\frac{dt_{90}}{dW_{\mathrm{r},i}}\right)\left(\frac{R - R_i}{R_{\mathrm{H2O}}}\right). \tag{9.21}$$

There are two cases of interest.

Uncertainty in actual temperature difference

If the actual temperature difference is of interest then the uncertainty is determined by the uncertainties in the resistance measurements and any dynamic or static temperature differences between the SPRT and cell temperatures:

$$u^2(\Delta t) = \left(\frac{dt_{90}}{dW_i}\right)^2 \frac{1}{R_{\mathrm{H2O}}^2}\left[u^2(R) + u^2(R_i) + 2u^2(R_{\mathrm{meas}}) + u^2(R_{\mathrm{ox}}) + u^2(R_{\mathrm{drift}}) + u^2(R_{\mathrm{ins}})\right], \tag{9.22}$$

where $u(R_{\mathrm{ox}})$, $u(R_{\mathrm{drift}})$, and $u(R_{\mathrm{ins}})$ are the uncertainties due to change in the oxidation state, vacancy state, and insulation resistance of the SPRT between the two measurements. The uncertainty $u(R_{\mathrm{ox}})$ is important for Ga, In, Sn, and Zn measurements, $u(R_{\mathrm{drift}})$ is important for measurements at the Al and Ag points, and $u(R_{\mathrm{ins}})$ is important for the Hg, H_2O, Ga, and Ag points. The other terms are given by

$$u^2(R_i) + u^2(R) = \left(R_i \frac{dW_i}{dt}\right)^2 \left[u^2(\Delta t_{\mathrm{liq},i}) + u^2(\Delta t_{\mathrm{ther},i}) + u^2(\Delta t_{\mathrm{dyn},i}) + u^2(\Delta t_{\mathrm{liq}}) + u^2(\Delta t_{\mathrm{ther}}) + u^2(\Delta t_{\mathrm{dyn}})\right] \tag{9.23}$$

and

$$u^2(R_{\text{meas}}) = \frac{R_S^2}{\left(I_2^2 - I_1^2\right)^2}\left[\left(I_2^4 + I_1^4\right)\left(u^2(\Delta X_{\text{DNL}}) + X^2\beta^2 u^2(t_{\text{bath}})\right) + I_2^4 u^2(X_{1,\text{noise}}) + I_1^4 u^2(X_{2,\text{noise}})\right] + 8R_S^2\left(\Delta X_{\text{sh},i} - \Delta X_{\text{sh}}\right)^2 \frac{I_2^4}{\left(I_2^2 - I_1^2\right)^2}\left(\frac{u^2(I)}{I^2}\right). \quad (9.24)$$

Equation (9.23) gathers the terms due to uncertainties in the cell temperatures and the thermal connection between the SPRT and the cells, while (9.24) gathers terms associated with the measurement of the SPRT resistance. Note that the term due to the bridge-current mismatch uncertainty in (9.24) is negligible if the self heating of the SPRT is the same in both cells.

The uncertainty in the difference between realised temperatures

In most fixed-point comparisons, the quantity of interest is the realised temperature of the cells, i.e. the temperature after all of the fixed-point corrections have been applied. In that case, Equation (9.23) should have additional terms due to the uncertainties in corrections for impurities, hydrostatic effect, residual gas pressure, and isotopic composition:

$$u^2(R_i) = \left(R_i \frac{dW_i}{dt}\right)^2 \left[u^2(\Delta t_{\text{liq},i}) + u^2(\Delta t_{\text{ther},i}) + u^2(\Delta t_{\text{dyn},i}) + u^2(\Delta t_{\text{liq}}) + u^2(\Delta t_{\text{ther}}) + u^2(\Delta t_{\text{dyn}}) + u^2(\Delta t_{\text{hyd},i} - \Delta t_{\text{hyd}}) + u^2(\Delta t_{p,i} - \Delta t_p) + u^2(\Delta t_{\text{imp},i} - \Delta t_{\text{imp}}) + u^2(\Delta t_{\text{iso},i} - \Delta t_{\text{iso}})\right]. \quad (9.25)$$

Some of the extra terms have been written as uncertainties in the difference of the corrections to account for correlations between the uncertainties in the corrections for the two cells. Consider, for example, the difference in the hydrostatic corrections for the two cells (Section 2.2):

$$\Delta t_{\text{hyd},i} - \Delta t_{\text{hyd}} = \frac{dt}{dh}\left(h_{\text{liq},i} - h_{\text{liq}}\right), \quad (9.26)$$

which is independent of the location of the SPRT sensing element (so long as it has the same nominal position at the bottom of the thermometer well for the two measurements). Hence the uncertainty in the difference between the two corrections is

$$u^2\left(\Delta t_{\text{hyd},i} - \Delta t_{\text{hyd}}\right) = \left(\frac{dt}{dh}\right)^2\left[u^2(h_{\text{liq},i}) + u^2(h_{\text{liq}})\right] + \left(h_{\text{liq},i} - h_{\text{liq}}\right)^2 u^2\left(dt/dh\right). \quad (9.27)$$

Note that the uncertainty is insensitive to the uncertainty in the correction coefficient if the two liquid heights are the same. Similarly, the uncertainty in the temperature due to uncertainty in the residual gas pressure is zero if the two cells are operated from the same gas system (because the two pressures are the same), and similar correlations may occur with the isotope corrections, and possibly the impurity corrections.

Glossary

Throughout the text the following symbols are used for the main variables (some symbols are used for more than one variable, but the meaning should be apparent from context):

A	Isotopic depression constant for isotopes expressed in permil, temperature coefficient parameter for SPRTs, cryoscopic constant
C	capacitance, either electrical or thermal analogue
D	diffusion coefficient
E_g	Energy gap
F	liquid fraction of fixed-point substance
g	acceleration due to gravity
$g(W)$	non-uniqueness function
H	enthalpy
h	vertical elevation of liquid levels in fixed points
I	sensing current of resistance bridge
K_f	cryoscopic constant
k	Boltzmann's constant, distribution coefficient for impurities, depression constant for deuterium isotope measured as isotope ratio (in e-H_2 point)
L	$1/e$ characteristic length for propagation of thermal influences
m_S or m_L	slopes of solidus and liquidus lines in phase diagram
n	number of moles
P	Power or heat flux
p	pressure
R	resistance, may be thermal or electrical, molar gas constant, isotopic ratio
T or t	temperature
u(.)	standard uncertainty of the quantity within parentheses
V	volume, velocity, voltage
W	resistance ratio for the SPRT
X	concentrations of isotopes or impurities measured as mole fraction, bridge reading as resistance ratio
Z	Berry's SPRT oxidation parameter

γ	pressure coefficient for standard resistors, interfacial tension
β	standard resistor temperature coefficient
δ	diffusion length for impurities, measure of isotopic concentration
μ	coupling constant between fixed-point cell and furnace
ρ	density
τ	time
ω	angular frequency

The symbols may be used with the prefixes:

Δ	to indicates change, error or correction in the quantity immediately following
d *or* δ	to indicate differential in the quantity immediately following

The symbols may be used with the following subscripts:

0	reference value, as in p_0, the reference pressure
1, 2, …	numerical index to indicate first, second, third, etc.
a	ambient
ac-dc	related to ac-dc difference of standard resistor
c	capillary
bath	associated with the standard resistor bath
cal	indicates measurements performed using unique equipment operated by the calibration laboratory

client	indicates measurements performed outside the calibration laboratory with the client's equipment
D	deuterium
drift	drift
DNL	differential non-linearity in the resistance bridge
dyn	dynamic
f	fusion, final
f(W)	fixed-point sensitivity coefficients
fp	associated with fixed point
furnace	furnace
h	elevation
H2O, e-H2, Ne, O2, Ar, Hg, Ga, Hg, In, Sn, Zn, Al, Ag: the various fixed points	
hyd	hydrostatic pressure
i	initial, also used for fixed-point index, ranges from e-H2 to Ag; $i = 1$ corresponds to H2O
in	inwards
ideal	ideal
imp	impurity
INL	integral non-linearity in the resistance bridge
iso	isotopic
l	liquidus
L	lead (of resistance bridge)
liq	liquid
meas	the measured value
melt	melt
min	minimum
noise	noise
NU	Non-uniqueness (Type 3)
ox	oxidation effect
out	outwards
OME	overall maximum estimate (impurity)
p	pressure
peak	peak
power	related to power coefficient of standard resistor
pure	pure fixed-point substance
r	reference, as in reference resistance ratio W_r
R	resistance, associated with the resistance value or resistance measurement
*R*s	standard resistor
s	solidus
SIE	Sum of individual estimates (impurity)
sh	self heating
SLAP	standard light Antarctic precipitation (isotopic standard for water)
SMOW	standard mean ocean water (isotopic standard for water)
SPRT	associated with the SPRT
SRI	Non-uniqueness (Type 1 – subrange inconsistency)
st	static
T or t	temperature, as in uncertainty in temperature u_t
thm	Thermal as in thermal resistance R_{thm}
tot	total
vac	vacancy or contamination effect
W	resistance ratio
*W*r	reference resistance ratio
X	bridge ratio

Appendix A: Summary of typical ranges of fixed-point uncertainties (in μK)

Fixed point	**e-H_2**	**Ne**	**O_2**	**Ar**	**Hg**	**H_2O**	**Ga**	**In**	**Sn**	**Zn**	**Al**	**Ag**
Source of uncertainty												
Fixed point effects												
Hydrostatic pressure	1-5	5-20	5-20	15-160	30-100	5-20	5-60	15-160	10-100	10-150	10-150	30-300
Residual gas pressure					0-20	0-20	0-200	5-500	5-300	5-400	10-700	10-600
Impurities	1-5	2-40	10-200	10-100	2-50	5-100	5-40	50-500	100-500	50-500	300-3000	1000-3000
Isotopic composition	5-65	175				5-35						
Strain, crystal defects	10-50	10-50	10-50	10-50		10-300						
Static thermal effects	5-50	5-50	5-50	5-50	5-20	5-10	5-20	5-100	10-100	10-150	15-400	20-1000
Dynamic thermal effects	5-50	5-50	5-50	5-50								
SPRT effects												
Oxidation					5-40	5-400	5-500	20-850	40-1000	100-1100		
Strain, vacancies, contamination										0-50	20-200	200-2000
Insulation leakage					0 - 20	0-100	0-20				2-50	100-3000
Resistance measurement												
Standard resistor stability	0-2	0-5	0-10	0-20	1-100	1-100	1-100	2-200	2-200	3-300	5-500	7-700
Misc. cable effects	0-100	0-100	0-100	0-100	0-100	0-100	0-100	0-100	0-100	0-100	0-100	0-100
Bridge errors	7-70	1-15	10-500	10-500	10-500	10-500	10-500	10-500	10-500	15-500	15-600	15-700
Self-heating correction	5-200	5-200	5-200	5-200	5-200	5-200	5-200	5-200	5-200	5-200	5-200	5-200
TOTAL	**20-250**	**180-300**	**20-550**	**25-550**	**35-550**	**20-600**	**15-600**	**30-1250**	**50-1250**	**120-1350**	**60-1300**	**250-4000**

Appendix B: Table of sensitivity coefficients and useful constants for the fixed points

Fixed point substance	Molecular mass g mol^{-1}	Temperature T_{90} /K	Temperature t_{90} /°C	$W_r(T_{90})$	dWr/dT_{90} /K^{-1}	dT_{90}/dWr K	Latent heat of fusion, L_f / kJmol^{-1}	First cryoscopic constant K_f^{-1} / K^{-1}	First cryoscopic constant K_f / K	dT/dP (Note 1)	dT/dl (Note 2)	Density / g.ml^{-1} Liquid at T_f	Density / g.ml^{-1} Liquid at 20 °C	Volume change on fusion /%
e-H_2(T)	2.01588	13.8033	−259.3467	0.001 190 07	0.000241	4157.62	0.117	0.0739	14	34	0.25	0.0770		11.5
Ne (T)	20.1797	24.5561	−248.5939	0.008 449 74	0.001227	815.24	0.335	0.0668	15	16	1.9	1.2		13.1
O_2 (T)	31.9988	54.3584	−218.7916	0.091 718 04	0.003903	256.22	0.444	0.0181	55	12	1.5	1.3		3.3
Ar (T)	39.948	83.8058	−189.3442	0.215 859 75	0.004342	230.33	1.188	0.0203	49	25	3.3	1.4		12.8
Hg (T)	200.59	234.3156	−38.8344	0.844 142 11	0.004037	247.72	2.301	0.00504	198	5.4	7.1	13.691	13.546	3.6
H_2O (T)	18.01528	273.16	0.01	1.000 000 00	0.003989	250.72	6.008	0.00968	103	−7.5	−0.73	0.9998	0.9982	−8.3
Ga (M)	69.723	302.9146	29.7646	1.118 138 89	0.003952	253.01	5.585	0.00732	136	−2.0	−1.2	6.09	5.91	−3.2
In (F)	114.818	429.7485	156.5985	1.609 801 85	0.003801	263.09	3.291	0.00214	467	4.9	3.3	7.023	7.29	2.3
Sn (F)	118.710	505.078	231.928	1.892 797 68	0.003713	269.34	7.162	0.00338	296	3.3	2.2	7.000	7.285	2.5
Zn (F)	65.409	692.677	419.527	2.568 917 30	0.003495	286.09	7.068	0.00177	564	4.3	2.7	6.575	7.135	4.6
Al (F)	26.981538	933.473	660.323	3.376 008 60	0.003205	312.02	10.79	0.00149	672	7.0	1.6	2.377	2.698	7.2
Ag (F)	107.8682	1234.93	961.78	4.286 420 53	0.002841	352.01	11.3	0.00089	1124	6.0	5.4	9.346	10.49	4.5

Notes:

1. **dT/dP is the rate of change of the temperature with pressure. The units are 10^{-8} K.Pa^{-1}, which is equivalent to millikelvin per atmosphere.**
2. **dT/dl is the rate of change of the temperature with depth. The units are 10^{-3} K.m^{-1}, which is equivalent to millikelvin per metre.**
3. **The units for K_f are equivalent to microkelvin per (µmol/mol) mole fraction.**

Appendix C: The ITS-90 Interpolations and Propagation of Uncertainty

For many users of this document, the total-uncertainty equations of Section 9 will be sufficient for most needs. This appendix provides the mathematical framework for developing uncertainty equations for cases not covered in Section 9. In doing so it also:

(i) presents a tutorial description of the mathematics underlying ITS-90 interpolations;
(ii) explains the basis of some of uncertainty expressions used throughout the text, including Section 9;
(iii) explains the rationale for some measurement practices that reduce uncertainty.

The approach to the analysis involves rewriting the SPRT interpolations in terms of a set of orthogonal interpolating functions (White and Saunders (2000, 2007), and White (2001)).

C.1 *The mathematical structure of ITS-90*

The mathematical definition of T_{90} in the SPRT subranges of ITS-90 (Preston-Thomas 1990) follows three algebraic steps:

Step 1: Calculate the resistance ratio
The resistance ratio for an SPRT is defined as

$$W = \frac{R(T)}{R(0.01\,^{\circ}\mathrm{C})} = \frac{R}{R_{\mathrm{H2O}}}, \tag{C.1}$$

where R is the resistance of the SPRT at temperature T, and R_{H2O} is the resistance of the SPRT at the triple point of water. Ideally, if every SPRT had the same electrical resistivity as a function of temperature, the $W(T)$ functions for all SPRTs would be the same.

Step 2: Interpolate a value for the reference resistance ratio
To compensate for the slight differences in the resistivity-temperature behaviour of different SPRTs, each SPRT is used to interpolate between reference resistance ratios, W_{r}, defined for each fixed point. The SPRT interpolating equations all have the form[6]

$$W_{\mathrm{r}}(W) = W - \Delta W(W), \tag{C.2}$$

where the deviation functions, $\Delta W(W)$, are polynomials in $W - 1$ and/or $\ln(W)$.

Step 3: Calculate the temperature according to ITS-90
Once the W_{r} value has been calculated, the temperature is calculated using the $W_{\mathrm{r}}(T_{90})$ function. The function is defined by ITS-90 in two segments, one for temperatures below 0.01 °C and one for temperatures above 0 °C. The $W_{\mathrm{r}}(T_{90})$ definition is an exact one-to-one relationship and introduces no uncertainty or non-uniqueness into ITS-90.

To illustrate the interpolation process, consider the interpolation in the water–aluminium subrange, for which the ITS-90 interpolating equation is

$$W_{\mathrm{r}} = W - a(W-1) - b(W-1)^2 - c(W-1)^3. \tag{C.3}$$

[6] The description of the interpolation at Step 2 differs from that presented by the designers of ITS-90 (Crovini *et al* 1991) and understood by many users of ITS-90. The mathematical structure of the SPRT sub-ranges of ITS-90 evolved from the four low-temperature SPRT sub-ranges of IPTS-68 and conventionally relates the reference function to the measured resistance ratios using $W = W_{\mathrm{r}}(T_{90}) + \Delta W$. That is, with the conventional perspective, the mapping is from W_{r} ➔ W (rather than W ➔ W_{r} as in (2)), and the values of the deviations are found by interpolating between the measured deviations at the fixed points. This perspective explains the nomenclature of the deviation functions and the negative sign in (2). When the equations are solved algebraically and written in full (see C.5 and C.6a-d), it is clear that the interpolation is between reference resistance-ratios, W_{r}.

The values of the coefficients *a*, *b*, and *c* are determined by requiring Equation (C.3) to be satisfied at each of the defining fixed points:

$$\begin{aligned} W_{\mathrm{r,Sn}} &= W_{\mathrm{Sn}} - a(W_{\mathrm{Sn}} - 1) - b(W_{\mathrm{Sn}} - 1)^2 - c(W_{\mathrm{Sn}} - 1)^3, \\ W_{\mathrm{r,Zn}} &= W_{\mathrm{Zn}} - a(W_{\mathrm{Zn}} - 1) - b(W_{\mathrm{Zn}} - 1)^2 - c(W_{\mathrm{Zn}} - 1)^3, \\ W_{\mathrm{r,Al}} &= W_{\mathrm{Al}} - a(W_{\mathrm{Al}} - 1) - b(W_{\mathrm{Al}} - 1)^2 - c(W_{\mathrm{Al}} - 1)^3, \end{aligned} \qquad \text{(C.4a, b, c)}$$

where W_{Sn} , W_{Zn}, and W_{Al} are the measured values of resistance ratio at the fixed points, and $W_{\mathrm{r,Sn}}$, $W_{\mathrm{r,Zn}}$ and $W_{\mathrm{r,Al}}$ are the values of reference resistance ratio assigned to the fixed points by ITS-90. Note that there are three equations and three unknowns; *a*, *b*, and *c*. Once the values of *a*, *b*, and *c* have been determined, the value of W_{r} can be calculated for any measured *W* at an unknown temperature using (C.3).

The values of *a*, *b*, and *c* determined from (C.4a-c) can also be substituted back into (C.3), and the ITS-90 equation rearranged as

$$W_{\mathrm{r}}(W) = W_{\mathrm{r,H2O}}\, f_{\mathrm{H2O}}(W) + W_{\mathrm{r,Sn}}\, f_{\mathrm{Sn}}(W) + W_{\mathrm{r,Zn}}\, f_{\mathrm{Zn}}(W) + W_{\mathrm{r,Al}}\, f_{\mathrm{Al}}(W), \qquad \text{(C.5)}$$

where

$$\begin{aligned} f_{\mathrm{H2O}}(W) &= \frac{(W - W_{\mathrm{Sn}})(W - W_{\mathrm{Zn}})(W - W_{\mathrm{Al}})}{(W_{\mathrm{H2O}} - W_{\mathrm{Sn}})(W_{\mathrm{H2O}} - W_{\mathrm{Zn}})(W_{\mathrm{H2O}} - W_{\mathrm{Al}})}, \qquad f_{\mathrm{Sn}}(W) = \frac{(W - W_{\mathrm{H2O}})(W - W_{\mathrm{Zn}})(W - W_{\mathrm{Al}})}{(W_{\mathrm{Sn}} - W_{\mathrm{H2O}})(W_{\mathrm{Sn}} - W_{\mathrm{Zn}})(W_{\mathrm{Sn}} - W_{\mathrm{Al}})}, \\ f_{\mathrm{Zn}}(W) &= \frac{(W - W_{\mathrm{H2O}})(W - W_{\mathrm{Sn}})(W - W_{\mathrm{Al}})}{(W_{\mathrm{Zn}} - W_{\mathrm{H2O}})(W_{\mathrm{Zn}} - W_{\mathrm{Sn}})(W_{\mathrm{Zn}} - W_{\mathrm{Al}})}, \qquad f_{\mathrm{Al}}(W) = \frac{(W - W_{\mathrm{H2O}})(W - W_{\mathrm{Sn}})(W - W_{\mathrm{Zn}})}{(W_{\mathrm{Al}} - W_{\mathrm{H2O}})(W_{\mathrm{Al}} - W_{\mathrm{Sn}})(W_{\mathrm{Al}} - W_{\mathrm{Zn}})}. \end{aligned} \qquad \text{(C.6a-d)}$$

Despite appearances, the rearranged interpolating equation (C.5) is identical to the ITS-90 equation (C.3), but is written in the normal form for a mathematical interpolation: a sum of four interpolating functions each multiplied by a constant (in this case the constants are the four reference resistance ratios). If you have not seen the ITS-90 equations written this way, it is well worth spending a few minutes successively substituting $W = 1$, $W = W_{\mathrm{Sn}}$, $W = W_{\mathrm{Zn}}$, and $W = W_{\mathrm{Al}}$ into (C.6a-d) to see how the interpolation works. You should find that each of the interpolating functions has the value 1.0 at the fixed point for which it is named, and is zero for all other fixed points. This is a property of all $f_i(W)$ functions for all subranges.

Although the ITS-90 interpolation equation has only three free parameters, *a*, *b*, and *c*, the equation actually passes through four points: (1, 1), (W_{Sn}, $W_{\mathrm{r,Sn}}$), (W_{Zn}, $W_{\mathrm{r,Zn}}$), and (W_{Al}, $W_{\mathrm{r,Al}}$). Note too that we have explicitly included the variables $W_{\mathrm{r,H2O}}$ and W_{H2O} in (C.5) and (C.6a-d) to highlight the form of the equations, although both are equal to 1 by definition.

Figure C.1 plots the four interpolating functions, $f_i(W)$, of (C.6a-d). Each takes the value 1.0 exactly at the fixed point for which it is named and is zero at the other fixed points. Note that each of the interpolating functions is a cubic function of *W*, and any linear combination of them, such as (C.5), will be cubic.

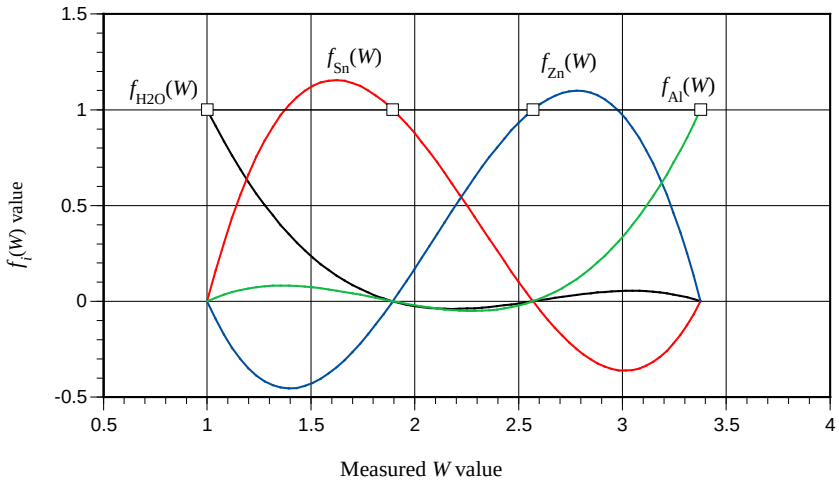

Figure C.1: The four ITS-90 interpolating functions for the water-aluminium subrange.

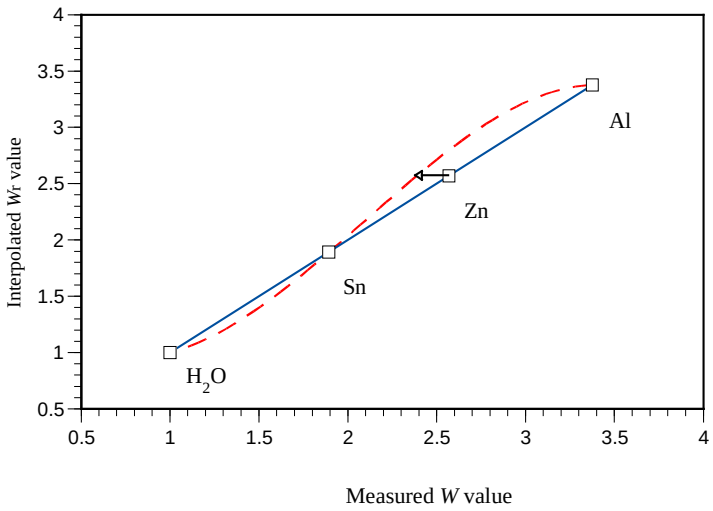

Figure C.2: The influence of an error in a fixed-point measurement. The solid line shows an interpolation between the measured W values and the W_r values. The dashed line shows the effect of a small error in the measured W_{Zn} value. The difference between the two curves is proportional to the $f_{Zn}(W)$ function.

Figure C.2 shows a graph of two water–aluminium interpolating equations. The solid curve passes through all four marked points. In the second, dashed curve, a small error has been introduced into the measured zinc-point value, W_{Zn}. The new curve passes through the new point but continues to pass through the other original points. The difference between the two curves is proportional to the $f_{Zn}(W)$ function of Figure C.1. This shows that the interpolating functions identified in (C.6a-d) are the sensitivity coefficients for errors and uncertainties associated with the fixed points. Ready identification of the fixed-point sensitivity coefficients is one of the benefits of expressing the ITS-90 equations in the more formal mathematical form.

C.2 *Propagation of uncertainty*

All of the ITS-90 interpolating equations can be expressed in the same form as (C.5), a sum of interpolating functions multiplied by the corresponding reference resistance ratios:

$$W_r(W) = \sum_{i=1}^{N} W_{r,i}\, f_i(W)\,, \tag{C.7}$$

where the numerical index i refers to the sequence of fixed points used to calibrate the SPRT (e.g. H_2O, Sn, Zn, etc). We reserve the index $i = 1$ for the water triple point. The $f_i(W)$ are a different set of interpolating functions for each ITS-90 subrange. Algebraic approximations to the interpolating functions for each subrange, and two methods for calculating them are described in detail in Appendix D.

In any general interpolation, where the equation is forced through N points, there are N pairs of coordinate values representing those points. For the ITS's-90 interpolations, the coordinates are pairs of the form (W_i, W_{ri}). There are therefore a total of $2N + 1$ independent parameter values determining the interpolation; the $2N$ coordinate values, and the W value at the unknown temperature. Differentiation of (C.7) with respect to all $2N + 1$ parameters leads to the most general form of the propagation-of-error equation[7] (White and Saunders 2007):

$$dW_r = \sum_{i=1}^{N} f_i(W) dW_{r,i} - \sum_{i=1}^{N} f_i(W) \left(\left. \frac{\partial W_r}{\partial W} \right|_{W=W_i} \right) dW_i + \frac{\partial W_r}{\partial W} dW\,. \tag{C.8}$$

For ITS-90 interpolations, (C.8) can be simplified because ITS-90 defines the values of many of the parameters, and they are, therefore, without error or uncertainty. Specifically:

- The reference resistance ratios at the fixed points, $W_{r,i}$, are defined, and hence all of the $dW_{r,i}$ terms are equal to zero;
- All resistance ratios for the triple point of water are equal to 1 by definition, hence $dW_{H2O} = 0$;

[7] Strictly, this equation relates the differential of W_r to differentials in the other quantities. The propagation-of-error equation is obtained by replacing the d symbol by Δ, e.g. $dW \rightarrow \Delta W$.

- The derivative dW_r/dW is very close to 1.0 (within 0.03% typically) because $W \approx W_r$.

Hence, the propagation-of-error equation for ITS-90 interpolations is

$$dW_r \approx -\sum_{i=2}^{N} f_i(W) dW_i + dW \ . \tag{C.9}$$

The simplifications have reduced the number of terms to N, and eliminated the derivatives. Most importantly, (C.9) shows that the interpolating functions, $f_i(W)$, are very good approximations to the sensitivity coefficients for errors and uncertainties in the fixed-point resistance ratios. Note too that the sum omits the term with the index $i = 1$, which corresponds to the triple point of water.

Although (C.9) is simple, it is not ideal for computing uncertainty. Each W value includes influence effects common to other W values (especially due to the water-triple-point measurements), and direct use of (C.9) would lead to a significant number of correlation terms in any uncertainty expression. These types of correlation problems are best simplified by expanding the equations in terms of the measured quantities. The first step is to express the equation in terms of measured resistance by repeatedly applying the identity

$$dW = \frac{1}{R_{H2O}} \left(dR - W dR_{H2O} \right), \tag{C.10}$$

which follows from the definition of W (C.1). This leads to the expression

$$dW_r = \frac{1}{R_{H2O}} \left[\left(dR - W dR_{H2O} \right) - \sum_{i=2}^{N} f_i(W) \left(dR_i - W_i dR_{H2O,i} \right) \right], \tag{C.11}$$

where $R_{H2O,i}$ are the triple-point-resistance values used to calculate each W_i (This may be different for each W_i value. Where a specific R_{H2O} value is required for the uncertainty analysis, any of the measured values will do). Equation (C.11) eliminates all of the correlation terms that would arise from effects associated with the realisation of the water triple point and most effects associated with the SPRT itself. However, resistance is still not the measured quantity; this is actually the bridge ratio at non-zero current. Therefore, there remain possible correlations due to effects associated with the resistance measurements and the self-heating corrections, and we need to make two more substitutions. The first is based on $R = XR_S$ where X is the zero-current bridge reading (resistance ratio) and R_S is the standard resistor value:

$$dR = dX R_S + dR_S X \ . \tag{C.12}$$

The second substitution expresses the zero-current bridge reading in terms of the bridge reading at the two different currents used to correct for self-heating:

$$dX(0) = \frac{I_2^2}{I_2^2 - I_1^2} dX(I_1) + \frac{I_1^2}{I_1^2 - I_2^2} dX(I_2) \ . \tag{C.13}$$

For the moment, we will not make the last two substitutions into (C.11). Instead, to keep this section as simple as practical, these effects are addressed in Section 8 (Resistance Measurement).

If, for the moment, we assume the uncertainties associated with each resistance measurement in (C.11) are not correlated (i.e. the contributing uncertainties due to the water-triple-point cells and resistance measurements are independent), we can immediately write down the corresponding expression for the uncertainty in the interpolated W_r value from (C.11):

$$u^2(W_r) = \frac{1}{R_{H2O}^2} \left[\left(u^2(R) + W^2 u^2(R_{H2O}) \right) + \sum_{i=2}^{N} f_i^2(W) \left(u^2(R_i) + W_i^2 u^2(R_{H2O,i}) \right) \right]. \tag{C.14}$$

The first term in parentheses collects the two terms that arise in the use of the SPRT (to measure an unknown temperature), while the second set of terms under the summation propagates the uncertainties resulting from the calibration at the fixed points. Equation (C.14) is the first of three basic forms of the propagation-of-uncertainty equation for the ITS-90 interpolations, and is a very good approximation if the uncertainties associated with the water triple point and resistance measurements are negligible (see Section 9.5). More accurate expressions for

the total uncertainty are derived in Section C.3 below. The main differences are in the propagation of uncertainties associated with measurements at the triple point of water. Figure C.3 compares the propagation of uncertainty for the water-triple-point uncertainties with (C.14) (curve a) with the more accurate equations derived below (curves b and c).

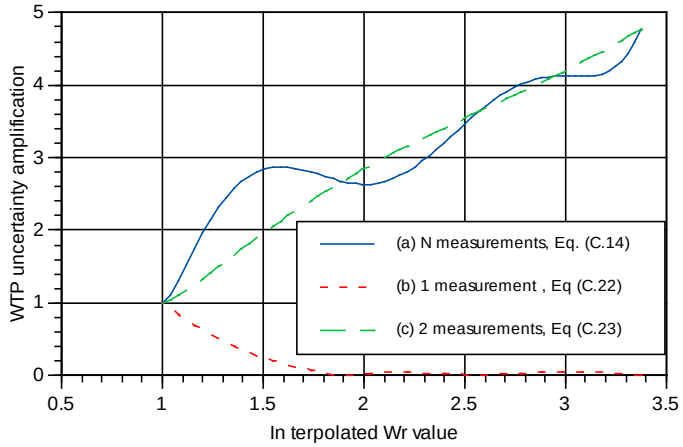

Figure C.3: The propagation of water-triple-point uncertainties versus measurement practice in the water–aluminium subrange. (a) Independent water-triple-point measurements for each W value, (b) one water-triple-point measurement for all W values, (c) one water-triple-point measurement for calibration (W_i, values) and one water-triple-point measurement for the unknown temperature (W value). It is assumed that each water-triple-point measurement has the same magnitude for the uncertainty, and all the uncertainties are uncorrelated.

In addition to the uncertainties associated with the actual measurements, ITS-90 has another source of uncertainty: non-uniqueness (see Section 7 for details). Ideally, each of the interpolation equations, applied to every ITS-90 compliant SPRT, would map the measured W values to the same W_r value and, hence, to the same temperature. In practice, for a number of reasons, this does not happen. That is, ITS-90 is not a unique temperature scale, but a family of scales that all agree within (typically) a few tenths of millikelvin (see Section 7). Therefore, once we have calculated the propagated uncertainty in the W_r values we must add uncertainties due to the non-uniqueness. The total uncertainty in the measured temperature can then be calculated as

$$u^2\left(T_{\text{total}}\right) = \left(\frac{dT}{dW}\right)^2 \left[u^2\left(W_r\right) + u^2\left(\Delta W_{r,\text{SRI}}\right) + u^2\left(\Delta W_{r,\text{NU}}\right)\right], \qquad \text{(C.15)}$$

where $u(\Delta W_{r,\text{SRI}})$ and $u(\Delta W_{r,\text{NU}})$ are the uncertainties, expressed in resistance ratio, in the interpolated W_r values due to Type 1 non-uniqueness (subrange inconsistency) and Type 3 non-uniqueness, respectively.

C.3 *Simplifying and reducing the uncertainty*

Throughout the uncertainty analysis, there are opportunities for both reducing the uncertainty and simplifying the mathematical expressions. To achieve these reductions we must adopt particular measurement procedures. This section explains the rationale for these procedures and gives the corresponding simplified uncertainty expressions. The simplifications all arise from particular properties of the interpolating functions, $f_i(W)$.

There are a very large number of ways of rearranging and presenting the ITS-90 interpolating equations. For example, the ITS-90 gives them as deviation functions, each the sum of a series of simpler functions, $F_j(W)$ that may be terms of a polynomial in $W - 1$ or $\ln(W)$:

$$\Delta W(W) = A_1 F_1(W) + \ldots + A_N F_N(W)\,. \qquad \text{(C.16)}$$

Remarkably, it can be shown that each of the functions, $F_j(W)$, or any linear combination of them, satisfies the mathematical identity

$$\sum_{i=1}^{N} f_i(W) F_j(W_i) = F_j(W)\,. \qquad \text{(C.17)}$$

Equation (C.17) tells us that any function that can be interpolated exactly by the ITS-90 equations can be written as a linear combination of the $f_i(W)$ interpolating functions. Two particular forms of this identity apply to all of the ITS's-90 interpolations and prove to be particularly useful in simplifying uncertainty expressions:

$$\sum_{i=1}^{N} f_i(W) W_i = W \ , \tag{C.18}$$

and

$$\sum_{i=1}^{N} f_i(W) = 1 . \tag{C.19}$$

The validity of (C.19) for the water-aluminium subrange is apparent in Figure C.1. (The sum of the functions is equal to 1.0 at each of the fixed points, and the only cubic equation that passes through all four points has a constant value of 1.0.)

We now investigate some examples of procedures that exploit these identities.

Use the same water-triple-point cell or water-triple-point resistance for all W values

The total uncertainty expression (C.14) contains terms for uncertainties in each of *N* different water-triple-point resistance measurements, each with its own corresponding uncertainty term. Suppose we use just one water-triple-point measurement to calculate all of the *W* values. Then the propagation-of-error equation is obtained by collating all of the dR_{H2O} terms in (C.11):

$$dW_{\mathrm{r}} = \frac{dR}{R_{\mathrm{H2O}}} - \sum_{i=2}^{N} f_i(W) \frac{dR_i}{R_{\mathrm{H2O}}} + \frac{dR_{\mathrm{H2O}}}{R_{\mathrm{H2O}}} \left(\sum_{i=2}^{N} f_i(W) W_i - W \right) . \tag{C.20}$$

The term in parentheses at the end of this expression can now be simplified using the identity (C.18) to obtain

$$dW_{\mathrm{r}} = \frac{1}{R_{\mathrm{H2O}}} \left(dR - \sum_{i=1}^{N} f_i(W) dR_i \right) . \tag{C.21}$$

The summation now runs from $i = 1$ (water triple point) instead of $i = 2$, so that terms associated from the water triple point are treated separately from the terms for the other fixed points. The corresponding equation for the total uncertainty can now be written down as

$$u^2(W_{\mathrm{r}}) = \frac{1}{R_{\mathrm{H2O}}^2} \left(u^2(R) + \sum_{i=1}^{N} f_i^2(W) u^2(R_i) \right) . \tag{C.22}$$

With this simplification, the total propagated uncertainty due to uncertainty in the water-triple-point value has been significantly reduced. It now only affects measurements made near the water triple point (see curve (b) of Figure C.3). This should be compared to curve (a), where the cumulative effects of water-triple-point uncertainties scale approximately in proportion to *W*.

This simplification can be made very easily for the cryogenic subranges ($t < 0$ °C) (Section 9.8), but not so easily for the higher temperature ranges where separate triple-point measurements are required to compensate for the oxidation and SPRT of the SPRT (see Section 6.1). However, most of the reduction in uncertainty can be achieved by always using the same water-triple-point cell. This expression is the basis for the detailed expressions of total uncertainty for SPRTs used 'in-house' as given in Sections 9.7 and 9.9.

The simplification leading to (C.22) cannot usually be applied where a user of the SPRT (e.g., a client of the calibration laboratory) does not have access to the same water-triple-point cell as the calibration laboratory. In this case, the simplification is not complete:

$$u^2(W_r) = \frac{1}{R_{\mathrm{H2O}}^2} \left[\left(u^2(R) + W^2 u^2(R_{\mathrm{H2O,client}}) \right) + \sum_{i=2}^{N} f_i^2(W) u^2(R_i) + \left(W - f_{\mathrm{H2O}}(W) \right)^2 u^2(R_{\mathrm{H2O,cal}}) \right] . \tag{C.23}$$

As before, the terms in the first parentheses are those associated with the client's measurements (i.e., the user of the SPRT), and the remaining terms propagate the uncertainties associated with the calibration. An example of this equation is curve (c) of Figure C.3. In this case, the propagated uncertainty is similar to that for (C.14).

Equation (C.23) is the basis of the total uncertainty expressions for SPRTs used outside the calibration laboratory, as given in Sections 9.8 and 9.10.

Measure resistance ratios with the same standard resistor
Consider a resistance ratio, $W(T)$, measured using a bridge operated with two different standard resistors $R_{S,T}$ and $R_{S,H2O}$, for each of the resistance measurements at the temperature T and the triple point of water:

$$W = \frac{R}{R_{H2O}} = \frac{R_{S,T}\,X}{R_{S,H2O}\,X_{H2O}}\,. \tag{C.24}$$

The propagation-of-error equation for this case is (from (C.10) and (C.12))

$$dW = W\left(\frac{dX}{X} + \frac{dR_{S,T}}{R_{S,T}} - \frac{dX_{H2O}}{X_{H2O}} - \frac{dR_{S,H2O}}{R_{S,H2O}}\right), \tag{C.25}$$

which has the corresponding uncertainty expression

$$u^2(W) = W^2\left(\frac{u^2(X)}{X^2} + \frac{u^2\left(R_{S,T}^2\right)}{R_{S,T}^2} + \frac{u^2\left(X_{H2O}\right)}{X_{H2O}^2} + \frac{u^2\left(R_{S,H2O}^2\right)}{R_{S,H2O}^2}\right), \tag{C.26}$$

and contains terms in the uncertainties for the values of both standard resistances. If we use, instead, the same standard resistor, $R_{S,T} = R_{S,H2O}$, for both resistance measurements, then the two terms in (C.25) cancel and

$$u^2(W) = W^2\left(\frac{u^2(X)}{X^2} + \frac{u^2\left(X_{H2O}^2\right)}{X_{H2O}^2}\right). \tag{C.27}$$

Now the uncertainty depends only on the uncertainty in the two bridge readings. (Actually, two small remnant terms depending on the stability of the resistor, see Section 8.1) This result means that it is not necessary to know the value of the standard resistor in order to measure temperature with the SPRT, it is sufficient that its value is stable and that it is used for both measurements of resistance used to calculate the W value.

Measure all resistance values with the same resistance bridge and connecting cables
There are a few errors occurring in resistance measurements that can be expressed as a simple quadratic or cubic function of the measured resistance (see Section 8). Suppose that these effects give rise to errors, ΔR, for each resistance value. From (C.21) we get the following expression for the error in the interpolated resistance ratio:

$$\Delta W_r = \frac{1}{R_{H2O}}\left(\Delta R - \sum_{i=1}^{N} f_i(W)\Delta R_i\right). \tag{C.28}$$

If the function describing the resistance error, ΔR, can be described or interpolated exactly by the ITS-90 equations, the term in parentheses simplifies to zero because of the identity (C.17). For example, the cubic interpolating equations for the water-aluminium subrange will interpolate exactly any offset, linear, quadratic or cubic error. In practice, so long as the function describing the error in the resistance measurements, ΔR, is not too non-linear, the term in parentheses in (C.28) is always very close to zero. In effect, the resistance bridge and the SPRT are calibrated together: any non-linearity in the resistance measurement is included in the SPRT deviation function.

A number of minor sources of uncertainty can be eliminated or reduced by this simplification, including: effects associated with the connecting cables; integral non-linearity (INL) in the bridge readings; the power coefficient of the standard resistor; and, to a lesser extent, the effect of current-ratio errors in self-heating corrections, but it does require the same bridge and set of cables to be used for all resistance measurements.

If the user of the SPRT and the calibration laboratory use a different resistance bridge, then the equivalent result for the error in the interpolated W_r value is

$$\Delta W_{\mathrm{r}} = \frac{1}{R_{\mathrm{H2O}}}\left(\Delta R_{\mathrm{client}} - \Delta R_{\mathrm{cal}}\right). \tag{C.29}$$

If the range of the unknown error is characterised by an uncertainty, then the uncertainty in the W_{r} value is

$$u^2\left(W_{\mathrm{r}}\right) = \frac{1}{R_{\mathrm{H2O}}^2}\left(u^2\left(R_{\mathrm{client}}\right) + u^2\left(R_{\mathrm{cal}}\right)\right). \tag{C.30}$$

Appendix D: The ITS-90 SPRT interpolating functions

Much of the uncertainty analysis depends on having functional forms for the interpolating functions, or equivalently, the sensitivity coefficients for the fixed-point uncertainties. This appendix describes two methods for calculating the functions, and gives the functional forms for each subrange.

D.1 Two methods for calculating the sensitivity coefficients

Method 1

The most obvious method for calculating the sensitivity coefficients is numerical, and historically this has been the most common approach (e.g. Preston-Thomas and Quinn 1992).

First, complete the numerical calculation that determines the coefficients for the interpolating function from the various measurements of resistance ratio; call this result $W_r(W,1,W_2,...,W_N)$. To determine the sensitivity coefficient for the second fixed point, recalculate the interpolating equation with a small change made to the measured W_2 value; call this result $W_r(W,1,W_2+\Delta W_2,...,W_N)$. The sensitivity coefficient for the second fixed point is

$$\frac{dW_r}{d\Delta W_2} = \frac{dW_r}{dW}\bigg|_{W=W_2} \quad f_2(W) = \frac{W_r(W,1,W_2+\Delta W_2,...,W_N) - W_r(W,1,W_2,...,W_N)}{\Delta W_2}, \tag{D.1}$$

where $f_2(W)$ is the second interpolating function. This technique can be applied successively to determine all of the sensitivity coefficients except the one for the water triple point, $f_{H2O}(W)$, which is most easily calculated using identity (C.19):

$$f_{H2O}(W) = 1 - \sum_{i=2}^{N} f_i(W).$$

Note that this method provides an exact value for the dW_i sensitivity coefficients, including the derivative terms in dW_r/dW_i (see (D.1) and discussion following (C.8)).

Method 2

This method is suited for use with algebraic mathematics applications such as Maple®, Mathematica®, and Mathcad®. The set of identities (C.17) applied to each ITS-90 interpolation provide a set of N equations relating the normal form of the ITS-90 interpolations (C.16) to the more formal form (C.7). These can be solved directly for the sensitivity coefficients:

$$\begin{bmatrix} f_1(W) \\ f_2(W) \\ \vdots \\ f_N(W) \end{bmatrix} = \begin{bmatrix} 1 & W_2 & \cdots & W_N \\ 0 & W_2 - 1 & \cdots & W_N - 1 \\ \vdots & \vdots & \ddots & \vdots \\ 0 & F_N(W_2) & \cdots & F_N(W_N) \end{bmatrix}^{-1} \begin{bmatrix} W \\ W - 1 \\ \vdots \\ F_N(W) \end{bmatrix}. \tag{D.2}$$

This method gives exact values for the $f_i(W)$ functions, but they are approximations (within 0.03%) to the actual sensitivity coefficients for the dW_i because they omit the derivative terms (see the numerical method above and the discussion following (C.8)).

D.2 *The interpolating functions for each subrange*

The following subsections list the interpolating functions for each of the ITS-90 subranges covered by this uncertainty guide. Each subsection presents the ITS-90 equation, formulae for the interpolating functions, and a graph showing the interpolating functions as a function of temperature. All of the graphs are expressed in temperature rather than resistance ratio; both axes are scaled so that the graphs plot the propagated temperature error divided by the temperature error at the specified fixed point.

Water-Gallium Subrange: 0.01 ºC to 29.7646 ºC

The ITS-90 equation for this subrange is

$$W_r(W) = W - a(W-1)\,, \tag{D.3}$$

where the a coefficient is determined by calibration of the SPRT at the melting point of gallium. The interpolation is rewritten as

$$W_r(W) = \frac{(W - W_{Ga})}{(1 - W_{Ga})} + W_{r,Ga}\frac{(W-1)}{(W_{Ga}-1)}\,, \tag{D.4}$$

from which the sensitivity coefficients are identified as

$$f_{H2O}(W) = \frac{(W - W_{Ga})}{(1 - W_{Ga})} \tag{D.5a}$$

and

$$f_{Ga}(W) = \frac{(W-1)}{(W_{Ga}-1)}\,. \tag{D.5b}$$

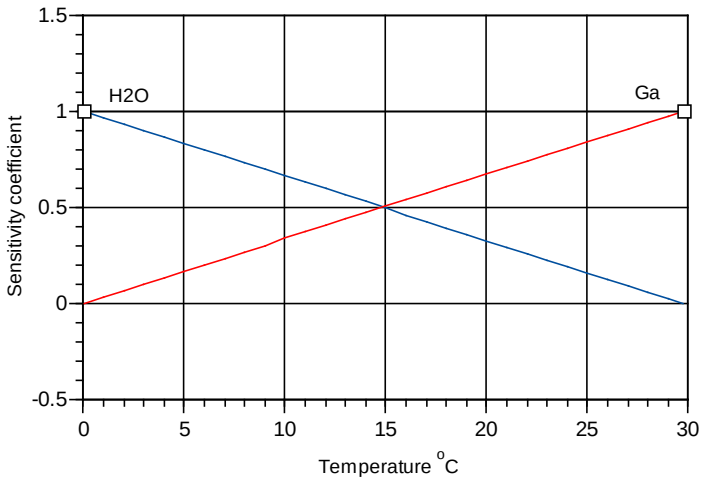

Figure D.1: Sensitivity coefficients for the water-gallium subrange. The curves show the propagated error in millikelvin for a 1 mK error at each of the fixed points.

Water-Indium Subrange: 0.01 ºC to 156.5985 ºC

The ITS-90 interpolation equation is

$$W_r(W) = W - a(W-1)\,, \tag{D.6}$$

where the *a* coefficient is determined by calibration of the SPRT at the freezing point of indium. The interpolation equation can be written in the form

$$W_r(W) = \frac{(W - W_{In})}{(1 - W_{In})} + W_{r,In}\frac{(W-1)}{(W_{In}-1)}\,, \tag{D.7}$$

from which the sensitivity coefficients are identified as

$$f_{H2O}(W) = \frac{(W - W_{In})}{(1 - W_{In})} \tag{D.8a}$$

and

$$f_{In}(W) = \frac{(W-1)}{(W_{In}-1)}\,. \tag{D.8b}$$

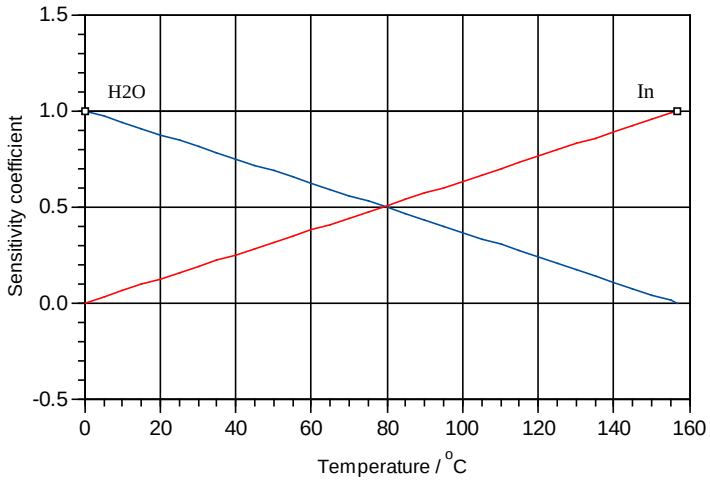

Figure D.2: The sensitivity coefficients for the water-indium subrange. The curves show the propagated error in millikelvin for a 1 mK error at each of the fixed points.

Mercury-Gallium Subrange: –38.8344 ºC to 29.7646 ºC

The ITS-90 interpolation equation is

$$W_r(W) = W - a(W-1) - b(W-1)^2 , \tag{D.9}$$

where the *a* and *b* coefficients are determined by calibration of the SPRT at the triple point of mercury and the melting point of gallium. The interpolation equation may be written in the form

$$W_r(W) = W_{r,Hg}\frac{(W-1)(W-W_{Ga})}{(W_{Hg}-1)(W_{Hg}-W_{Ga})} + \frac{(W-W_{Hg})(W-W_{Ga})}{(1-W_{Hg})(1-W_{Ga})} + W_{r,Ga}\frac{(W-W_{Hg})(W-1)}{(W_{Ga}-W_{Hg})(W_{Ga}-1)}, \tag{D.10}$$

from which the sensitivity coefficients are identified as

$$f_{Hg} = \frac{(W-1)(W-W_{Ga})}{(W_{Hg}-1)(W_{Hg}-W_{Ga})}, \tag{D.11a}$$

$$f_{H_2O} = \frac{(W-W_{Hg})(W-W_{Ga})}{(1-W_{Hg})(1-W_{Ga})} , \tag{D.11b}$$

and

$$f_{Ga} = \frac{(W-W_{Hg})(W-1)}{(W_{Ga}-W_{Hg})(W_{Ga}-1)} . \tag{D.11c}$$

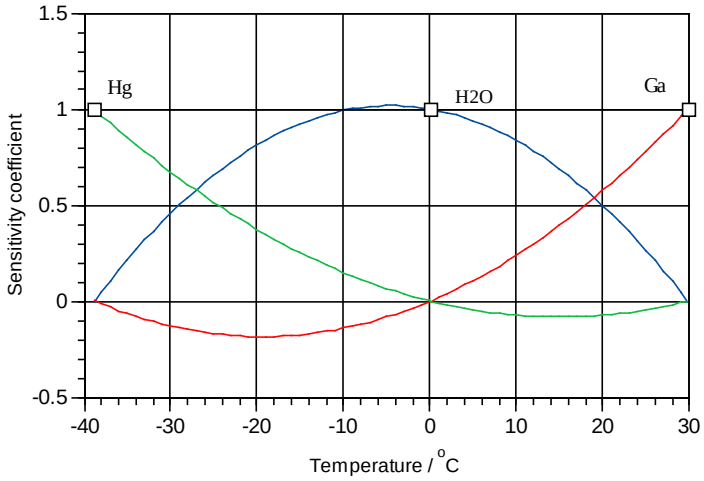

Figure D.3: The sensitivity coefficients for the mercury-gallium subrange. The curves show the propagated error in millikelvin for a 1 mK error at each of the fixed points.

Water-Tin Subrange: 0.01 ºC to 231.928 ºC

The ITS-90 interpolation equation is

$$W_r(W) = W - a(W-1) - b(W-1)^2 , \tag{D.12}$$

where the *a* and *b* coefficients are determined by calibration of the SPRT at the freezing points of indium and tin. The interpolation equation may be written in the form

$$W_r(W) = \frac{(W-W_{In})(W-W_{Sn})}{(1-W_{In})(1-W_{Sn})} + W_{r,In}\frac{(W-1)(W-W_{Sn})}{(W_{In}-1)(W_{In}-W_{Sn})} + W_{r,Sn}\frac{(W-1)(W-W_{In})}{(W_{Sn}-1)(W_{Sn}-W_{In})}, \tag{D.13}$$

from which the sensitivity coefficients are identified as

$$f_{H2O} = \frac{(W-W_{In})(W-W_{Sn})}{(1-W_{In})(1-W_{Sn})}, \tag{D.14a}$$

$$f_{In} = \frac{(W-1)(W-W_{Sn})}{(W_{In}-1)(W_{In}-W_{Sn})}, \tag{D.14b}$$

and

$$f_{Sn} = \frac{(W-1)(W-W_{In})}{(W_{Sn}-1)(W_{Sn}-W_{In})}. \tag{D.14c}$$

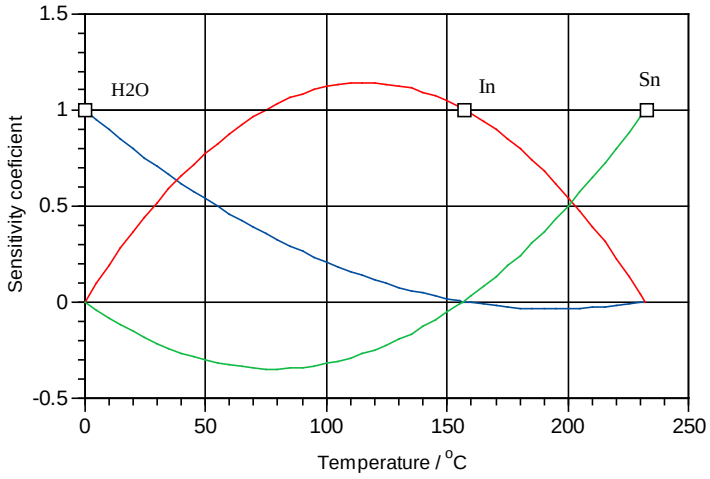

Figure D.4: The sensitivity coefficients for the water-tin subrange. The curves show the propagated error in error for a 1 mK uncertainty at each of the fixed points.

Water-Zinc Subrange: 0.01 ºC to 419.527 ºC

The ITS-90 interpolation equation is

$$W_r(W) = W - a(W-1) - b(W-1)^2 , \tag{D.15}$$

where the *a* and *b* coefficients are determined by calibration of the SPRT at the freezing points of tin and zinc. The interpolation equation may be written in the form

$$W_r(W) = \frac{(W-W_{Sn})(W-W_{Zn})}{(1-W_{Sn})(1-W_{Zn})} + W_{r,Sn}\frac{(W-1)(W-W_{Zn})}{(W_{Sn}-1)(W_{Sn}-W_{Zn})} + W_{r,Zn}\frac{(W-1)(W-W_{Sn})}{(W_{Zn}-1)(W_{Zn}-W_{Sn})} , \tag{D.16}$$

from which the sensitivity coefficients are identified as

$$f_{H2O} = \frac{(W-W_{Sn})(W-W_{Zn})}{(1-W_{Sn})(1-W_{Zn})} , \tag{D.17a}$$

$$f_{Sn} = \frac{(W-1)(W-W_{Zn})}{(W_{Sn}-1)(W_{Sn}-W_{Zn})} , \tag{D.17b}$$

and

$$f_{Zn} = \frac{(W-1)(W-W_{Sn})}{(W_{Zn}-1)(W_{Zn}-W_{Sn})} . \tag{D.17c}$$

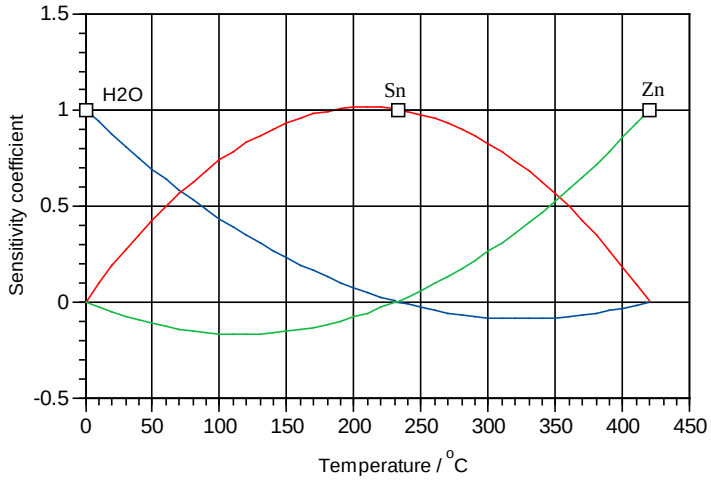

Figure D.5: The sensitivity coefficients for the water-zinc subrange. The curves show the propagated error in millikelvin for a 1 mK error at each of the fixed points.

Water-Aluminium Subrange: 0.01 ºC to 660.323 ºC

The ITS-90 interpolation equation is

$$W_r(W) = W - a(W-1) - b(W-1)^2 - c(W-1)^3 , \tag{D.18}$$

where the *a*, *b* and *c* coefficients are determined by calibration of the SPRT at the freezing points of tin, zinc and aluminium. The interpolation equation may be written in the form

$$W_r(W) = f_{H_2O} + W_{r,Sn} f_{Sn} + W_{r,Zn} f_{Zn} + W_{r,Al} f_{Al} , \tag{D.19}$$

where the sensitivity coefficients are

$$f_{H2O} = \frac{(W-W_{Sn})(W-W_{Zn})(W-W_{Al})}{(1-W_{Sn})(1-W_{Zn})(1-W_{Al})} , \tag{D.20a}$$

$$f_{Sn} = \frac{(W-1)(W-W_{Zn})(W-W_{Al})}{(W_{Sn}-1)(W_{Sn}-W_{Zn})(W_{Sn}-W_{Al})} , \tag{D.20b}$$

$$f_{Zn} = \frac{(W-1)(W-W_{Sn})(W-W_{Al})}{(W_{Zn}-1)(W_{Zn}-W_{Sn})(W_{Zn}-W_{Al})} , \tag{D.20c}$$

$$f_{Al} = \frac{(W-1)(W-W_{Sn})(W-W_{Zn})}{(W_{Al}-1)(W_{Al}-W_{Sn})(W_{Al}-W_{Zn})} . \tag{D.20d}$$

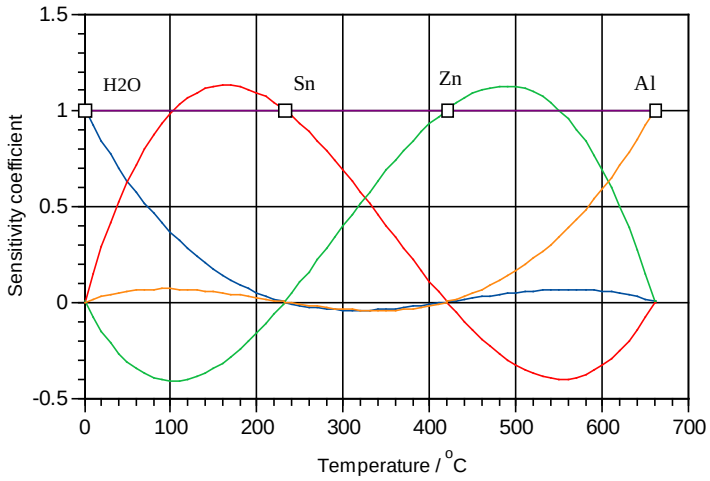

Figure D.6: The sensitivity coefficients for the water-aluminium subrange. The curves show the propagated error in millikelvin for a 1 mK error at each of the fixed points.

Water-Silver Subrange: 0.01 ºC to 961.78 ºC

The ITS-90 interpolation equation takes the form

$$W_r(W) = W - a(W-1) - b(W-1)^2 - c(W-1)^3 - d(W - W_{Al})^2, \qquad \text{(D.21)}$$

where the *a*, *b* and *c* coefficients are the same as determined from the water–aluminium subrange, and the *d* coefficient is determined by calibration of the SPRT at the freezing point of silver. The equation is applicable only over the temperature range between the aluminium and silver points (660.323 °C to 961.78 °C). The interpolation equation may be written in the form

$$W_r(W) = f_{H_2O} + W_{r,Sn} f_{Sn} + W_{r,Zn} f_{Zn} + W_{r,Al} f_{Al} + W_{r,Ag} f_{Ag}, \qquad \text{(D.22)}$$

where the sensitivity coefficients (applicable only above 660.323 °C) are

$$f_{H_2O} = f_{H_2O}^{Al}(W) - f_{H_2O}^{Al}(W_{Ag})\left(\frac{W - W_{Al}}{W_{Ag} - W_{Al}}\right)^2, \qquad \text{(D.23a)}$$

$$f_{Sn} = f_{Sn}^{Al}(W) - f_{Sn}^{Al}(W_{Ag})\left(\frac{W - W_{Al}}{W_{Ag} - W_{Al}}\right)^2, \qquad \text{(D.23b)}$$

$$f_{Zn} = f_{Zn}^{Al}(W) - f_{Zn}^{Al}(W_{Ag})\left(\frac{W - W_{Al}}{W_{Ag} - W_{Al}}\right)^2, \qquad \text{(D.23c)}$$

$$f_{Al} = f_{Al}^{Al}(W) - f_{Al}^{Al}(W_{Ag})\left(\frac{W - W_{Al}}{W_{Ag} - W_{Al}}\right)^2, \qquad \text{(D.23d)}$$

$$f_{Ag} = \left(\frac{W - W_{Al}}{W_{Ag} - W_{Al}}\right)^2, \qquad \text{(D.23e)}$$

where the F_i^{Al} are the sensitivity coefficients for the water-aluminium subrange, as given by (D20a-d). For temperatures below 660.323 °C, Equations (D20a-d) apply.

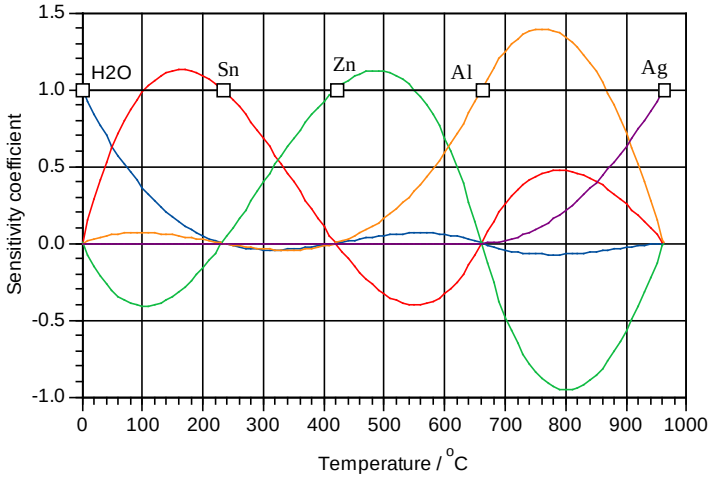

Figure D.7: The sensitivity coefficients for the water-silver subrange. The curves plot the propagated error in millikelvin for a 1 mK error at each of the fixed points. Below 660.323 °C (the aluminium point) the curves are identical to those in Figure D.6.

Argon-Water Subrange: 83.058 K to 273.16 K

The ITS-90 interpolation equation is

$$W_r = W - a(W-1) - b(W-1)\ln(W)\,, \tag{D.24}$$

where the *a*, and *b* coefficients are determined by calibration of the SPRT at the triple points of argon and mercury. The interpolation may be written in the form

$$W_r(W) = f_{H_2O} + W_{r,Hg} f_{Hg} + W_{r,Ar} f_{Ar}\,, \tag{D.25}$$

where the sensitivity coefficients are

$$f_{H_2O} = \frac{(W-1)(W_{Hg}-W_{Ar})\ln W + (W_{Hg}-1)(W_{Ar}-W)\ln W_{Hg} - (W_{Hg}-W)(W_{Ar}-1)\ln W_{Ar}}{(W_{Hg}-1)(W_{Ar}-1)(\ln W_{Hg} - \ln W_{Ar})}, \tag{D.26a}$$

$$f_{Hg} = \frac{(W-1)(\ln W - \ln W_{Ar})}{(W_{Hg}-1)(\ln W_{Hg} - \ln W_{Ar})}, \tag{D.26b}$$

$$f_{Ar} = \frac{(W-1)(\ln W - \ln W_{Hg})}{(W_{Ar}-1)(\ln W_{Ar} - \ln W_{Hg})}. \tag{D.26c}$$

The sensitivity coefficient for the triple point of water is most easily calculated as $f_{H_2O} = 1 - f_{Hg} - f_{Ar}$.

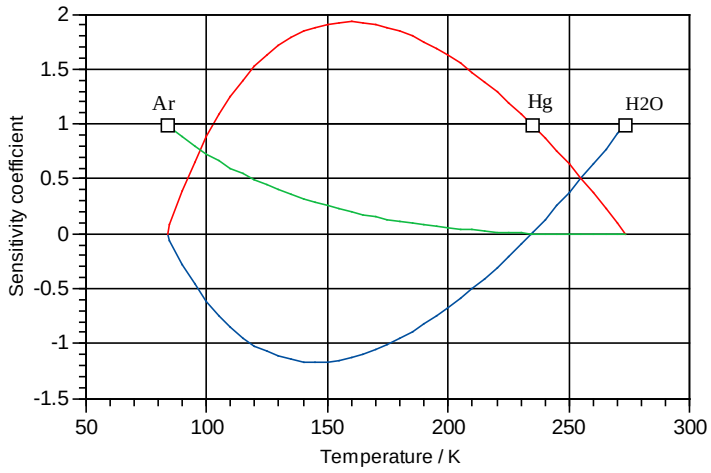

Figure D.8: The sensitivity coefficients for the argon-water subrange. The curves show the propagated error in millikelvin for a 1 mK error at each of the fixed points.

Oxygen-Water Subrange: 54.3584 K to 273.16 K

The ITS-90 interpolation equation takes the form

$$W_r(W) = W - a(W-1) - b(W-1)^2 - c\left(\ln W\right)^2, \tag{D.27}$$

where the *a*, *b* and *c* coefficients are determined by calibration of the SPRT at the triple points of oxygen, argon and mercury. The interpolation may be written in the form

$$W_r = f_{H20} + W_{r,Hg} f_{Hg} + W_{r,Ar} f_{Ar} + W_{r,O2} f_{O2}, \tag{D.28}$$

where the sensitivity coefficient for the oxygen point is

$$f_{O2}(W) = \frac{(\ln W)^2 (W_{Hg}-1)(W_{Ar}-1)(W_{Ar}-W_{Hg}) - (\ln W_{Ar})^2 (W_{Hg}-1)(W-1)(W-W_{Hg}) + (\ln W_{Hg})^2 (W-1)(W_{Ar}-1)(W-W_{Ar})}{(\ln W_{O2})^2 (W_{Hg}-1)(W_{Ar}-1)(W_{Ar}-W_{Hg}) - (\ln W_{Ar})^2 (W_{Hg}-1)(W_{O2}-1)(W_{O2}-W_{Hg}) + (\ln W_{Hg})^2 (W_{O2}-1)(W_{Ar}-1)(W_{O2}-W_{Ar})}. \tag{D.29}$$

The equations for the argon and mercury functions can be found by permuting the indices (e.g., swap the Ar and O2 subscripts to obtain the $f_{Ar}(W)$ function), and the water function found from $f_{H2O} = 1 - f_{O2} - f_{Ar} - f_{Hg}$. Alternatively, the following numerical approximations may be used:

$$\begin{aligned}
f_{O2} &= -1.598425679 + 3.403991489W - 1.805565809W^2 + 0.4032254894\left(\ln W\right)^2, \\
f_{Ar} &= +3.930746333 - 8.465193581W + 4.534447249W^2 - 0.5593488293\left(\ln W\right)^2, \\
f_{Hg} &= -4.044936086 + 16.33613127W - 12.29119519W^2 + 0.4643043265\left(\ln W\right)^2, \\
f_{H2O} &= +2.712615432 - 11.27492918W + 9.562313751W^2 - 0.3081809866\left(\ln W\right)^2.
\end{aligned} \tag{D.30a-d}$$

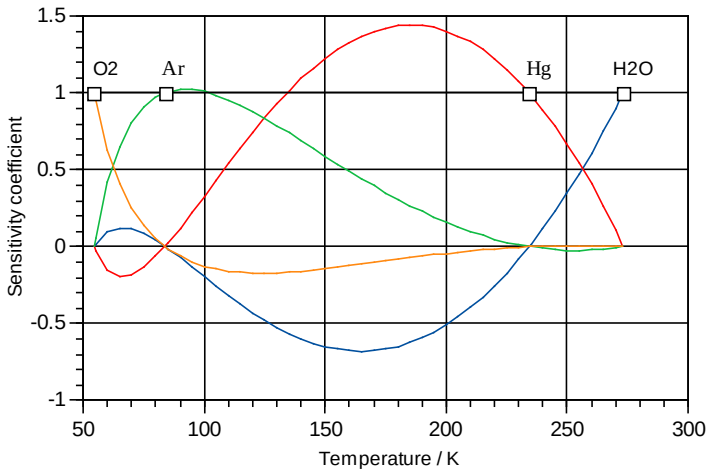

Figure D.9: The sensitivity coefficients for the oxygen-water subrange. The curves show the propagated error in millikelvin for a 1 mK error at each of the fixed points.

Neon-Water Subrange: 24.5561 K to 273.16 K

The ITS-90 interpolation equation is

$$W_r = W - a(W-1) - b(W-1)^2 - c\ln W - d(\ln W)^2 - e(\ln W)^3, \qquad \text{(D.31)}$$

where the *a*, *b*, *c*, *d*, and *e* coefficients are determined by calibration of the SPRT at the triple points of equilibrium hydrogen, neon, oxygen, argon and mercury. The interpolation may be written in the form

$$W_r = f_{H2O} + W_{r,Hg} f_{Hg} + W_{r,Ar} f_{Ar} + W_{r,O2} f_{O2} + W_{r,Ne} f_{Ne} + W_{r,e\text{-}H2} f_{e\text{-}H2}\,. \qquad \text{(D.32)}$$

The sensitivity coefficients in this case are too complex to write down in algebraic form. The following numerical approximations may be used:

$$f_{Hg} = -24.30265740 + 42.99793720W - 18.69528095W^2 - 14.20610018\ln(W) - 2.778961721\ln^2(W) - 0.1788181624\ln^3(W),$$
$$f_{Ar} = +33.02979668 - 46.64306946W + 13.61327293W^2 + 20.51522598\ln(W) + 4.195086350\ln^2(W) + 0.2785479955\ln^3(W),$$
$$f_{O_2} = -29.45087407 + 39.79347654W - 10.34260259W^2 - 19.77485453\ln(W) - 4.269113231\ln^2(W) - 0.2941747479\ln^3(W),$$
$$f_{Ne} = +7.413452875 - 9.508661062W + 2.095208241W^2 + 5.423905534\ln(W) + 1.384488984\ln^2(W) + 0.1102290468\ln^3(W),$$
$$f_{H} = -1.715380724 + 2.160321157W - 0.4449404100W^2 - 1.291145588\ln(W) - 0.3520630280\ln^2(W) - 0.03269335415\ln^3(W),$$
$$f_{H2O} = +16.02566264 - 28.80000438W + 13.77434278W^2 + 9.33296879\ln(W) + 1.820562646\ln^2(W) + 0.1169092222\ln^3(W).$$

(D.33a-f)

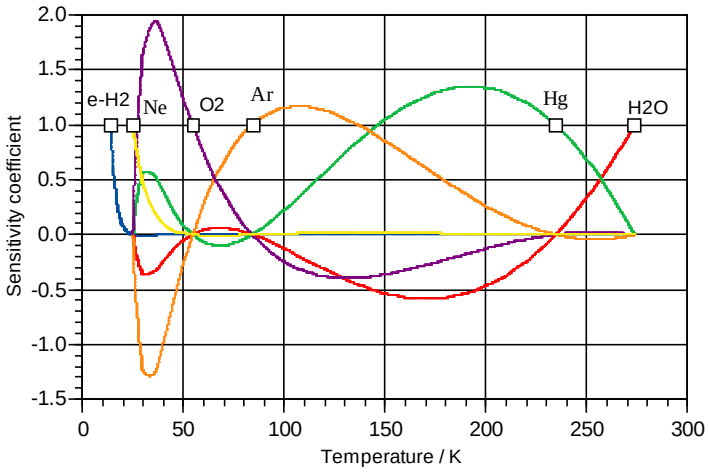

Figure D.10: The sensitivity coefficients for the neon-water subrange. The curves plot the propagated error in millikelvin for a 1 mK error at each of the fixed points. Note that the subrange extends only down to the Neon point (24.5561 K), although the hydrogen point is below this temperature.

References

Ahmed M.G., Hermier Y., Moussa M.R., and Bonnier G., (2003), Argon Triple-point Device to Calibrate Long-Stem Thermometers in Quasi Adiabatic Conditions, in *Temperature: its Measurement and Control in Science and Industry, Vol. 7* Ed. D.C. Ripple, AIP, New York, 167-172.

Ahmed M.G., (2005), Investigation of the ITS-90 subrange inconsistencies for 25.5 Ω SPRT's in the range 0 °C – 660 °C, Proc. TEMPMEKO 2004, Ed. Davor Zvizdic, Faculty of Mechanical Engineering and Naval Architecture, Zagreb, 271-274.

Ancsin J., (1982), Melting curves of H_2O, in *Temperature its Measurement and Control in Science and Industry Vol. 5*, Ed. J. F. Schooley, AIP, New York, 281-284.

Ancsin J., and Murdock E.G., (1990), An intercomparison of platinum resistance thermometers between 0 °C and 630 °C, *Metrologia*, **27**, 201-209.

Ancsin J., (1996), Non-uniqueness of the ITS-90, *Metrologia*, **33**, 5-17.

Ancsin J., (2003), Oxidation of platinum resistance thermometers, in *Temperature: Its measurement and control in Science and Industry, Vol. 7*, Ed D.C. Ripple, AIP, New York, 345-349.

Ancsin J., (2004), A comparison of PRTs at the Cu-Ag eutectic point (760 °C), *Metrologia*, **41**, 198-203.

Ancsin J, (2006), Non-uniqueness of ITS-90 at 548.2°C and at 156.6°C, *Metrologia*, **43**, 461-469.

ASTM, (2002), *Standard Guide for use of water triple point cells*, E1750-02, American Society for Testing and Materials, West Conshohoken, PA, USA.

Ballico.M., (1999), A technique for *in situ* measurement of the conductivity of water in 'triple point of water cells, *Meas. Sci Technol.* **40**, L33-L36.

Baker H. *et al*., (1992), *ASM Handbook, Volume 3, Alloy Phase Diagrams*, Ed. Baker, H., ASM Int., Metals Park.

Batagelj,V., Bojkovski, J., Drnovsek, J. and Pusnik, I., (2003), Influence of SPRT self-heating on measurement uncertainty in Fixed point calibration and calibration by comparison, in *Temperature: Its measurement and control in Science and Industry, Vol. 7*, Ed D.C. Ripple, AIP, New York, 315-320.

Batagelj V., Bojkovski J., Drnovsek J. (2005), *The Numerical Analyses of the Temperature Gradients inside the Fixed-point cell*, Proc. TEMPMEKO 2004, Ed. Davor Zvizdic, Faculty of Mechanical Engineering and Naval Architecture, Zagreb, 209-214.

Bojkovski, J Batagelj,V.., (2007), The immersion profile in a triple point of water fixed point cell for different SPRTs of the same type. Presented to TEMPMKO 2007, Lake Louise, Canada.

Berry R.J., (1959, The Temperature-Time Dependence of the Triple Point of Water, *Can. J. Phys.*, **37**, 1230-1248

Berry R.J., (1962), The stability of platinum Resistance Thermometers at Temperatures up to 630 ºC, in *Temperature its Measurement and Control in Science and Industry, Vol 3*, Ed C.M. Herzfeld, Rheinhold, New York, 301-311.

Berry R.J.,(1963), Relationship between the real and ideal resistively of platinum, *Can J. Phys*. **41**, 946-982.

Berry R.J., (1966), Platinum resistance thermometry in the range 630 – 900 °C, *Metrologia*, **2**, 80-90.

Berry R.J., (1967), Platinum Resistance Thermometry Below 10 °K, *Metrologia*, **3**, 53-57.

Berry R.J., and Lamarche J.L.G., (1970), Departures from Matthiessen's Rule for Vacancies in Platinum, *Phys. Lett*., **31A**, 319-320

Berry R.J., (1972), The influence of crystal defects in platinum on platinum resistance thermometry, in *Temperature: Its Measurement and Control in Science and Industry Vol 4*, Ed. R.P. Hudson, ISA Pittsburg, 937-949

Berry R.J., (1978), Study of multilayer surface oxidation of platinum by electrical resistance technique, *Surface Science*, **76**, 415-442.

Berry R.J., (1982a), Evaluation and control of platinum oxidation errors in standard platinum resistance thermometers, in *Temperature its measurement and Control in Science and Industry*, Vol. 5, Ed. J.F. Schooley, AIP, New York, 743-752.

Berry R.J., (1982b), Oxidation, stability and insulation characteristics of Rosemount standard platinum resistance thermometers, in *Temperature its measurement and Control in Science and Industry*, Vol. 5, Ed. J.F. Schooley, AIP, New York, 743-752.

Berry R.J., (1983), Thermal strain effect in standard platinum resistance thermometers, *Metrologia*, **19**, 37-47.

Berry R.J., (1995), Analysis and control of electrical insulation leakage in platinum resistance thermometers up to 1064C, *Metrologia*, **32**, 11-25.

Bureau International des Poids et Mesures, (1990), *Supplementary Information for the ITS-90*, BIPM, Sevres (Available at http://www.bipm.org/en/committees/cc/cct/publications_cc.html).

Bureau International des Poids et Mesures, (1997), *Supplementary Information for the International Temperature Scale of 1990*, (available at http://www.bipm.org/en/committees/cc/cct/publications_cc.html).

Bureau International des Poids et Mesures, (2005), The International System of Units, 8th Edition, (Available at http://www.bipm.fr/en/si/si_brochure/).

Bureau International des Poids et Mesures, (2006), *Mise en Pratique for the definition of the kelvin* (available at http://www.bipm.org/en/committees/cc/cct/publications_cc.html).

Bloembergen P., Bonnier G., Ronsin H., (1990), An International Intercomparison of Argon Triple Point Calibration Facilities, Accommodating Long-stem Thermometers, *Metrologia*, **27**, 101-106.

Bonnier, G., Diril, A.,Arai, M.,Ballico, M.,Chimenti, V.,Duris, S.,Filipe, E., Ivanova, A.G., Kartal Dogan, A., Mendez-Lango, E., Meyer, C., Pavese, F., Peruzzi, A., Renaot, E., Seidel, J., Stock, M., Ugur, S., White, D.R., (2005), Uncertainty budgets for SPRT Calibrations at the Fixed Points", Proc. TEMPMEKO 2004, Ed. D. Zvizdic, University of Zagreb,1119-1140.

Bonnier G., and Hermier Y., (1982), Thermal behaviour of sealed cells and of a multi-compartment cell, in *Temperature its measurement and control in science and industry Vol 5*, Ed. J. F. Schooley, AIP, New York, 231-237.

Bowen, G. J. and Revenaugh J., (2003), Interpolating the isotopic composition of modern meteoric precipitation. *Water Resources Research*, **39**, 10. See also the on-line isotope in precipitation calculator (OIPC) at http://es.ucsc.edu/~gbowen/OIPC_Main.html.

Burton J.A., Prim R.C., and Slichter W.P., (1953), The Distribution of Solute in Crystals Grown from the Melt. Part I. Theoretical *J. Chem. Phys.* **21**, 1987.

CIPM, (1999), Mutual Recognition of National Measurement Standards and of Calibration and Measurement Certificates Issued by National metrology Institutes, BIPM, Sèvres.

Connolly J.J., McAllan J.V., (1980), Limitations on Metal Fixed Points Caused by Trace Impurities, *Metrologia*, **16**, 127-132.

Craig, H., (1961), Isotope variations in meteoric waters, *Science* **133**, 1702-1703.

Crovini L., Jung H.J., Kemp R.C., Ling Shan-Kang, Mangum B.W., Sakurai H., (1991), The Platinum Resistance Thermometer Range of the International Temperature Scale of 1990, *Metrologia*, **28**, 317-325.

del Campo, D, Chimenti, V, Reyes, J, Rodriguez Castrillon, J A, Moldovan, M, Garcia Alonso, J I, (2008) Assembly and study of different mercury cells with known impurity content and isotopic composition, Proc. TEMPMEKO 2007, *Int. J. Thermophys*, **29**, 93-103.

Eriksson G., Hack K., (1990), A Computer Program for the Calculation of Complex Chemical Equilibria, M*etallurgical Transactions B*, **21B**, 1013-1023.

Evans J.P., and Wood S.D., (1971), An Intercomparison of High Temperature Platinum Resistance Thermometers and Standard Thermocouples, *Metrologia*, **7**, 108-130

Evans J. P., (1984), Evaluation of some high-temperature platinum resistance thermometers, *Journal of Research of the National Bureau of Standards*, **89**, 384-373.

Fahr M., and Rudtsch S., (2008), A new method for the quantification and correction of thermal effects on the realisation of fixed points, Proc.TEMPMEKO 2007, *Int. J. Thermophys*., **29**, 126-138

Fellmuth, B., Berger,D., and Wolber L., (1999), An international star comparison of low temperature fixed point cells using sealed triple point cells, Proc. TEMPMEKO 1999, Ed. J.F. Dubbeldam and M.J. DeGroot, NMi Van Swinden Laboratorum, 233-238.

Fellmuth B, Fischer J., and Tegeler E., (2001), Uncertainty budgets for characteristics of SPRTs calibrated according to the ITS-90, working document of BIPM Consultative Committee on Thermometry, CCT/2001-02.

Fellmuth *et al*. (2003a) Comments on the underestimation of the change of fixed-point temperatures by impurities due to a non-justified application of Raoult's law, Working document of the BIPM Consultative Committee on Thermometry, CCT/03-12.

Fellmuth B., Berger D., Wolber L., de Groot M., Head D., Hermier Y., Mao Y. Z., Nakano T., Pavese F., Shkraba V., Steele A. G., Steur P. P. M., Szmyrka-Grzebyk A., Tew W. L., Wang L., White D. R., (2003b), An International Star Intercomparison of Low-Temperature Fixed Points Using Sealed Triple-Point Cells, in *Temperature: Its Measurement and Control in Science and Industry, Vol. 7*, Ed. D. C. Ripple. AIP, NY,885-890.

Fellmuth B, Tegeler E and Fischer J., (2005a), Uncertainty of the characteristics of SPRTs calibrated according to the ITS-90, Proc. TEMPMEKO 2004, Ed. D. Zvizdic, Faculty of Mechanical Engineering and Naval Architecture, Zagreb, 1135-1140.

Fellmuth B., Wolber L., Hermier Y., Pavese F., Steur P.P.M., Peroni I., Szmyrka-Grzebyk A., Lipinski L., Tew W.L., Nakano T., Sakurai H., Tamura O., Head D., Hill K.D., Steele A.G., (2005b), Isotopic and other influences on the realization of the triple point of hydrogen, *Metrologia*, **42**, 171-193.

Fellmuth B., Hill K.D., Bloembergen P., de Groot M., Hermier Y., Matveyev M., Pokhodun A., Ripple D., and Steur P. P. M., (2005c), Methodologies for the estimation of uncertainties and the correction of fixed-point temperatures attributable to the influence of chemical impurities, Working document of the BIPM Consultative Committee on Thermometry, CCT/2005-08.

Fellmuth B., and Hill K.D., (2006), Estimating the influence of impurities on the freezing point of tin, *Metrologia*, 2006, **43**,71-83.

Ferrick M.G., Calkins D.J., Perron N.M., Cragin J.H., and Kendall C., (2002), Diffusion model validation and interpretation of stable isotopes in river and lake ice, *Hydol.Process*, **16**, 851-872.

Filipe E., (2008), Components of a variance model for the analysis of repeated measurements in fixed point comparisons, Proc. TEMPMEKO 2007, *Int. J. Thermophys*, **29,** 871-880.

Furukawa G.T. (1972), Vapor Pressures of Natural Neon and of the Isotopes ^{20}Ne and ^{22}Ne from the Triple Point to the Normal Boiling Point, *Metrologia*, **8**, 11-27.

Furukawa G.T., and Bigge W.R.,(1982), Reproducibility of some triple point of water cells, in *Temperature its Measurement and Control in Science and Industry Vol. 5*, Ed. J. F. Schooley, AIP, New York, 291-297.

Furukawa G.T., Mangum B.W., and Strouse G.F., (1997), Effects of different methods of preparation of ice mantles of triple point of water cells on the temporal behaviour of the triple-point temperature, *Metrologia* **34**, 215-233.

Furukawa G.T., Strouse G.F., (2001), Investigation of the non-uniqueness of the ITS-90 in the range 660 °C to 962 °C, Proc, TEMPMEKO 2001, Ed. Fellmuth B., Seidel J., Scholz G., VDE Verlag, Berlin, 553-558.

Gonfiantini, R.,(1978), Standards for stable isotope measurements in natural compounds, *Nature* **271**, 534 – 536.

Gramich, J W, and Machlan, L A, (1985), Isotopic variations in commercial high-purity gallium, *Anal. Chem.*, **57**, 1788-1790

Head D. I., (1997), A EUROMET intercomparison of capsule platinum resistance thermometers between 13 K and 273 K, Proceedings of the International Seminar on Low Temperature Thermometry and Dynamic Temperature Measurement, Ed. A. Szmyrka-Grzebyk, IMEKO, Wrocław, L36 – L41.

Hermier, Y, and Bonnier G., (1990), An adiabatic calorimeter for calibration at the triple point of argon, Proc TEMPMEKO 1990, Helsinki, 95-104.

Hintelmann, H, and Lu, S Y, (2003), High precision isotope ratio measurements of mercury isotopes in cinnabar ores using multi-collector inductively coupled plasma spectrometry, *Analyst*, **128**, 635-639

Hill K.D., and Woods D.J., (1992), A preliminary assessment of the non-uniqueness of the ITS-90 in the range 500 ºC to 660 ºC as measured with a caesium-filled pressure-controlled, heat-pipe furnace, in *Temperature, its Measurement and Control in Science and Industry, Vol 6*, ed J.F Schooley, AIP, New York, 215-219.

Hill K.D., (2001), Is there are long-term drift in triple point of water cells?, *Metrologia*, **38**, 79-82.

Hill K.D., and Steele A.G., (2003), The non-uniqueness of the ITS-90: 13.8033 K to 273.16 K, in *Temperature: Its Measurement and Control in Science and Industry*; Ed. D.C Ripple, AIP, New York, 53-58.

Ilin A.U., (2003), A criterion for Uniformity of a Temperature Field in Realisation of the ITS-90 Fixed Points, in *Temperature: Its Measurement and Control in Science and Industry*; Ed. D.C Ripple, AIP, New York, 297-301.

ISO (1993) *International Vocabulary of Basic and General Terms in Metrology*; International Organization for Standardization, Genève, Switzerland, ISBN 92-67-01075-1.

ISO (1995) *Guide to the Expression of Uncertainty in Measurement*; International Organization for Standardization, Genève, Switzerland, ISBN 92-67-10188-9.

IUPAC (1997) *Isotopic composition of the elements*, International Union of Pure and Applied Chemistry. (Published as K. J. R. Rosman and P. D. P. Taylor, *Pure Appl. Chem.* **70**, 217-235,1998, available at http://ciaaw.org/publications.htm)

IUPAC (1994) *Reporting of stable hydrogen, carbon, and oxygen isotopic abundances*, International Union of Pure and Applied Chemistry. (Published as Coplen, T.B., *Pure & Appl. Chem.*, **66**, 273-276, 1994, available at http://ciaaw.org/publications.htm)

Ivanova A.G., and Ilin A.U., (2004), Influence of the realising method on the freezing temperature of zinc, Presented to TEMPMEKO 2004, *Izmeritelnaj Technika*, **11**, 2004, 43-46 (Translation: *Measurement Techniques*, **47**, 1096-1099).

Jansson B., Jönsson B., Sundman B., Ågren J., (1993), The Thermo-calc project, *Thermochim. Acta*, **214**, 93-96.

Jimeno-Largo P., Bloembergen P., and Ancsin J., (2005), An experimental and theoretical analysis of the effect of the impurities on the adiabatic melting curve of silver", Proc. TEMPMEKO 2004, Ed. D. Zvizdic, Faculty of Mechanical Engineering and Naval Architecture, Zagreb, 233-238.

Karlsson H., and Sørlsdal T., (1995/96), Pressure Coefficients of a 1 W Thomas-Type Resistance Standards, *Metrologia*, **32**, 389-391.

Kiyosawa, K., (1991), Freezing point mixtures of $H_2{}^{16}O$ and $H_2{}^{18}O$, *J. Soln. Chem.* **20**, 583-588.

Kibble B.P., and Rayner, G.H., (1984), *Coaxial AC Bridges*, Adam Hilger, Bristol.

LaMer, V.K., and Baker, W.N., (1934), The Freezing point of Mixtures of H_2O and D_2O. The Latent Heat of D_2O. *J. Am. Chem. Soc.* **56**, 2641-2643.

Mangum, B. W., and Thornton, D.D., (1979), Determination of the triple point of gallium, *Metrologia*, **15**, 201-215

Mangum B.W., Pfeiffer E.R., Strouse G.F., (1990), Non-uniqueness of some standard platinum resistance thermometers over the temperature range from 13 K to 1235 K, Proc. TEMPMEKO 1990, Helsinki, 17-36.

Mangum B.W., Bloembergen P., Chattle M.V., Fellmuth B., Marcarino P., Pokhodun A.I., (1997), On the International Temperature Scale of 1990 (ITS-90), *Metrologia*, **34**, 427-429.

Magnum B.W., Bloembergen P., Chattle M.V., Fellmuth B., Marcarino P., Pokhodun A. I., (1999a), On the influence of impurities on fixed point temperatures, 2000, working document of BIPM Consultative Committee on Thermometry, CCT/99-11.

Mangum B.W., Bloembergen P., Chattle M.V., Fellmuth B., Marcarino P., Pokhodun A.I.,(1999b), On the International Temperature Scale of 1990 (ITS-90). Part II: Recommended techniques for comparisons, at the highest level of accuracy, of fixed-point cells used for contact thermometry, *Metrologia*, **36**, 79-88.

Magnum B.W., Bloembergen P., Chattle M.V., Fellmuth B., Marcarino P., Pokhodun A. I., (2000a), Optimal realization of the defining points of the ITS-90 that are used in contact thermometry, working document of BIPM Consultative Committee on Thermometry, CCT/2000-13.

Mangum B.W., Strouse G.F., Guthrie W.F., Pello R., Stock M., Renaot E., Hermier Y., Bonnier G., Marcarino P., Gam K.S., Kang K.H., Kim Y.-G., Nicholas J.V., White D.R., Dransfield T.D., Duan Y., Qu Y., Connolly J., Rusby R.L., Gray J., Sutton G.J.M, Head D.I., Hill K.D., Steele A., Nara K., Tegeler E., Noatsch U., Heyer D., Fellmuth B., Thiele-Krivoj B., Duris S., Pokhodun A.I., Moiseeva N.P., Ivanova A.G., de Groot M.J., Dubbeldam J.F., (2002b), Key Comparison: Summary of comparison of realizations of the ITS-90 over the range 83.8058 K to 933.473 K: CCT key comparison CCT-K3, *Metrologia*, **39**, 179-205.

Marcarino P. and Dematteis R.,(1999), Calibration of SPRTs affected by humidity in the subrange between the fixed points of Hg and Ga, Proc.TEMPMEKO 1999, Ed. J.F Dubbeldam and M.J. de Groot, NMi Van Swinden Laboratorium.

McAllan J.V., (1982), The effect of pressure on the water triple point temperature, in *Temperature its Measurement and Control in Science and Industry Vol. 5*, Ed. J F Schooley, AIP, New York, pp 285-290.

McMartin M. P., and Kusters, N.L., (1966), A direct-Current-Comparator Ratio Bridge for Four-Terminal Resistance Measurements, *IEEE Tans. Instrum. Meas*., **IM-15**, 212-220.

Massalski T.B., *et al*. (1990), *Binary alloy phase diagrams*, 2nd ed., Editor-in-chief, Massalski T. B.; Editors, Okamoto H., Subramanian P.R., Kacprzak L., Materials Park, Ohio, ASM International, 1990.

Meijer, H. A., and Li, W. J., (1998), *Isotopes Environ. Health Sudie*, **34**, 349-369.

Mendez-Lango E., (2002), A non-destructive method to evaluate the impurity content in triple point of water cells, Proc. TEMPMEKO 2001, Ed. Fellmuth B., Seidel J., Scholz G., VDE Verlag, Berlin, 465-470.

Meyer C.W., and Tew W., (2006), ITS-90 non-uniqueness from PRT subrange inconsistencies over the Range 24.56 K to 273.16 K, *Metrologia*, **43**, 341-352.

Meyer C. W., and Ripple, D.C., (2006), Determination of the uncertainties for ITS-90 realization by SPRTs between fixed points**,** *Metrologia*, **43**, 327-340.

Moiseeva N.P., Pokhodun A.I., (1992), Investigation of the non-uniqueness and subrange inconsistency of ITS-90 using platinum resistance thermometers in the 0-961.78 °C range, in *Temperature: Its Measurement s and Control in Science and Industry, Vol 6* Ed. J.F. Schooley, AIP, New York,187-191.

Moiseeva N.P., (2005), Improved design for 0.6-ohm HTSPRTS: reducing the leakage error and increasing the stability. Proc. TEMPMEKO 2004, Cavtat, Ed. Davor Zvizdic, Faculty of Mechanical Engineering and Naval Architecture, Zagreb, 433-438.

Nakanishi M., and Sakurai H., (2005), Precise Determination of Hydrostatic Pressure Correction Coefficient of Triple Point of Water Cells using Cryogenic Current Compator Bridge, *Jap. J. Appl. Phys*. **44**, 4206-4208.

Nakano T., Tamura O., Sakurai H., (2003), New sealed cells for the realization of Cryogenic fixed points at NMIJ/AIST, in *Temperature: Its Measurement and Control in Science and Industry*, Vol 7, Ed. Ripple D.C. AIP, New York, 185-190.

Nakano, T., Tamura, O., and Sakurai, H., (2005a), Melting curves of low temperature fixed points of the ITS-90 used sealed cells. Proc. TEMPMEKO 2004, Cavtat, Ed. D. Zvizdic, Faculty of Mechanical Engineering and Naval Architecture, Zagreb,159-164.

Nakano, T., Tamura, O., and Sakurai, H., (2005b), Anomalous Increase of Heat Capacity below the Triple Point of e-H_2 Caused by Porous Catalyst. Proc. TEMPMEKO 2004, Cavtat, Ed. D. Zvizdic, Faculty of Mechanical Engineering and Naval Architecture, Zagreb,147-152.

Nakano T., Tew W.L., Tamura O., and Sakurai H., (2005c), Double anomalous peak in the heat capacity just below the triple point of saturated e-H2 with FeO(OH), Proc TEMPMEKO 2007, *Int. J. Thermophys*., **29**, 83-94.

Nguyen M. K., and Ballico M., (2008), Comparison of 5 Isotope-corrected water triple point cells with the NMIA-2002 WTP ensemble, Proc. TEMPMEKO 2007, *Int. J. Thermophys*, **29**, 1761-1771

Nicholas J.V., White D.R., Dransfield T.D., (1997), Isotope Influences on the Triple point of water and the definition of the kelvin, Proc. TEMPMEKO 1996, Ed. Marcarino P., Levrotto and Bella, Torino, 57-62.

Nubbemeyer H.G., Fischer J., (2002), Final report on key comparison CCT-K4 of local realizations of aluminium and silver freezing-point temperatures, *Metrologia*, **39**, Tech. Suppl., 03001.

Palenčár R., Ďuriš S., Brdečka R., (2000), Contribution to the Evaluation of the Uncertainties of the SPRT Calibration in the Defining Fixed Points. CCT working document, CCT/2000-23.

Papon P., Leblond J., and Meijer P.H.E., (2002), *The Physics of Phase Transitions*, Springer Verlag, Berlin.

Pavese F., Ancsin J., Astrov D.N., Bonhoure J., Bonnier G., Furukawa G.T., Kemp R.C., Maas H., Rusby R.L., Sakurai H., Ling Shan-Kang, (1984), An International Intercomparison of Fixed Points by Means of Sealed Cells in the Range 13.81 K - 90.686 K, *Metrologia*, **20**, 127-144.

Pavese F. and Molinar G., (1992), *Modern Gas-based Temperature and Pressure Measurements*, Plenum, New York.

Pavese F., and Tew, W.L., (2000), On the isotopic composition of commercial hydrogen vs “natural isotopic composition” and the problems for the ITS-90 definition, working document of BIPM Consultative Committee on Thermometry, CCT/2000-19.

Pavese, F., Tew, W.L. and Steele, A., (2002), Archival and theoretical considerations for isotopic dependence in the e-H2 fixed points, Proc TEMPMEKO 2001, Ed. Fellmuth B., Seidel J., Scholz G., VDE Verlag, Berlin, 429-434.

Pavese F., Fellmuth B., Head D., Hermier Y., Peruzzi A., Szmyrka-Grzebyk A., and Zanin L., (2003), MULTICELLS: A European Project on Cryogenic Temperature Fixed Points in Sealed Cells", in *Temperature: its Measurement and Control in Science and Industry Vol. 7* , Ed. D.C. Ripple, AIP, New York, 161-166.

Pavese F., (2005a), On problems in the definition of the International Temperature Scale arising from the variability of the isotopic composition of some substances used for the fixed-points, *Metrologia*, **42**, 194-200.

Pavese, F., Fellmuth, B., Head, D., Hermier, Y., Hill, K.D., Valkiers, S., (2005b), Evidence of a Systematic Deviation of the Isotopic Composition of Neon from Commercial Sources with its Isotopic composition in Air, *Anal. Chem*., **77**, 5076-5080.

Pavese F., (2009), Critical review of information relevant to the correction of the effect of chemical impurities in gases used for the realization of ITS-90 fixed points *Metrologia*, **46**, 47-61

Peruzzi A., Kerkhof O., and de Groot M.J., (2007), Isotope and impurity content in water triple point cells manufactured at NMi VSL, Proc. TEMPMEKO 2007, *Int. J. Thermophys*, **28**, 1931-1940

Pond, S. L., (2003), Argon Triple-Point Apparatus for SPRT Calibration, *Temperature: Its Measurement and Control in Science and Industry, Vol. 7*, Ed. D. C. Ripple, AIP, New York, 203-208.

Preston-Thomas H., (1990), The International Temperature Scale of 1990, *Metrologia*, **27**, 3-10, also erratum: *Metrologia*, **27**, 107 1990. (The full text of the amended version of ITS-90 is available at http://www.bipm.fr/en/committees/cc/cct/publications_cc.html).

Prince, A., (1966), *Alloy Phase Equilibria*, Elsevier, Amsterdam (on-line copy at http://www.matport.com/research/free-tools/aprince/ap-book.html).

Quinn T.J., (1990), *Temperature*, Monographs in Physical Measurement, Academic Press, London.

Renaot E., Valin M.H., Bonnier G., White M., Van der Linden A., Bairy G., Kovacs T., Nemeth S., Bojkovski J., Kuna R., Weckstrom T., Ivarsson J., Rauta C., Helgesen F., Uytun A., Ugur S., Kryl J., Adunka F., Ranostaj J., Duris S., Anagnostou M., Kokkini E., Pauza A., aand Augevicius V., (2005), Comparison of realisations of the triple point of water (Euromet project No. 549), Proc. TEMPMEKO 2004, Cavtat, Ed. D. Zvizdic, Faculty of Mechanical Engineering and Naval Architecture, Zagreb, 1009-1015.

Renaot E., Valin M. H., and Elgourdu M., (2008a), Analaysis of the Comparison of TPW Realizations in Europe in Light of CCT Recommendation 2 (CI-2005), Proc. TEMPMEKO 2007, *Int.. J. Thermophys.*, **29**, 791-798.

Renaot E., Valin M.H., and Elgourdu M., (2008b), Influence of Impurities and Filling Protocol on the Aluminium Fixed Point, Proc. TEMPMEKO 2007, *Int J. Thermophys.*, **29**, 852-860.

Ripple D.C., Gam K. S., Hermier Y., Hill K., Rusby R., Steele A., Steur P.P.M., Stock M., Strouse G.F., and White D.R., (2005), Summary of Facts Relating to Isotopic Effects and the Triple Point of Water: Report of the BIPM -CCT ad hoc Task Group on the Triple Point of Water, working document of BIPM Consultative Committee on Thermometry, CCT/05-07.

Ripple D., Pokhodun A., Steur P., Strouse G., Tamura O. (2008), Recommended List of Common Impurities for Metallic Fixed-point Materials of the ITS-90, working document of BIPM Consultative Committee on Thermometry, CCT/08-16/rev.

Rudtsch, S., Ramm, G., Heyer, D., Vollmert, R., (2005), Comparison of Test and Calibration Methods for Resistance Ratio Bridges", Proc. TEMPMEKO 2004, Cavtat, Ed. D. Zvizdic, Faculty of Mechanical Engineering and Naval Architecture, Zagreb, 773-780.

Sadli M., Renaot E., Bonnier G., (1998), Propagation of HTSPRT Calibration Uncertainties from 0.01 ºC up to 961.78 ºC, Proc. Euromet workshop in temperature Paris 1998, BNM-INM. 13-18.

Sakurai H., (1998), Realization of the Triple Point of Equilibrium Hydrogen Using a Closed Cycle GM refrigerator, *Trans. Soc. Control. Eng*. **34**, 1553-1558.

Sakurai H., (1999), Precise determination of the triple points of equilibrium hydrogen and argon using a closed cycle refrigerator, Proc. TEMPMEKO 1999, Ed. Dubbeldam J.F. and de Groot M.J., NMi Van Swinden Laboratorium, Delft, 124-128.

Sakurai H., (2002), Hydrostatic correction coefficient of triple point cell of water, *Trans. of the Society of Instrument and Control Engineers* (Japan) **38**, 590-593.

Sloan G.J. and McGhie A.R., (1988), *Techniques of Melt Crystallisation*, John Wiley & Sons, New York.

Steele A.G., Fellmuth B., Head D.I., Hermier Y., Kang K.H., Steur P.P.M., Tew W.L., (2002a), Key Comparison: CCT-K2: Key comparison of capsule-type standard platinum resistance thermometers from 13.8 K to 273.16 K *Metrologia*, 2002, **39**, 551-571.

Steele A., (2002b), Revisiting the Triple Point of Spin-equilibrated Hydrogen at National Research Council of Canada, Proc. TEMPMEKO 2001, Ed Fellmuth B. Seidel J., Scholz G., VDE Verlag Berlin 417-422.

Steele A.G., (2005), ITS-90 Subrange inconsistency below the triple point of water, *Metrologia*, **42**, 289-297.

Steur P. P. M., Hermier Y., Gam, K.S., Hill K.D., Fellmuth B., Pokhodun A., Ripple D., (2005), Isotopic effects in the hydrogen fixed points: working document of BIPM Consultative Committee on Thermometry, CCT/2005-06.

StimsonF.H., (1945), The Measurement of some Thermal Properties of water, *Journal of the Washington Academy of Sciences*, **35**, July 15, 1945.

Stock M., and Solve S., (2006), CCT-K7: Key comparison of water triple point cells Report B (available at www.bipm.fr).

Strouse G.F., (1992a), Investigation of the ITS-90 subrange inconsistencies for 25.5 Ω SPRTs, in *Temperature: Its Measurement and Control in Science and Industry*, Vol. 6, Ed. J.F. Schooley, AIP, New York, 165-168.

Strouse G.F., (1992b), NIST assessment of ITS-90 non-uniqueness for 25.5 W SPRTs at gallium, indium and cadmium fixed points, in *Temperature: Its Measurement and Control in Science and Industry*, Vol. 6. Ed. J.F. Schooley, AIP, New York, 1992, 175-178.

Strouse, G.F. and Hill, K.D., (2003a), Performance Assessment of resistance Ratio Bridges Used for the Calibration of SPRTs, in *Temperature: Its Measurement and Control in Science and Industry, Vol 7*, 2003, Ed. Dean C. Ripple, AIP, New York, 327-332.

Strouse G.F., (2003b), NIST methods of estimating the impurity uncertainty component for ITS-90 fixed-point cells from the Ar TP to the Ag FP, working document of BIPM Consultative Committee on Thermometry, CCT/03-19.

Strouse G.F., (2005), NIST certification of ITS-90 Fixed-point cells from 83.8058 K to 1234.93 K: Methods and Uncertainties, Proc. TEMPMEKO 2004, Cavtat, Ed. D. Zvizdic, Faculty of Mechanical Engineering and Naval Architecture, Zagreb, 879-884.

Strouse G.F., and Zhao M., (2007), The impact of isotopic concentration, impurities and cell aging on the water triple point temperature, Proc. TEMPMEKO 2007, *Int. J. Thermophys*, **28**, 1913-1922.

Tavener J.P., (2002), Fully defined water triple point cells, *Proceedings of TEMPMEKO 2001*,Ed. Fellmuth B., Seidel J., Scholz G., VDE Verlag, Berlin, 471-475.

Tavener J.P., (2006), Private communication with D R White.

Tavener J.P., and Davies N., (2007), The establishment of ITS-90 water triple point references to ±2 μK, and the assessment of 100 water triple point cells made between 2001 and 2006, presented to TEMPMEKO 2007, Lake Louise, canada.

Tew W.L., and White D.R., (2005), Comment on 'Freezing Point Mixtures of $H_2{}^{16}O$ with $H_2{}^{17}O$ and those of Aqueous CD_3CH_2OH and $CH_3{}^{13}CH_2OH$ Solutions', *J. Soln. Chem.*, **34**, 10, 1191-1196.

Tew W.L., (2008), Estimating the Triple-point Isotope Effect and the Corresponding Uncertainties for Cryogenic fixed points. Proc. TEMPMEKO 2007, *Int. J. Thermophys.*, **29**, 67-81.

Ubbelohde A.R., (1965), *Melting and Crystal Structure*, Clarendon press, Oxford, pp31-36.

Villars P., Prince A., Okamoto H., (1995), *Handbook of ternary alloy phase diagrams*, Materials Park, OH, ASM International.

Wang,C, Yeh, C., (1998), Effects of particle size on the progressive oxidation of nanometer platinum by dioxygen, *J. Catal*., **178**, 450-456.

Ward S.D., Compton J.P., (1979), Intercomparison of Platinum Resistance Thermometers and T_{68} Calibrations, *Metrologia*, 1979, **15**, 31-46.

White D. R., (1996), A method for calibrating resistance thermometry bridges, Proc. TEMPMEKO 1996, Levrotta & Bella, Torino, Ed. P. Marcarino, Levrotto and Bella, Torino, 129-134.

White D.R. and Saunders P., (2000), The propagation of uncertainty on interpolated scales with examples from thermometry, *Metrologia*, **37**, 285-293.

White D.R., (2001), The propagation of uncertainty with non-Lagrangian interpolation, *Metrologia*, **38**, 63-69.

White D.R, Dransfield T.D., Strouse G.F., Tew W.L., Rusby R.L., Gray J., (2003a), Effects Of Heavy Hydrogen and Oxygen on the Triple-Point Temperature of Water" in *Temperature: its Measurement and Control in Science and Industry*, Vol 7 , Ed. D. C. Ripple, AIP, New York, 221—226.

White D.R., (2003b), Contribution of Uncertainties in Resistance Measurements to Uncertainty in ITS-90, *Temperature: Its Measurement and Control in Science and Industry, Vol. 7*, Ed. D. C. Ripple, AIP, New York, 321-326.

White D.R., (2004), Measuring the residual air pressure in triple-point-of-water cells, *Meas. Sci. Technol*. **15**, 2004, N15-N16.

White D.R. and Dransfield T.D., (2005a), Buoyancy Effects on the Temperature Realised by Triple-Point-of-Water Cells, Proc. TEMPMEKO 2004, Ed. D. Zvizdic, Faculty of Mechanical Engineering and Naval Architecture, Zagreb, 313-318.

White D.R., Downes C.J., Dransfield T.D., Mason R.S., (2005b), Dissolved Glass in Triple-Point-of-Water Cells, Proc. TEMPMEKO 2004, Cavtat, Ed. D. Zvizdic, Faculty of Mechanical Engineering and Naval Architecture, Zagreb, 251-256.

White D.R., and Saunders P., (2007), Propagation of uncertainty with calibration equations, *Meas. Sci. & Tehnol*, **18**, 2157-2169.

White D.R. and Strouse G.F., (2009), Observations on sub-range inconsistency in the SPRT interpolations of ITS-90, *Metrologia*, **45**, 101–108

White D.R., Arai M., Bittar A., Yamazawa K., (2007), A Schottky-Diode Model of the Nonlinear Insulation Resistance Effects in SPRTs, Proc. TEMPMEKO 2007, *Int. J. Thermophys.* **28**, 1855-1881.

Wise, S.A., and Watters, (2005) R.L., NIST Report of investigation: reference materials 8535, 8536, 8537 (available at **www.nist.gov**.)

Widiatmo, J.V., Katsuhiko H, Arai, M., (2005), Assessment Of High-Temperature Metal Fixed Points On The Basis Of The Continuous Freezing Method, Proc. TEMPMEKO 2004, Cavtat, Ed. D. Zvizdic, Faculty of Mechanical Engineering and Naval Architecture, Zagreb, 239-244.

Widiatmo J.V., Harada K., Yamazawa K., Arai M., (2006), Estimation of impurity effect in aluminium fixed-point cells based on thermal analysis, *Metrologia*, **43**, 561-572.

Widiatmo J.V., Harada K., Yamazawa K., and Arai M., (2008), Impurity Effect in Silver point Realization, Proc. TEMPMEKO 2007, *Int. J. Thermophys*. **29** 158-170

Wilkins F.J. and Swan M.J., (1970), Precision ac/dc resistance standards, *Proc. IEE*, **117**, 841-849.

Witt T.J., (1998), Electrical Resistance Standards and the Quantum Hall Effect, *Rev. Sci. Inst.* **69**, 2823-2843.

Wolber L., and Fellmuth B., (2008), Influence of the Freezing and Annealing Conditions on the Realization of Cryogenic Fixed Points, Proc. TEMPMEKO 2007, *Int. J. Thermophys,*. **29**, 82-92.

Yamazawa K. and Arai M., (2003), Measurement of the insulation resistance for the development of high temperature platinum resistance thermometers with a guard electrode", in *Temperature: Its Measurement and Control in Science and Industry, Vol. 7*, Ed. D.C. Ripple, AIP, New York, 363-368.

Yamazawa K. and Arai M., (2005), Design improvement against the lead leakage effect for high temperature SPRTs up to 1085 °C, Proc. TEMPMEKO 2004, Cavtat, Ed. D. Zvizdic, Faculty of Mechanical Engineering and Naval Architecture, Zagreb, 409-414.

Yamazawa K. Arai., White D.R., (2007a), A Schottky-Diode Model of the Nonlinear Insulation Resistance in HTSPRTs, Proc. TEMPMEKO 2007, *Int. J. Thermophys*, **28**, 1843-1854.

Yamazawa K. Widaiatmo J.V., and Arai M., (2007b), Thermal analysis of the heater induced realization of the tin point, Proc. TEMPMEKO 2007, *Int. J. Thermophys*, **28**, 1941-1956.

Zhao, M., Li, X., and Chen, D., (2003), Experimental Study of Different Filling gases on the Stability of Metal-sheathed Standard Platinum Resistance Thermometers, in *Temperature: Its Measurement and Control in Science and Industry, Vol. 7*, Ed. D.C. Ripple, AIP, New York, 330-344.

Zhang J. and Berry R.J., (1985), Ac and Dc Insulation Leakage in platinum Resistance Thermometers up to 750 ºC, *Metrologia*, **21**, 207-223.

Zhiru K, Jingbo L and Xiaoting L., (2002), Study of the ITS-90 non-uniqueness for the standard platinum resistance thermometer in the subrange 0 °C to 419.527 °C, *Metrologia*, **39**, 127-133.

Zief M., and Speights R., (1972), *UltraPurity Methods and Techniques*, Marcel Decker, New York,173-191.